

University of New Hampshire

University of New Hampshire Scholars' Repository

Master's Theses and Capstones

Student Scholarship

Spring 2023

USING UNPILOTED AERIAL VEHICLE STRUCTURE FROM MOTION AND SNOWMODEL TO MAP SPATIAL DISTRIBUTION OF WIND DEPOSITED SNOW IN MOUNT WASHINGTON, NH AVALANCHE TERRAIN

Cameron Wagner

University of New Hampshire, Durham

Follow this and additional works at: <https://scholars.unh.edu/thesis>

Recommended Citation

Wagner, Cameron, "USING UNPILOTED AERIAL VEHICLE STRUCTURE FROM MOTION AND SNOWMODEL TO MAP SPATIAL DISTRIBUTION OF WIND DEPOSITED SNOW IN MOUNT WASHINGTON, NH AVALANCHE TERRAIN" (2023). *Master's Theses and Capstones*. 1728.
<https://scholars.unh.edu/thesis/1728>

This Thesis is brought to you for free and open access by the Student Scholarship at University of New Hampshire Scholars' Repository. It has been accepted for inclusion in Master's Theses and Capstones by an authorized administrator of University of New Hampshire Scholars' Repository. For more information, please contact Scholarly.Communication@unh.edu.

**USING UNPILOTED AERIAL VEHICLE STRUCTURE FROM MOTION AND
SNOWMODEL TO MAP SPATIAL DISTRIBUTION OF WIND DEPOSITED SNOW IN
MOUNT WASHINGTON, NH AVALANCHE TERRAIN**

By

Cameron Wagner

Bachelor of Science in Environmental Engineering, University Of New Hampshire, 2021

THESIS

Submitted to the University of New Hampshire

in Partial Fulfillment of

the Requirements for the Degree of

Master of Science

in

Civil and Environmental Engineering

May, 2023

This thesis has been examined and approved in partial fulfillment of the requirements for the degree of Master of Science in Civil Engineering by:

Thesis Director, Dr. Jennifer M. Jacobs
Professor of Civil and Environmental Engineering

Dr. Julie Paprocki
Assistant Professor of Civil and Environmental
Engineering

Dr. Michael Palace
Associate Professor of Earth Sciences

On April 19th, 2023

Original approval signatures are on file with the University of New Hampshire Graduate School.

ACKNOWLEDGEMENTS

This project would not be possible without the support and guidance of the people I am surrounded by. First, I would like to thank my girlfriend, Sarah, for her unconditional support, and willingness to join on data collection efforts throughout the year. I would also like to thank my advisor, Dr. Jennifer Jacobs, for her guidance and input throughout my entire project from planning to manuscript editing. I would also like to thank the Jacobs Research Group: A. Hunsaker, T. Hoheneder, E. Cho, F. Sullivan, M. Verfaillie, J. Johnston, I. Khan, M. Moradi, and L. Dwyer for offering input along the way. Furthermore, I would like to thank my other committee members, Dr. Michael Palace, and Dr. Julie Paprocki, for their involvement in the defense process. The extremely arduous data collection would have not been possible without the help of all of those who have joined. Additionally, I would like to thank Frank Carus, Pat Scanlon, Ryan Lewthwaite, Jeff Fongemie, and the rest of the MWAC for their continued backing of my research efforts as well as occasional gear and personnel transport to the study areas. The SnowModel portion of this work would not be possible without Dr. Glen Liston and Adele Reinking. Their willingness to take time out of their day was appreciated thoroughly. I am grateful for Adam LeWinter and the others at the RS/GIS CX at CRREL. Their willingness to provide the cloud ODM SfM processing workflow was integral to the project's success. Finally, I am deeply thankful for my family and friends who have offered unwavering belief in my success throughout this entire project.

This material is based upon work supported by the Broad Agency Announcement Program and the Cold Regions Research and Engineering Laboratory (ERDC-CRREL) under contract number W913E5-18-C-006. Any opinions, findings and conclusions or recommendations in this material are those of the author(s) and do not necessarily reflect the views of the Broad Agency Announcement Program and the Cold Regions Research and Engineering Laboratory.

TABLE OF CONTENTS

ACKNOWLEDGEMENTS	iii
TABLE OF CONTENTS	iv
LIST OF FIGURES	vi
LIST OF TABLES	viii
ABSTRACT	ix
1 INTRODUCTION	1
2 CHAPTER 2 – SITE DESCRIPTION	7
2.1 Mount Washington and The Presidential Range	7
2.2 Tuckerman Ravine	9
2.3 Boott Spur Gullies	13
3 CHAPTER 3 – METHODS	16
3.1 UAV Data Acquisition	16
3.1.1 Base Station Positioning	17
3.1.2 UAV Flight Planning and Hardware Specifications	19
3.1.3 UAV Flight Procedure	20
3.2 Post-Processing and Digital Surface Model Creation	22
3.2.1 Structure from Motion Workflow	22
3.2.2 Snow Depth Calculation	22
3.3 Snow Depth SfM Campaigns and Manual Validation	23
3.4 SnowModel Processing	24
3.4.1 SnowModel Overview	24
3.4.2 SnowModel Processing Workflow	27
4 CHAPTER 4 – RESULTS	29
4.1 Winter 2021-2022 Summary	29
4.2 SfM Snow Depth Validation	31
4.3 UAV SfM Snow Depth	33
4.3.1 Tuckerman Ravine	33
4.3.2 Boott Spur Gullies	38
4.4 UAV SfM Snow Depth Change	43
4.4.1 Tuckerman Ravine	43
4.4.2 Boott Spur Gullies	48
4.5 SnowModel Derived Snow Depth	51
4.5.1 SnowModel Time Series	51
4.5.2 SnowModel and UAV SfM Snow Depth Change Comparison	58
4.6 Winter 2021-2022 Case Studies	64
4.6.1 February BSG Snow and Rain Event Case Study	64
4.6.2 Late March Tux Wind Slab Formation and 4/01/22 Avalanche Case Study	68

5	CHAPTER 5 – DISCUSSION	71
5.1	Snow Accumulation Patterns in Tuckerman Ravine and Boott Spur Gullies	71
5.2	UAV and SnowModel Snow Redistribution	72
5.3	Experimental Error	73
5.4	SnowModel	76
5.5	Future Directions	78
6	CHAPTER 6 – CONCLUSION	81
	LIST OF REFERENCES	83
	APPENDIX A – USDA WMNF RESEARCH PERMIT	90
	APPENDIX B – GROUND SAMPLING LOCATIONS	92
	APPENDIX C – WEB ODM REPORT AND SETTINGS FOR TUX MARCH 9TH	93
	APPENDIX D – PUBLIC OUTREACH AND MOUNT WASHINGTON AVALANCHE CENTER (MWAC) INVOLVEMENT	95
	APPENDIX E – SNOWMODEL PARAMETERS	98
	APPENDIX F – BLOWING SNOW FLUX ADJUSTMENT PARAMETER AND TABLER SLOPE ADJUSTMENT SCALING FACTOR TESTING	100
	APPENDIX G – UAV SFM AND SNOWMODEL SNOW DEPTH CHANGE COMPARISON MAPS	102
	APPENDIX H – SNOWMODEL LANDCOVER INPUT	109

LIST OF FIGURES

Figure 1: Mount Washington’s Eastern Aspect. Credit: Red Line Guiding 2017	7
Figure 2: Overview of Study Area with Boott Spur Gullies (BSG), Tuckerman Ravine (Tux), Bigelow Lawn, and SnowModel Input Area show. Mount Washington Summit is Located at Elevation 1917 m in the Center of the Map.	11
Figure 3: Study Area Map with Bigelow Lawn, Boott Spur Gullies (BSG), and Tuckerman Ravine (TUX) Delineated	12
Figure 4: Photographs of Tuckerman Ravine (Tux) (A) and Boott Spur Gullies (BSG) (B) Study Areas Credit: Cameron Wagner.....	12
Figure 5: Areas of Interest Within the Tuckerman Ravine and BSG Study Areas, the Two UAV Launch Locations, and other Referenced Features	13
Figure 6: DJI D-RTK2 Base Station Set up for Tuckerman Ravine (A) and BSG (B) Surveys ..	18
Figure 7: Study Area Map Showing Sample Flight Lines in Tuckerman Ravine (Tux) and Boott Spur Gullies (BSG)	20
Figure 8: SnowModel Process Visualization in Context of this Study.....	25
Figure 9: SnowModel Component SnoTran-3D Transport Processes. Source: (Liston et al., 2007)	26
Figure 10: Tabler Slope Adjustment Scaling Factor (S) Particle Distribution Credit: (Liston et al., 2007)	28
Figure 11: 10/28/21 to 4/25/22 Wind Rose at the MWOBS.....	30
Figure 12: 10/29/21 to 4/30/22 Average Daily Wind Speed, Temperature, and Cumulative Snowfall at the MWOBS. Grey Vertical Lines Signify Days when a Tuckerman Ravine UAV Survey was Conducted.....	30
Figure 13: Comparison of UAV SfM Snow Depth to Avalanche Probe Snow Depth by Date and Location e.g., Tuckerman Ravine (Tux) and Boott Spur Gullies (BSG). Vertical Lines are \pm One Standard Deviation of the Three m Buffer Area SfM Snow Depth Values About Each Manual Probe Location.	32
Figure 14: Tuckerman Ravine Snow Depth Time Series. Note Each Date’s Extent is Based on the 10/29/21 Baseline Extent. AOI Map (Figure 5) Outlines Orange “Tux UAV Bounds” To Show Where Extents Above Reside with Areas of Interest and Points of Interest.	35
Figure 15: Tuckerman Ravine Snow Depth for the Areas of Interest (top) and Points of Interest (bottom) by Date	37
Figure 16: BSG Total Snow Depth Time Series Winter 2021-2022	40
Figure 17: BSG Snow Depth for the Areas of Interest (top) and Points of Interest (bottom) by Date	42
Figure 18: Tuckerman Ravine Snow Depth Change Time Series. Note Flights 10/29/21 – 1/21/22 Had a Smaller Flight Plan. A Red Outline Shows the Full Flight Plan That was Enacted on 2/1/22 and used for the Remainder of Data Collection.....	46
Figure 19: AOI Snow Depth Change Sensitivity to Tuckerman Ravine Snow Depth Change Scatterplot. The Dashed Line is the 1:1 Line.....	47
Figure 20: Boott Spur Gullies Snow Depth Change Time Series. Surveys from 10/29/21 Through 3/09/22 use a Slightly Smaller Flight Plan from the Three Remaining Flights (3/23/22 through 4/18/22). This Smaller Boundary is Shown in the Bottom Right Corner with a Teal Outline.	49

Figure 21: AOI Snow Depth Change Weighting on Boott Spur Gullies (BSG) Average Snow Depth Change. The Dashed Line is the 1:1 Line.	50
Figure 22: SnowModel Time Series Coinciding with UAV Flight Dates	54
Figure 23: SnowModel (SM) and UAV Comparison Time Series. Corrected Average SM is 1.29 m Less Than the Average SM Data Due to an Early Season Rainstorm That SnowModel Simulated Snow.	55
Figure 24: Landsat 8 and SnowModel Snow Cover Comparison of 4/25/2022	56
Figure 25: Normalized Difference Snow Index (NDSI) Derived from Landsat 8 Data Captured 4/25/2022. NDSI Map Above and Boxplots Showing SnowModel Snow Depth Below.....	57
Figure 26: Tuckerman Ravine SnowModel and UAV SfM Snow Depth Change Comparison by AOI. The Dashed Line is the 1:1 Line.	61
Figure 27: BSG SnowModel and UAV SfM Snow Depth Change Comparison by AOI. The Dashed Line is the 1:1 Line.	63
Figure 28: BSG Natural Avalanche Case Study. Snow Depth Change Map after Avalanche (A) Avalanche Crown Line in Hillman’s Highway. Credit: Brian Post (B). Orthomosaic Comparison Captured 2/01/22 (C) and 2/11/22 (D) with Avalanche Debris Delineated.....	66
Figure 29: BSG Snow Depth Change After Rain-On-Snow Event (A) with Photograph Taken by Cameron Wagner on 2/24/22 of Extreme Ablation Feature (B).....	67
Figure 30: 3/23/22 to 3/30/22 Tuckerman Ravine Wind Slab Snow Depth Change with Delineated Wind Slabs (A) Visual Observation and Delineation of a Wind Slab in the Runout of Left Gully (B) Credit: Cameron Wagner	69
Figure 31: Post-Avalanche Snow Depth Change Map (A) with Camera Images of Avalanche Debris (B) and Avalanche Crown Line (C) Credit: Ryan Lewthwaite (MWAC)	70
Figure A.1: United States Forest Service White Mountain National Forest Research Permit	91
Figure A.2: Ground Sampling Campaign Locations by Date.....	92
Figure A.3: Open Drone Map Sample Processing Report and Input Parameters	94
Figure A.4: GEE Products A. Total Snow Depth Viewer B. Snow Depth Change Viewer C. Tux Ortho Viewer D. BSG Ortho Viewer.....	96
Figure A.5: Wind Slab Notification Observation Posted to the MWAC's Public Observation Website on March 31 st , 2022.	97
Figure A.6: Backpack with UAV Data Collection Gear Backpack Mounted (A) and USFS Snowmobile Mounted (B).....	97
Figure A.7: Blowing Snow Flux Adjustment Parameter (BSFP) and Tabler Adjustment Scaling Factor (S) Testing on 30 m Resolution SnowModel Grid	101
Figure A.8: SnowModel and UAV Snow Depth Change Map Comparison in Tuckerman Ravine Time Series	108
Figure A.9: North American Land Change Monitoring System 2015 30 m	109

LIST OF TABLES

Table 1: Summary of the Winter 2021-2022 UAV Flights with SfM GPS Errors	24
Table 2: Tuckerman Ravine (Tux) Average Snow Depth (m) for the Areas of Interest (AOI) by Date	36
Table 3: Tuckerman Ravine (Tux) Snow Depths (m) for the Points of Interest (POI) by Date ...	36
Table 4: Boott Spur Gullies (BSG) Snow Depths (m) for the Areas of Interest (AOI) by Date ..	41
Table 5: Boott Spur Gullies (BSG) Snow Depths (m) for the Points of Interest (POI) by Date ..	41
Table 6: Tuckerman Ravine AOI SfM and SnowModel (SM) Willmott Statistics (meters).....	60
Table 7: Tuckerman Ravine POI SfM and SnowModel (SM) Willmott Statistics (meters)	60
Table 8: Boott Spur Gullies (BSG) AOI SfM and SnowModel (SM) Willmott Statistics (meters)	62
Table 9: Boott Spur Gullies (BSG) POI SfM and SnowModel (SM) Willmott Statistics (meters)	62

ABSTRACT

East of the Rocky Mountains, United States avalanche terrain is almost exclusive to Mount Washington, New Hampshire. Mount Washington's east-aspect glacial cirques are subject to frequent wind slab avalanche problems due to high winds and ample snowfall in fetch areas above the cirques. Quantification of these slabs' location, extent, and depth is an integral part of avalanche forecasting and risk assessment. This research used SnowModel, a spatially distributed snow-evolution model, to simulate wind slab depth maps using Mount Washington Observatory meteorologic station data on a 1 m grid. SnowModel's SnowTran-3D, a snow redistribution by wind algorithm, is tested for one of the first times in the Eastern United States. Snowpack seasonal evolution and accumulation event-based model performance is calibrated and validated using 15 snow depth maps collected throughout the winter of 2021-2022. Snow depth maps were constructed via Structure from Motion (SfM) analysis photogrammetry. SfM maps were derived from optical imagery collected using an Unpiloted Aerial Vehicle (UAV) and were able to quantify wind slab depth with a 5 cm spatial resolution.

Limited ground validation showed UAV SfM values are accurate with a 30 cm RMSE on the 2/01/2022 sample date. Total snow depth and snow depth change map time series of each study location consistently show wind-transported snow accumulation and erosion patterns on Mount Washington. SnowModel can capture Mount Washington's widespread snow redistribution trends but fails to quantify the magnitude and distribution of wind slabs as the UAV SfM can. SnowModel-derived snow depth was compared to Landsat 8's Normalized Difference Snow Index (NDSI) and shows a significant signal in snow depth increase when NDSI exceeds 0.4. This study provides the first of its kind approach for capturing Mount Washington's winter snowpack evolution using UAV SfM and a physically based snow evolution model.

1 INTRODUCTION

Snow avalanches are severe natural disasters that can destroy transportation and recreational infrastructure systems as well as human lives (Mock & Birkeland, 2000). The effects and dangers of these disasters may not be as geographically widespread as other natural disasters, such as tornados, tsunamis, and hurricanes, but are just as, if not more, challenging to forecast. Avalanche hazard areas are almost entirely comprised of slopes and flow paths (i.e., runout zone) which are nearly exclusive to mountainous areas. In the United States (US), avalanches are most prominent in high-elevation western mountain ranges such as the Rockies, Wasatch, San Juans, and Cascades. Three main components that contribute to avalanche formation are (1) steep terrain or slopes, (2) snowpack properties or arrangement of snow layers, and (3) weather. Important aspects of weather include the amount of new precipitation, wind speed, temperature, and solar radiation (Schweizer et al., 2003; Schweizer & Jamieson, 2001).

East of the Rocky Mountains, avalanches almost exclusively occur within the steep glacial cirques of Mount Washington, New Hampshire (Allen, 2000). Glacial cirques are large bowl-like land formations that have been carved into mountains in high elevations by moving glaciers. Mount Washington is located within the Presidential Mountain Range as part of the larger White Mountain National Forest complex in the Northeastern United States and has a 1,917 m summit elevation. Although the Presidential Range avalanche terrain area is only 275 km², its frequent use for recreation results in the potential for human casualties. There have been 17 recorded avalanche-caused fatalities on Mount Washington since 1950 (Crane, 2021). Although this number is relatively small compared to Colorado's 312 (CAIC, 2023), avalanches pose a life-threatening risk on Mount Washington.

The most predominant type of avalanche on Mount Washington is the wind slab avalanche. Snowfall events on Mount Washington are frequently associated with strong winds. The occurrence of high wind speeds leads to increased deposition of snow on the Mount Washington slopes with eastern-facing aspects (Allen, 2000). Wind slabs form when strong wind deposits and packs a dense layer of snow on the surface. They can be either formed by freshly fallen snow or by existing snow of low density that is transported by wind and then packed together.

Generally, the degree of wind slab avalanche risk can be quantified by measuring the depth and extent of the slab. Currently, the wind slabs on Mount Washington are detected by the expertise of local forecasters with visual delineation, or by digging snow pits to find density changes (Greene et al., 2010; Greene et al., 2015). For a wind slab to result in an avalanche, this dense layer must be situated on top of a weak, low-density layer. Identifying the depth of the slab contributes to awareness of where avalanche trigger locations are prominent. This helps forecasters by providing a quantitative data set to analyze when determining the avalanche danger rating of a given day (McClung, 2002).

Unpiloted Aerial Vehicles (UAVs) are a useful tool for collecting high-resolution remotely sensed data in difficult terrain (i.e., steep, remote). Avalanche terrain is inherently dangerous, thus, harnessing remote sensing techniques via UAVs to gather information such as optical imagery is extremely useful in isolating observers from danger. Structure from Motion (SfM) is a low-cost remote sensing technique for generating digital surface and elevation models (DSMs/ DEMs) of small study regions using optical imagery. Unlike other techniques for generating DEMs (e.g., LiDAR), SfM only requires an off-the-shelf digital camera as the primary sensor (Westoby et al., 2012). SfM-generated snow depth maps can be comparable to terrestrial laser scanner (TLS) depth maps with centimeter-level error (Adams et al., 2018). Aerial UAV mapping has the additional

advantage over TLS scanning because of the lack of shadowing from vegetation and/or terrain present in ground-based TLS scans.

As summarized by Verfaillie et al. (2023), previous studies have demonstrated the utility of UAVs SfM for avalanche detection. Eckerstorfer and Bühler (2015) and Eckerstorfer et al. (2016) identified remote sensing techniques relevant to avalanche forecasting (i.e., LiDAR, radar, optical) and their potential benefits. They determined that SfM is effective for generating 3D models with centimeter accuracy and resolution to study avalanche extent and debris. Gauthier et al. (2014) explored the use of SfM for modeling crown fractures (i.e., the profile of snow remaining above an avalanche that has slid), downed avalanches and their debris piles, and terrain mapping to better classify avalanche terrain. Their study collected red-green-blue (RGB) imagery from a helicopter using a full-frame single-lens reflex (SLR) camera. Another study carried out by Peitzsch et al. (2016) used a ground-based Nikon D-7100 digital SLR camera to capture glide snow avalanches (i.e., a phenomenon in which the entire snowpack down to the ground slides causing a large avalanche) along the Going-to-the-Sun Road corridor in Glacier National Park, Montana.

Other studies such as Masný et al. (2021) have used UAVs to collect photogrammetry to measure snow depth in alpine areas. Their research did not focus directly on avalanche forecasting but tested the ability of a fixed-wing real-time kinematic (RTK)-enabled UAV to map widespread high-resolution snow depth. They found that UAV SfM can measure snow depth at centimeter resolution in alpine environments. An emphasis on the importance of RTK was noted to eliminate the need to utilize ground control points in hard-to-access areas. Miller (2021) studied UAV-collected SfM in an avalanche path in the Bridger Range, Montana. Their 13 UAV-derived snow surface models helped to identify the snow depth and slope scale variability. In comparison to manual in-situ snow depth measurements, the UAV data had root mean square error (RMSE)

values in the range of 15 to 115 cm (Miller, 2021; Miller et al., 2022). Overall, UAVs have been shown capable of mapping snow depth with varying levels of error. In line with findings by Miller (2021), typical RMSE values for UAV-derived SfM snow depth depending on the land cover are 22 to 42 cm (Lendzioch et al., 2019), 8.5 to 13.7 cm (Harder et al., 2016), and 17 to 31 cm (Avanzi et al., 2018).

UAV data collection is an improvement over point data collected by avalanche forecasters, but modeling can provide similar insights without exposing surveyors or UAV pilots to the risks associated with avalanche-prone terrain. Mountainous environments, especially in the wintertime, are hazardous for deploying and flying UAVs. Restrictions such as cloud cover, cold temperatures, and wind also limit the days when UAV surveys can occur. Model-generated snow depth maps can eliminate the need for routine UAV data collection and instead use UAV measurements to calibrate and validate models.

SnowModel is a numerical model created by Dr. Glen Liston at Colorado State University's Cooperative Institute for Research in the Atmosphere (CIRA) to estimate snowpack evolution over varying temporal and spatial scales (Glen E. Liston & Kelly Elder, 2006). SnowModel has a wide breadth of applications from basin scale (100 m resolution) water resource management for the Upper Colorado River basin (Hammond et al., 2023) to Caribou migration resulting from snow depth study in Arctic Alaska (Pedersen et al., 2021). SnowModel has been proven effective in modeling snow depth in a variety of landscapes and regions (Litherland, 2013; Reynolds et al., 2021). An important component of SnowModel for this research, SnowTran-3D, redistributes snow due to wind effectively in high arctic sites with varying topography and landcover (Bruland et al., 2004). This component has also been used in alpine landscapes in Wyoming, USA (Hiemstra et al., 2006).

Greene (1999) investigated SnowTran-3D forced with meteorological station data and atmospheric conditions from the Climate Version of Regional Atmospheric Modeling System (ClimRAMS) data in the northern Colorado Rocky Mountains (Greene, 1999). Greene ran simulations on a 30 by 30 m grid and found both types of forcing data to be effective in simulating large-scale snow distribution features. This study demonstrated the effectiveness of SnowTran-3D for capturing snow distribution in complex mountainous terrain.

Gauer (2001) enhanced SnowTran-3D to include a two-layer numerical model to estimate the blowing and drifting of snow in alpine terrain. The model's upper layer describes the driving-wind field as well as the turbulent suspension, while the lower layer describes the transport by saltation (i.e., near-surface ballistic motion of particles) and erosion, and deposition of snow. Upon model-to-field data comparison, this new model is proven to be an effective tool for land-use planning and avalanche forecasting (Gauer, 2001).

Modeling techniques are an emerging method to gain information on avalanche forecast areas. Morin et al. (2020) investigated the potential for numerical snow models to aid in avalanche forecasting. They reviewed SNOWPACK (Lehning et al., 1999) from Switzerland, Crocus (Brun et al., 1989) from France, SNOWGRID (Olefs et al., 2013) from Austria, and seNORGE (Saloranta, 2012) from Norway. SNOWPACK is a one-dimensional model that is integrated into SnowModel along with other sub-models to describe all elements of the snow regime. Morin et al. (2020) determined that these models are effective for characterizing snow profiles, density changes, and the evolution of weak layers. However, none of these models described the snow redistribution by wind at a high enough resolution adequate for avalanche forecasting small wind slabs. Morin et al. (2020) also investigated how various countries use models within their avalanche forecasting workflows. European countries such as Switzerland, Italy, and Austria use

SNOWPACK to aid forecast generation, but the primary focus is on snowpack conditions rather than high-resolution redistribution by the wind. For a model to represent the Mount Washington snow regime, wind redistribution must be an integral part of the model.

UAV-collected SfM and numerical snowpack modeling both provide a means of gaining quantitative information without exposing forecasters to avalanche hazards. Models are typically validated with ground sampling points or meteorological station data such as SNOTEL. UAV snow depth data is also validated with ground sampling but when the study area is large and potentially dangerous to travel through, it can be challenging to collect ground observations suitable for validating snow depth returns. In this research study, these two products will be tested against each other so that in the future, snow depth change maps can be generated without needing to collect data with UAVs. SnowModel has yet to be used on a fine scale such as an individual basin over a snow season. Due to this, a time series of UAV SfM snow depth data will serve as the SnowModel validation.

The overall purpose of this research is to quantitatively identify the spatial extent and depth of wind-deposited snow with two complementary methods: UAV SfM and SnowModel. This will be accomplished by (1) carrying out an extensive UAV field data collection campaign, (2) Forcing SnowModel with local station data for the 2021-2022 winter, and (3) comparing these two methods of snow depth map generation to identify wind slab depth and extent.

2 CHAPTER 2 – SITE DESCRIPTION



Figure 1: Mount Washington's Eastern Aspect. Credit: Red Line Guiding 2017

2.1 Mount Washington and The Presidential Range

This study was conducted on Mount Washington (Figure 1) located in the White Mountain National Forest of central New Hampshire, United States (44.2706° N, 71.3033° W, 1917 m above sea level, ASL). The Presidential Range is the highest mountain range in the White Mountains and northeastern US with Mount Washington being the tallest peak (Figure 2). Mount Washington and the surrounding peaks in the Presidential Range are unique because they have the largest area (12.1 km^2) of true continuous alpine vegetation in the eastern United States (Bliss, 1963). Tree line begins at a relatively low elevation of approximately 1400 m (Grant et al., 2005) and is made up of spruce and fir boreal forest with northern hardwood species at lower elevations (Seidel et al., 2009). Another distinct characteristic of Mount Washington is the earning of a reputation for having “the worst weather in the world” (Smith, 1982).

The Mount Washington Observatory (MWOBS), a fully equipped metrological and research station, is situated on the Mount Washington summit (Figure 2). Air temperature, liquid precipitation, wind direction, wind speed, peak wind speed, prevailing visibility, sunshine minutes,

present weather phenomena, sky cover, clouds below summit, dewpoint temperature, wet bulb temperature, observer remarks, snowfall, snow depth, station pressure, and relative humidity are recorded by MWOBS. Year-round, Mount Washington and the surrounding Presidential Range often experience hurricane-force westerly winds up to 44.69 m/s (100 mph). From December through April, the daily average wind speed is 18.33 m/s (41 mph) and the temperature is -11.1 °C (12 °F) (MWOBS, 2023). Mount Washington receives an average of 645 cm of snowfall annually (Allen, 2000). A second weather station is present within the study domain called the Hermit Lake SNOTEL site (HLSN3) (Figure 5). This weather station records the same parameters as those collected by the MWOBS. The Hermit Lake Snotel is located 1 km (0.621 mi) due east of Tuckerman Ravine at an elevation of 1,143 m (3,750 ft).

There are three areas within Mount Washington that are important to study wind slab generation in this region. These areas, Bigelow Lawn, Tuckerman Ravine, and Boott Spur Gullies are close to each other (Figure 2) and each has a unique role in wind-transported snow and subsequent formation of wind slabs. The Tuckerman Ravine site was selected due to its varying aspect, and close down-wind proximity to the Bigelow Lawn. The Boott Spur Gullies site was selected to contrast with the terrain features and snow accumulation patterns found in the Tuckerman Ravine site. While Tuckerman Ravine avalanche terrain is widespread within its snow-covered bowl, the BSG area is made up of one gully and snowfield which isolates avalanche terrain to two main slopes. UAV flights are prohibited in White Mountain National Forest's Forest Protection Areas (FPAs), so a special use research permit was acquired (Appendix A).

Bigelow Lawn, a large fetch, or snow pickup is situated 0.77 km south-southeast of Mount Washington's summit (Figure 3). This area is referred to as a fetch because it is relatively flat compared to the surrounding terrain. Bigelow Lawn is entirely composed of alpine tundra land

cover, which is a rock-covered landscape lacking trees or any vegetation more substantial than grass and lichen. Due to the flat pitch and lack of substantial snow-holding vegetation, once snow fills in the gaps between the rocks, any additional snow accumulation will likely be transported during high winds. This results in wind slabs on downwind or lee eastern aspect steep slopes namely those within Tuckerman Ravine and Boott Spur Gullies.

2.2 Tuckerman Ravine

Tuckerman Ravine is a glacial cirque located 0.8 km southeast of Mount Washington's summit (Figure 2). The ravine is 0.18 km² in spatial extent with elevations ranging from 1,327 to 1,629 m above sea level. The land cover in the lower reaches of Tuckerman Ravine consists of large boulders with dense krummholz (i.e., deformed vegetation from continuous exposure to freezing winds). The upper sections are confined by rock buttresses, small alpine shrubbery, and grassland.

It is not uncommon to have 12 to 16 m of snow in the lower reaches of Tuckerman Ravine (Allen, 2000). Much of the snow within the ravine is transported from neighboring terrain by strong westerly winds. This study site was selected for its accessibility, range of orographic features, history of avalanche activity, and United States Forest Service (USFS) Snow Ranger presence. Figure 4-A shows a photograph of the ravine in the winter.

Tuckerman Ravine has many features; Figure 5 identifies areas of interest (AOIs) that will be used for subsequent analysis. Left Gully is the southernmost rock confined gully in Tuckerman Ravine. The Chute is just north of Left Gully. It is also rock confined with a distinct hourglass shape. Left Gully and Chute have similar snow accumulation patterns due to their similar aspect and geological formation. The Headwall area is the steepest (40-55°) section of Tuckerman Ravine. Many cliffs with icefall are present in this region. An area coined Scour Area is located at

the highest elevations of Tuckerman Ravine and is subject to extreme ridgeline wind speeds that scour most of the snow into the lower areas in the Ravine. Chicken Rock Gully is a small area east of the Headwall which fills in with the greatest snow depth of the entire study area. Snow-off survey of this region reveals a dihedral cliff formation which is when two cliffs join near a right angle. This area also has a waterfall running through the joining point of the cliffs. The east-facing terrain feature provides a sheltering effect from predominant western winds and blowing snow which leads to extreme accumulation of snow below the cliffs. The Ravine Floor is a nearly flat vegetated area that is filled in with avalanche debris from avalanche paths above. The Lunch Rocks area is composed of large car-sized boulders that are rarely snow-covered.

In each of the seven AOIs, a single point location was selected with the goal to capture specific evolution patterns that occur in exact locations within the AOIs. The point in Left Gully is about halfway up the gully where the deepest drifts reside. Chute's point is located just below the main constriction in the gully. The Scour Area AOI's point is at the southern end of the AOI near Chute. The point for the Headwall region is in the northern third of the AOI and is where deep wind slabs typically form. The Chicken Rock Gully point is about where the Ravine's deepest drifts form. The sample point in the Lunch Rocks AOI is on a boulder that does not get fully snow-covered. Finally, the Ravine Floor's point is near the eastern edge of the AOI and is representative of the Ravine's main avalanche runout path.

Access to Tuckerman Ravine involves a 4.43 km (2.75 mi) hike up the Tuckerman Ravine Trail which begins at the Appalachian Mountain Club's Pinkham Notch Visitor Center in Gorham, New Hampshire (44.2575° N, -71.2529° W, 619 m ASL). This section of trail ascends 692.5 m of elevation.

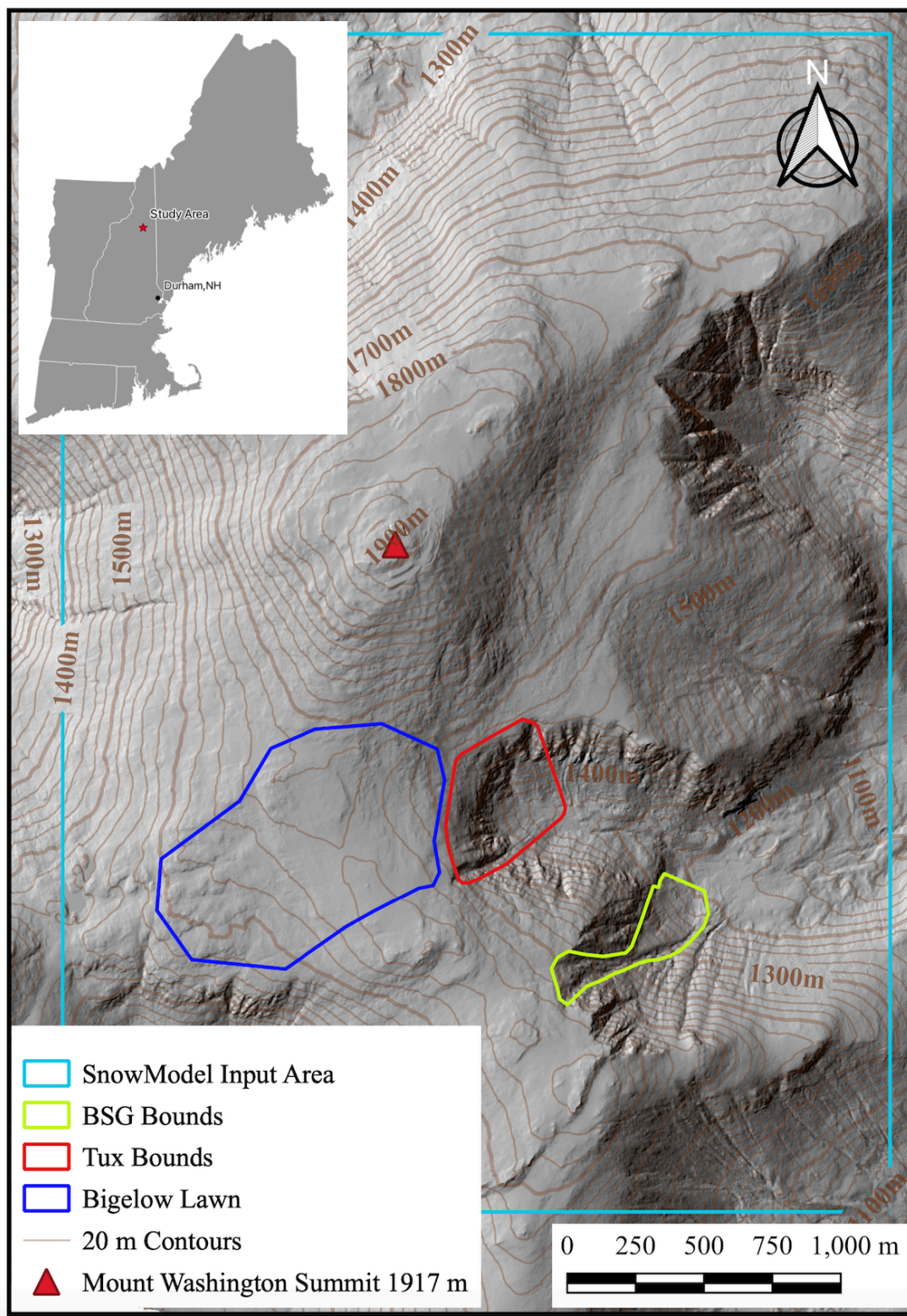


Figure 2: Overview of Study Area with Boott Spur Gullies (BSG), Tuckerman Ravine (Tux), Bigelow Lawn, and SnowModel Input Area show. Mount Washington Summit is Located at Elevation 1917 m in the Center of the Map.

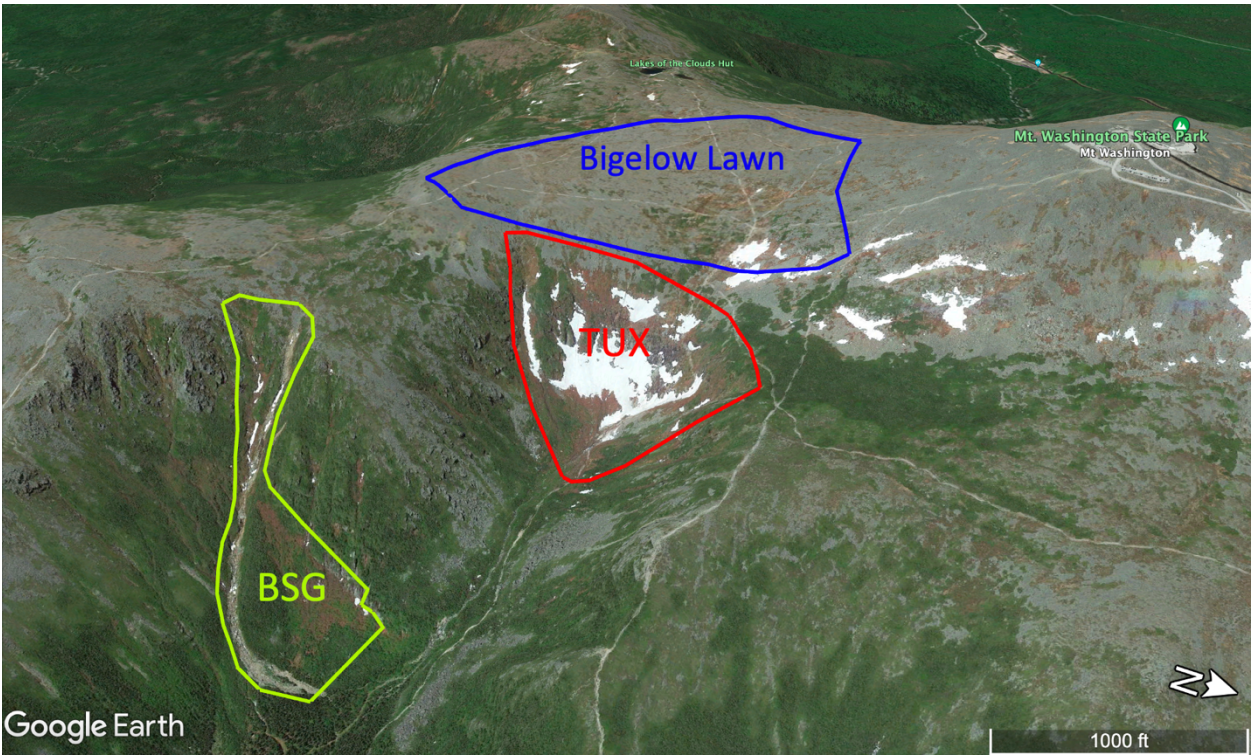


Figure 3: Study Area Map with Bigelow Lawn, Boott Spur Gullies (BSG), and Tuckerman Ravine (TUX) Delineated

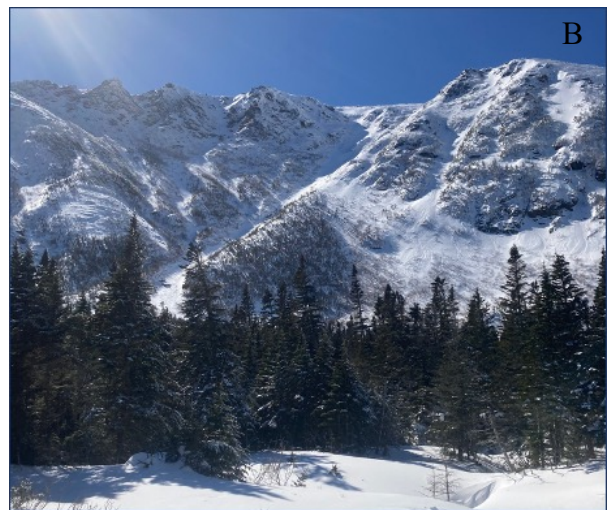
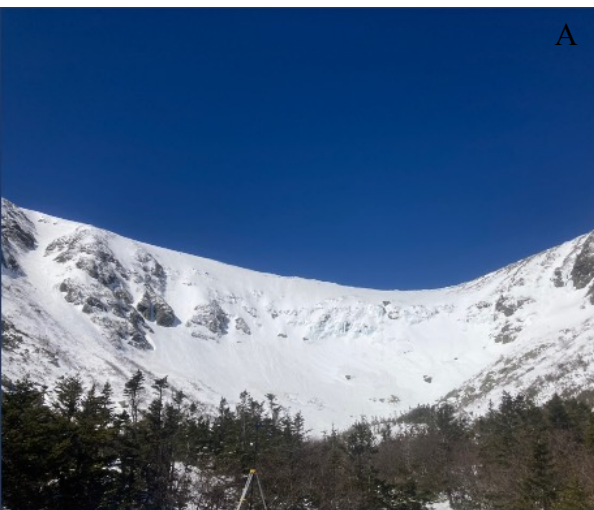


Figure 4: Photographs of Tuckerman Ravine (Tux) (A) and Boott Spur Gullies (BSG) (B) Study Areas Credit: Cameron Wagner

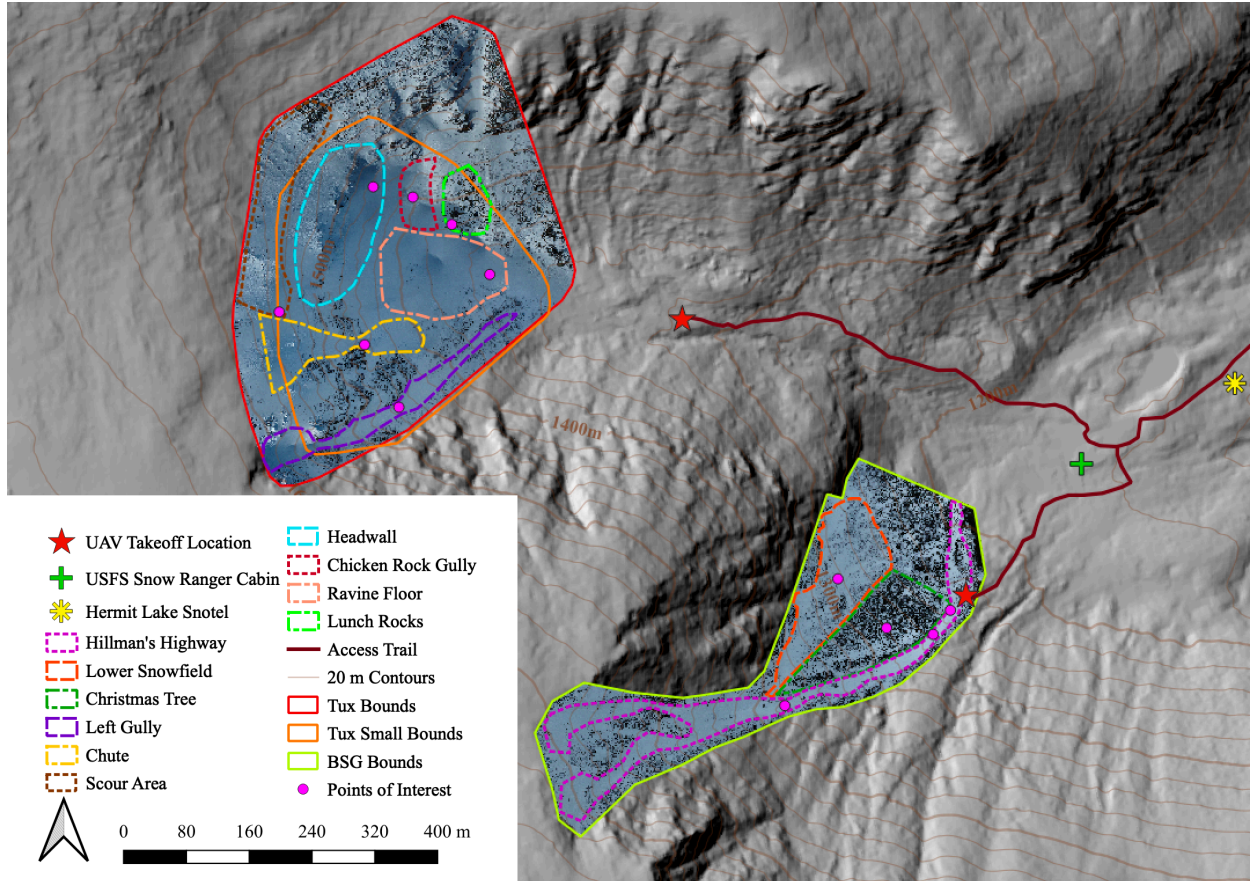


Figure 5: Areas of Interest Within the Tuckerman Ravine and BSG Study Areas, the Two UAV Launch Locations, and other Referenced Features

2.3 Boott Spur Gullies

The Boott Spur Gullies (BSG) study area is 0.4 km east-southeast of Tuckerman Ravine. The BSG site is 0.13 km² in extent, encompassing the popular backcountry ski descent Hillman's Highway and Lower Snowfield. Northeast aspect slopes are the dominant aspect in BSG, with the upper section of the Hillman's Highway gully facing east. The elevation in BSG ranges from 1,195 to 1,605 m above sea level. The land cover in the lower reaches of BSG consists of numerous large boulders, while the upper sections of BSG are confined by rock buttresses and have a smoother,

shale surface. The Lower Snowfield land cover is defined as low-height hardwood shrubbery vegetation with a mix of coniferous alpine shrubbery. An area called the Christmas Tree separates Hillman's Highway and the Lower Snowfield. This region is distinguishable by its triangular shape and coniferous vegetation that remains visible throughout the winter. Figure 5 delineates these areas for reference. Five points were selected across the BSG study area for analysis. The first point in the center of the Lower Snowfield is located in an area that becomes snow-covered early in the accumulation season. The next point is in the Christmas Tree AOI and is specifically located on a dense patch of coniferous vegetation that is never snow-covered. The last three points are within Hillman's Highway. Hillman's Highway 1 (HH1) is in the lower part of the gully adjacent to the UAV take-off location. Hillman's Highway 2 (HH2) is upslope of HH1 among large boulders and where a streambed blowout (i.e., isolated full snowpack depth ablation) occurs. Finally, Hillman's Highway 3 (HH3) is located in the center of the gully next to the apex of the Christmas Tree.

BSG typically has less snow transported from the Bigelow Lawn as compared to Tuckerman Ravine. This is due to a large Northeast ridge that separates the two study areas. This land formation blocks the Lower Snowfield and Hillman's Highway from westerly winds that transport snow from Bigelow Lawn. Figure 4-B illustrates this shadowing effect with the large ridge shown on the right side of the image. In contrast, Tuckerman Ravine is directly east and downwind of Bigelow Lawn.

Access to BSG involves a 4.02 km (2.5 mi) hike up the Tuckerman Ravine Trail which begins at the Appalachian Mountain Club's Pinkham Notch Visitor Center in Gorham, New Hampshire (44.2575° N, -71.2529° W, 619 m ASL). Upon taking a left turn at the USFS Snow Ranger Cabin shown on Figure 5, begin up the John Sherburne Ski Trail for 161 m and bear left to join the

Hillman's Highway Access trail. Follow this trail for another 193 m until the study area is reached.

A total of 604 m in elevation gain occurs when accessing the BSG study area from Pinkham Notch.

3 CHAPTER 3 – METHODS

3.1 UAV Data Acquisition

This study was designed to measure the spatial depth and extent of wind-transported snow in Mount Washington avalanche terrain. To achieve this, Real-time Kinematic (RTK) UAV flights were carried out with consistent base station locations to create 5 cm resolution Structure from Motion (SfM) Digital Surface Models (DSMs). RTK connection to a local base station or Continuously Operating Reference Stations (CORS) station is a recent advancement in GNSS technology that allows for up to 1 cm UAV positioning and subsequent geotagged images. With an RTK connection established, 1 to 3 cm horizontal and vertical GPS errors can be achieved (Stempfhuber & Buchholz, 2012). Following data collection, the images are stitched together using the scale-invariant feature transform (SIFT) (Lowe, 1999) by matching prominent points between images (i.e., tie points). SIFT is integral when there are large variations in scale and perspective throughout image capturing. This is especially important in steep study areas such as those present in this research because of the rapidly changing elevation of camera location and surface. These points make up the sparse point cloud which is then filled in using multiview stereo matching (MVS) to create the dense point cloud. The dense point cloud is a 3D reconstruction of the terrain colorized with values from the photos. Conversion from dense cloud to DEM results in a 2D raster file with each pixel value corresponding to that position's elevation. Typically, ground classification is needed to generate a DEM from the DSM. In this study, this process is unnecessary because the snow surface is the measurement of interest. Another useful SfM output is the orthophoto. This output is a large optical photograph of the survey area created from the

combination of individual photographs throughout the flight. The resolution of the orthophoto typically matches the individual photographs which leads to very high resolution-to-area ratios.

3.1.1 Base Station Positioning

Monument points were established to provide a known coordinate for the UAV's RTK base station, which is used in fixed point mode. Fixed point mode eliminates base station positional errors between flights. Without a monument and being set to fixed point mode, base stations need to establish coordinates prior to UAV connection. Offset between base station coordinates is presented when the base station needs to survey its current point. In this case, every subsequent data collection event will have a slightly different base station coordinate, resulting in an increased error. By uploading a consistent point for the base station transmission, georeferencing is not necessary to align subsequent models.

Figure 6 shows the base station and monument point locations for each study area. These sites were selected for their sufficient vantage points throughout the entire duration of the flight. They are also far enough away from avalanche risk to be considered safe. The point selected for Tuckerman Ravine is on top of a first aid cache, Connection Cache, which stands about 1.5 m above the ground. The point selected for Boott Spur Gullies (BSG) is on a large boulder that remains exposed above the snowpack throughout the entire snow season.

On October 17th, 2021, the monument points were created using a chisel and marked with a small dot of green spray paint in the Tuckerman Ravine and BSG study locations. The coordinates of these monument points were measured using a custom RTK GPS device with 1 cm positional accuracy. This device uses the Sparkfun ZED-F9P chip on the UBlox C099 application board. Base and rover modules are linked using a serial radio. The custom RTK base station was set nearby to survey-in mode and remained stationary for 30 minutes to gather a precise location before sending RTK data to the rover. Next, the rover was placed at each of the two monument points and used to collect their location. The Tuckerman Ravine base station location is (44.2612° N, -71.2933° W, 1290.2 m ASL) and BSG's is (44.2581° N, -71.2886° W, 1203.3 m ASL).



Figure 6: DJI D-RTK2 Base Station Set up for Tuckerman Ravine (A) and BSG (B) Surveys

3.1.2 UAV Flight Planning and Hardware Specifications

The UAV platform used for every flight was the DJI Phantom 4 RTK Edition with DJI Remote and D-RTK2 Base Station. This UAV is outfitted with a 1" CMOS 20MP optical RGB camera with an 84° field of view (Phantom 4 RTK - product information - DJI). The flight plans were made with the terrain following feature enabled. The 30 m spatial resolution Shuttle Radar Topography Mission (SRTM) data (Farr et al., 2007) was uploaded to the flight planning software to provide the terrain baseline to ensure the flight remained within the 120 m (400 ft) above the ground level ceiling set by FAA regulations found in Title 14 CFR 107.51(b).

Two flight passes for each study area were conducted using a double-grid flight plan. The Tuckerman Ravine flight plan had an altitude of 45 m above ground level (AGL) and a speed of 5.3 m/s. In total, 700 photos were taken in timed shooting mode per direction on each flight. The BSG flight plan was set to an altitude of 35 m AGL, and a speed of 4.1 m/s. In total, 350 photos were taken in timed shooting mode per direction on each flight. A 70% frontal and 70% side overlap were selected for both study areas. This relatively high overlap gives the tie point finding algorithm an improved ability to cross-reference between photos and, therefore, a more robust set of tie points. An off nadir gimble angle of 80° was selected to provide greater perspective in every frame. A greater perspective aids in the tie point-finding process and thus leads to greater accuracy in the SfM outputs.

UAV flight lines were created within the DJI proprietary flight planning software application. These lines were uploaded to the UAV which then autonomously flies along these lines taking overlapping photos at a set image overlap. Figure 7 shows the flight lines used for data collection. Photos are geotagged by the UAV's onboard GNSS (global navigational satellite system) unit.

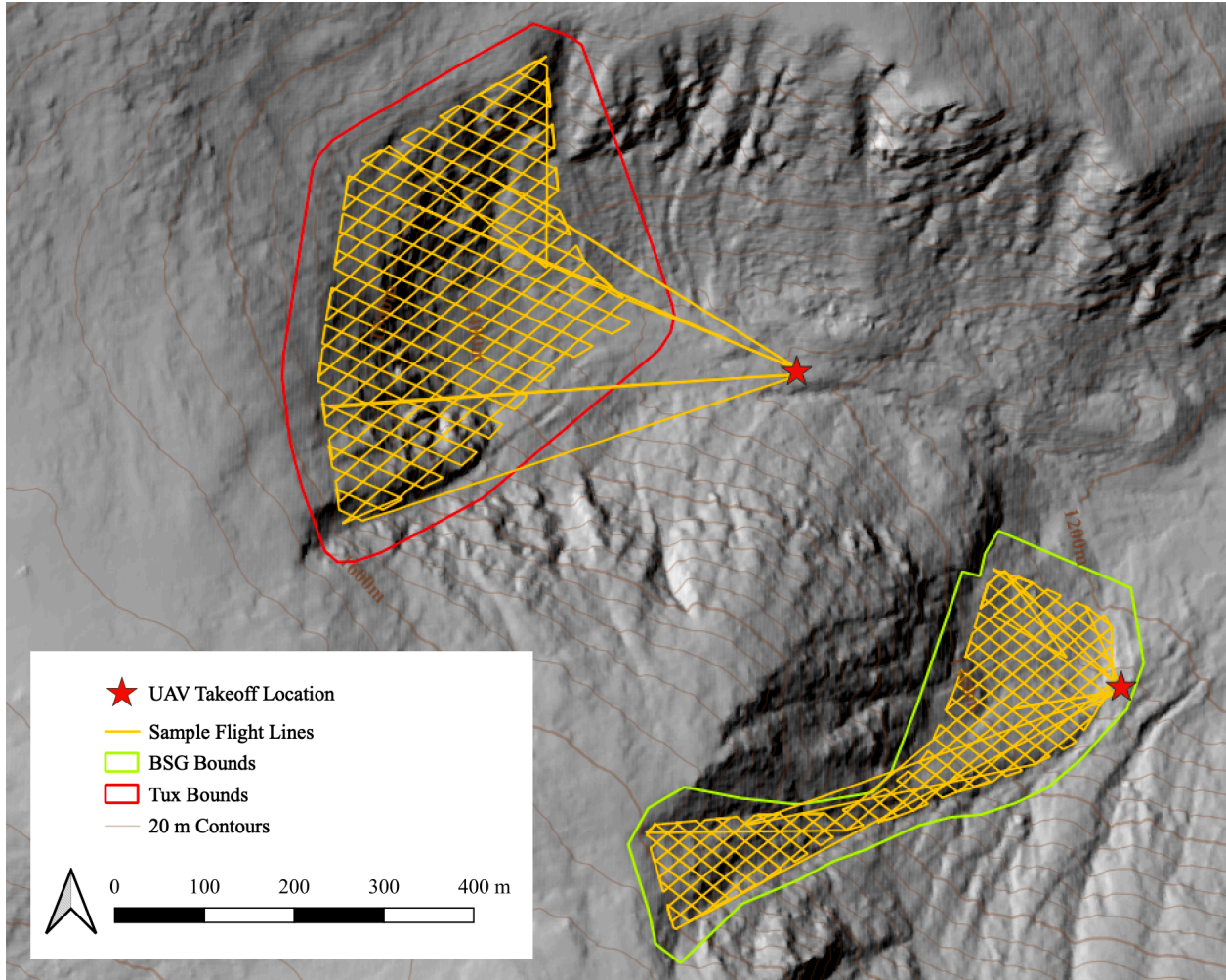


Figure 7: Study Area Map Showing Sample Flight Lines in Tuckerman Ravine (Tux) and Boott Spur Gullies (BSG)

3.1.3 UAV Flight Procedure

The same field procedure was followed for all campaigns. Upon arriving at the study area, the RTK base station was situated directly above the respective study area's monument. Next, the UAV's propellers were attached, and the UAV was set up on a flat area of the ground. Both the controller and UAV were powered on and the corresponding flight plan was opened. After linking the UAV to the RTK base station, the associated GNSS coordinate was uploaded to the base station. Once a successful RTK connection was established, there was a "ready to fly" message on

the controller, the flight plan was initiated. The UAV then took off and headed to the first waypoint. Throughout the flight, errors were checked, and if one presented itself that would prevent effective data collection, the flight was canceled. An example of an error worthy of canceling a flight would be the ‘RTK disconnected’ error. Constant RTK connection was vital to keep GPS error low. A ‘wind speed too high’ warning was presented often but did not compromise the flight. The battery cell error occurred when batteries were not kept sufficiently warm prior to swapping between flights. This was easily remedied by warming up the successive battery with body heat and blowing warm breath on the battery before swapping.

The UAV was programmed to return to the home point when the battery percentage dropped below a threshold value determined by the distance of the UAV from the home point. Typically, this threshold was between 20 and 30%. The UAV would return home but was landed manually. Hot swapping (i.e., the quick change of batteries) is done to ensure a quick turnaround time. This process turns off the UAV, swaps batteries with a fresh one, and then turns the UAV back on. To continue, the in-progress flight plan would be loaded, and data collection would resume based on where the UAV left off. For the Tuckerman Ravine study area on a day with minimal (e.g., 0 to 6.7 m/s) wind, four to five batteries were sufficient to complete the flight plan but could require up to eight batteries with moderate (e.g., 6.7 m/s to 13.4 m/s) wind. For most data collection campaigns, ten batteries were available. This process was repeated at the BSG study area with the BSG monument coordinates and flight plan. BSG has a smaller flight plan and is typically better sheltered from wind than Tuckerman Ravine. To complete the flight plan, days with minimal wind would use three to four batteries but could require up to six batteries with moderate wind.

3.2 Post-Processing and Digital Surface Model Creation

3.2.1 Structure from Motion Workflow

A Structure from Motion (SfM) workflow was used to create snow depth products. The US Army Corps of Engineers ERDC CRREL provided the use of their Amazon Web Service (AWS) cloud-based Open Drone Map (ODM) SfM workflow for this project. Photos gathered from the campaign were uploaded via the Cyberduck application to the AWS bucket in a respectively dated folder. A settings file (Appendix C) with SfM parameters, (e.g., processing quality and expected outputs) was also uploaded. Ultra-high processing quality was used for this project. Outputs from the processing include the orthophoto in a variety of image file formats, and digital surface and terrain models (DSM, DTM respectively) in .tiff file format. A process initiation file was uploaded following the successful upload of all photos and settings files. Typically, the Tux study area took about five hours and BSG took about three hours to process. The results are SfM outputs and a processing report which summarizes processing and errors (Appendix C). This report was used to decide if there was an acceptable GPS error. The orthophotos and DSMs for each study site were downloaded and imported to Quantum Geographical Information System (QGIS). All further analysis is carried out in QGIS.

3.2.2 Snow Depth Calculation

Total snow depth and snow depth change were calculated using the DSM rasters. For total snow depth, the baseline DSM collected on October 29th was subtracted from the current day snow-on DSM. The difference between the two is the total snow depth for that date. To find snow depth change, the difference between the most recent DSM and the previous DSM was calculated. This

change in snow depth resulted in positive and negative values indicating the snow loading and scouring, respectively.

3.3 Snow Depth SfM Campaigns and Manual Validation

Table 1 displays sampling campaigns of the 2021-2022 winter as well as SfM processing GPS errors. A total of 16 campaigns were completed with 14 in Tuckerman Ravine and 12 in BSG. The average GPS errors were 0.07 and 0.03 m in Tuckerman Ravine and BSG respectively, with an average error across both study areas of 0.05 m. Errors greater than 0.1 m occurred in five out of the twenty-six SfM processes. The greatest error (0.15 m) occurred from BSG on 1/4/22. Section 4.2 explains possible sources of error between manual sample dates.

A limited manual probing snow depth validation was conducted during the 12/15/21 and 2/01/22 campaigns. In-situ snow depths were collected using a 280 cm avalanche probe with 10 cm graduations and recorded with the CalTopo (CalTopo, 2019) mapping app on an Apple iPhone SE 2nd generation cell phone equipped with GPS/ GLONASS positioning. Snow depths were recorded when the probe reached the ground surface to capture the entire snowpack depth. The probe angle was angled as close to vertical as possible. A total of 20 probe measurements were collected: 11 on 12/15/21 in Tuckerman Ravine and nine on 2/01/22 with six in Tuckerman Ravine and three in BSG. All the measured points in Tuckerman Ravine were gathered on the floor of the ravine, lower reaches of the Chute, and Chicken Rock Gully. The BSG measured points were in Hillman's Highway below the top of the Christmas Tree. The exact location of these points can be seen in Appendix B.

Table 1: Summary of the Winter 2021-2022 UAV Flights with SfM GPS Errors

Survey Date	Tuckerman Ravine (Tux)	Boott Spur Gullies (BSG)	Surface Condition	MWOBS Cumulative Snow Depth (cm)	Manual Probing	Tux GPS Error (m)	BSG GPS Error (m)
Total	14	12			2		
10/29/21	X	X	Baseline	0		0.03	0.02
11/20/21	X	X	Snow-On	74.7		0.03	0.03
12/15/21	X		Snow-On	172.0	X	0.03	
1/4/22		X	Snow-On	214.9			0.15
1/8/22	X		Snow-On	232.4		0.02	
1/21/22	X	X	Snow-On	283.7		0.06	0.02
2/1/22	X	X	Snow-On	310.6	X	0.09	0.02
2/11/22		X	Snow-On	349.0			0.02
2/24/22	X	X	Snow-On	357.6		0.03	0.02
2/26/22	X	X	Snow-On	377.2		0.13	0.02
3/9/22	X	X	Snow-On	430.8		0.03	0.03
3/23/22	X	X	Snow-On	479.3		0.13	0.02
3/30/22	X	X	Snow-On	500.4		0.02	0.03
4/5/22	X		Snow-On	517.4		0.08	
4/18/22	X	X	Snow-On	570.2		0.11	0.02
4/25/22	X		Snow-On	587.5		0.14	
Average						0.07	0.03

3.4 SnowModel Processing

3.4.1 SnowModel Overview

SnowModel is a physics-based snow-evolution model capable of producing a time series of snow depth maps for a given study area. SnowModel has four sub-models. Micro-Met defines the meteorological forcing conditions. EnBal conducts surface energy exchanges. SnowPack calculates the snow depth and water-equivalent evolution over time. SnowTran-3D redistributes snow due to wind. The model is designed to run on sub-grid resolutions of 1 to 200 m and temporal

resolutions of 1 hour to 1 day (Glen E. Liston & Kelly Elder, 2006). SnowModel was selected for this research due to its robust documentation, active development, and incorporation of SnowTran-3D (Liston & Sturm, 1998) a proven snow redistribution model.

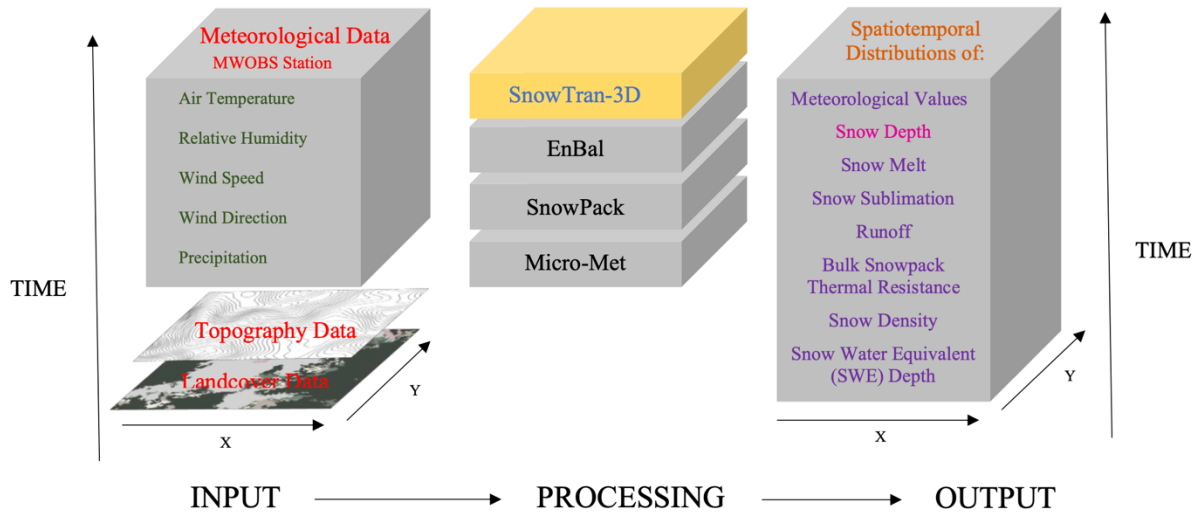


Figure 8: SnowModel Process Visualization in Context of this Study

SnowModel requires three inputs: (1) spatially distributed topography, (2) land cover raster data, and (3) a time series of air temperature, precipitation, wind speed and direction, and relative humidity. Using these inputs, SnowModel estimates snow accumulation, redistribution, sublimation, density evolution, ripening, melt, refreezing of meltwater, and runoff for each timestep. Figure 8 shows the workflow of SnowModel including inputs, processing layers, and outputs. The SnowTran-3D sub-model and snow depth output are highlighted to stress their influence and importance to this study. Interaction with the canopy such as snow interception and snow holding depth is estimated by the land cover.

SnowTran-3D is the component of SnowModel that applies wind-induced transport properties. The five main snow transport and redistribution mechanisms represented in the

SnowTran-3D sub-model shown in Figure 9 are (1) the wind-flow forcing field, (2) the wind-shear stress on the surface, (3) the transport of snow by saltation and turbulent suspension (the dominant wind-transport modes), (4) the sublimation of saltating and suspended snow and (5) the accumulation and erosion of snow at the snow surface (Liston et al., 2007).

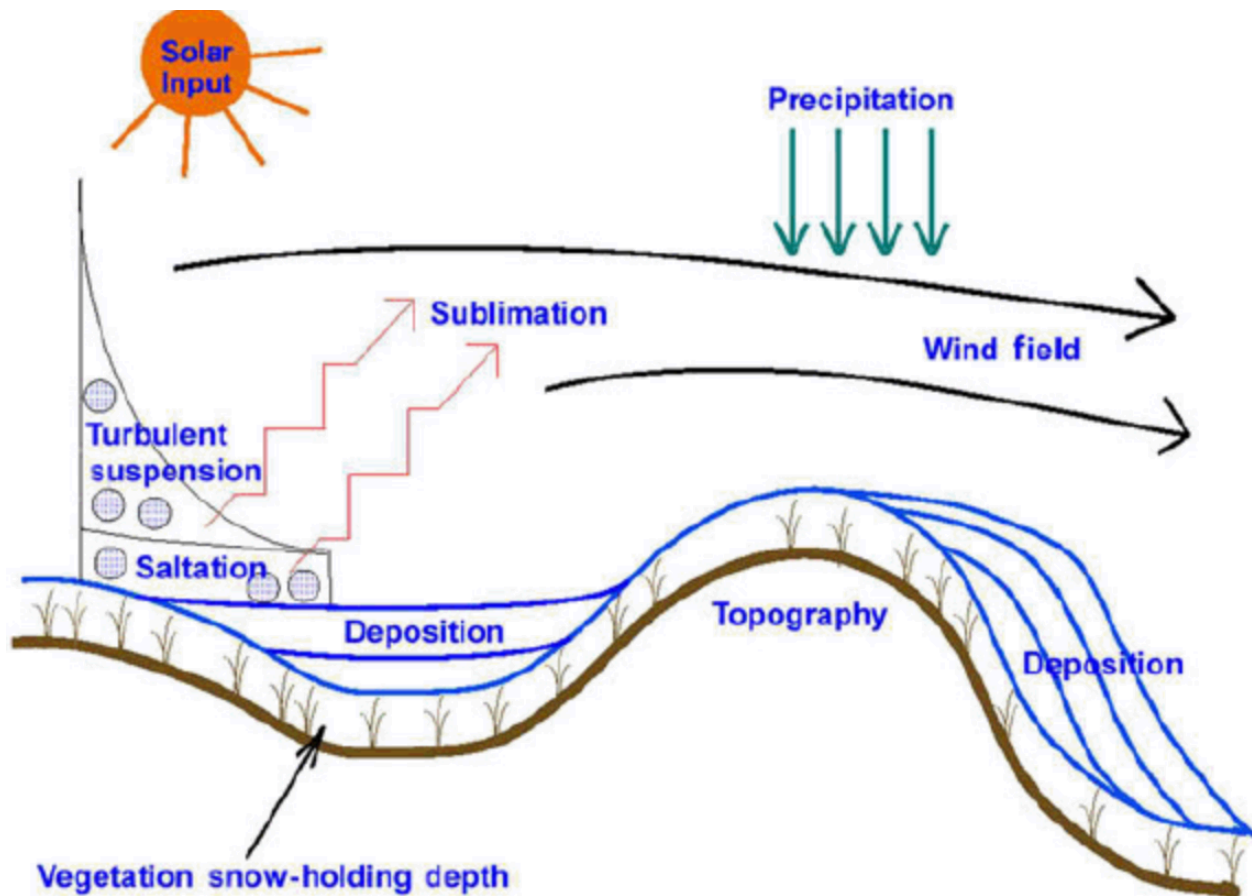


Figure 9: SnowModel Component SnoTran-3D Transport Processes. Source: (Liston et al., 2007)

3.4.2 SnowModel Processing Workflow

For this study, topography data was NHGRANIT's 1 ft aerial LiDAR dataset. This dataset was resampled to 1 m within QGIS. The 2015 North American Land Change Monitoring System (NALCMS) land cover dataset (Commission for Environmental Cooperation. "2015 Land Cover of North America at 30 Meters", North American Land Change Monitoring System, Ed. 2.0. 2020.) (Appendix H) was embedded into SnowModel and processed within QGIS to match the topography data's 1 m grid cells using the align raster tool. The input parameter file was updated with the study area coordinates, coordinate reference system, and grid cell resolution (e.g., 3028 by 4310) (Appendix E). The land cover and topography data were clipped to the bounding box and previously specified resolution of 1 m. The MWOBS meteorological station data was uploaded to Micro-Met, a spatially distributed meteorological downscaling algorithm. All the inputs were used to produce a snowmodel.par file which contained the model parameters. The basic inputs for this file were the simulation start date and time (e.g., 10/28/21, at 12:00) and time step (e.g., daily). Processing time for the 10/28/21 to 4/25/22 time period using a 1 by 1 m grid is seven hours. The main parameters for characterizing snow drifts are the blowing snow flux parameter and the Tabler slope adjustment scaling factor. The blowing snow flux parameter was the predominant wind direction. Although the input file provides wind speed and direction, this value overrides direction values with one static value. The Tabler slope adjustment scaling factor adjusts how the snow gets deposited on varying slope steepness. Figure 10 shows snow distribution changes with Tabler slope value. The blowing snow flux parameter chosen for the model run analyzed in this research was 140°. The Tabler slope adjustment scaling factor chosen was 2.1 (Appendix F). SnowModel computes all desired variables for the domain by the specified time step.

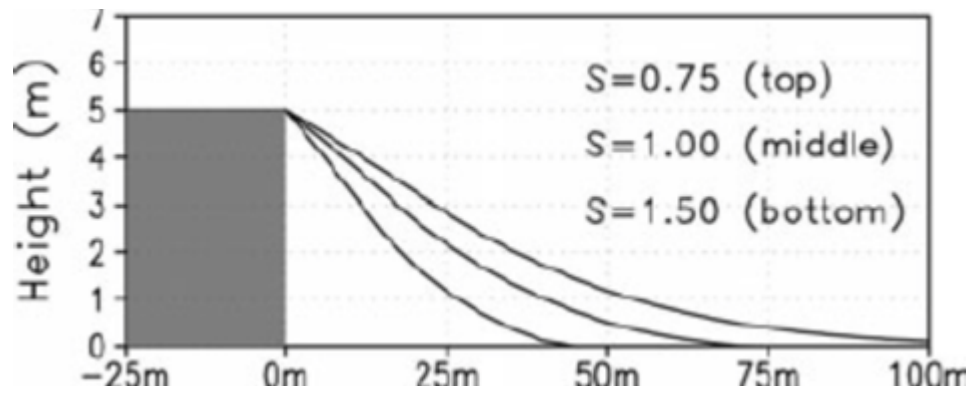


Figure 10: Tabler Slope Adjustment Scaling Factor (S) Particle Distribution Credit: (Liston et al., 2007)

4 CHAPTER 4 – RESULTS

4.1 Winter 2021-2022 Summary

Winter on Mount Washington typically begins with snowfall at the end of October and continues until late April and May when melt begins dominating. The 2021-2022 winter snowfall from 10/29/21 to 4/25/22 was 587.5 cm (Figure 12). Although an additional 40.4 cm of snow fell after 4/25/22, the winter total was 87.9 cm less than the Mount Washington annual average of 715.8 cm. Snowstorms occurred regularly during the winter starting on 11/2/21. The first snowfall during the 2021-2022 winter occurred from 11/2/21 to 11/3/21 with a 4.6 cm snow total. The maximum daily snowfall was 28.7 cm on 1/17/22. Mount Washington's historic average temperature from November to April is -10.29 °C. The 2021-2022 winter's November to April average temperature was -10.31 °C, matching the historic average value. Although the average temperature was well below freezing, the 2021-2022 winter had 24 days above freezing. Some of these days also had rain. This high number of above-freezing days led to many rain-on-snow and mid-winter ablation events. A rain-on-snow event occurred on 2/17/22 and 2/18/22 with a total of 17.8 mm (0.7 in) of rain. Over the winter, the daily average wind speed was 22.5 m/s and higher than 10 m/s 96% of the winter. The windiest day occurred on 12/12/21 with an average wind speed of 40.08 m/s. The wind rose shows that westerly winds prevail on Mount Washington (Figure 11). Southeastern winds were less common and were typically associated with a lower magnitude of speed.

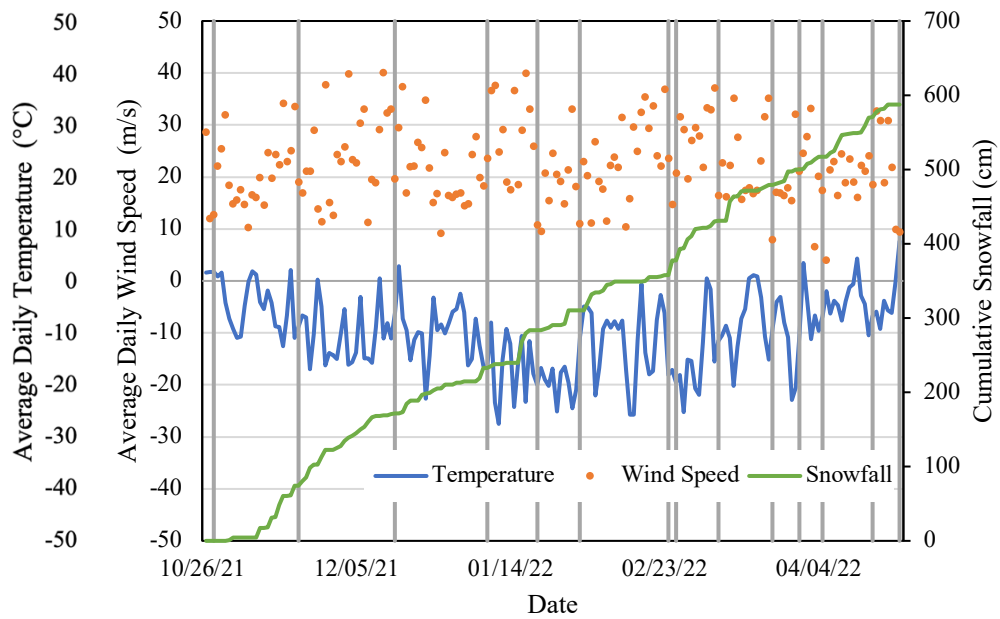


Figure 12: 10/29/21 to 4/30/22 Average Daily Wind Speed, Temperature, and Cumulative Snowfall at the MWOBS. Grey Vertical Lines Signify Days when a Tuckerman Ravine UAV Survey was Conducted.

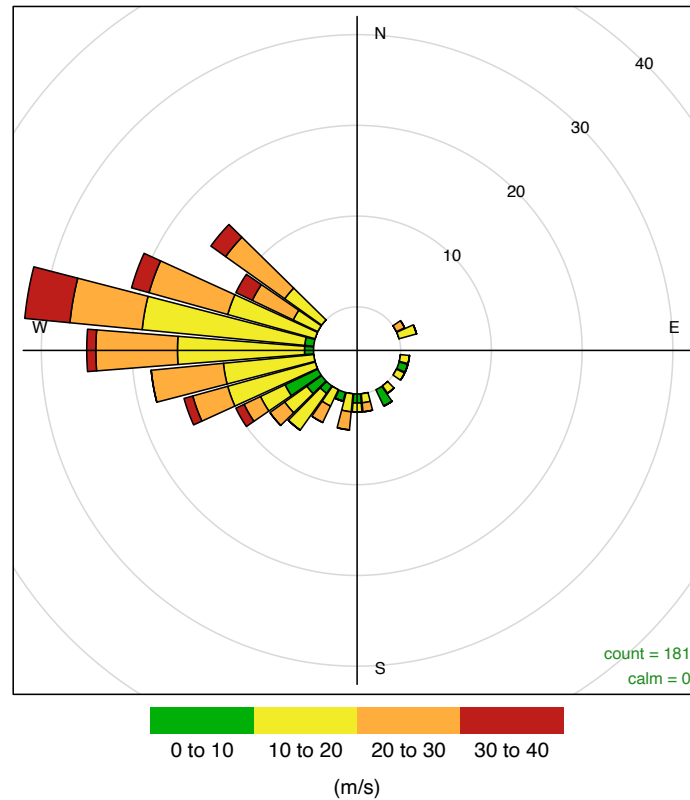


Figure 11: 10/28/21 to 4/25/22 Wind Rose at the MWOBS

4.2 SfM Snow Depth Validation

The SfM snow depth values were compared to 20 snow depth validation measurements (Figure 13). The average and standard deviation SfM snow depth data were determined using all 5 cm pixels within a 3 m buffer of each manual probe location. The linear trendline has a slope of 1.04, a y-intercept of -11.59 cm, and an R^2 value of 0.51 indicating a bias, but reasonable agreement. The average snow depth measured by the avalanche probe, 104.6 cm, was deeper than the SfM, 97.6 cm with a difference of 7 cm. Only 35% of the SfM snow depth measurements are deeper than their respective avalanche probe snow depth measurement. Most of these measurements occurred on 2/01/22. The root mean square error (RMSE) values for the 12/15/21 Tuckerman Ravine, 2/01/22 BSG, and 2/01/22 Tuckerman Ravine sampling events are 61.8 cm, 29.1 cm, and 26.5 cm, respectively. The February in-situ observations agreed much better with SfM values than the December in-situ observations. This is likely due to increased vegetation compaction later in the winter which limited over-probing. While not a comprehensive measurement of error due to the small number of measurements and the limited distribution across the entire study site, the results indicate that SfM can quantify the magnitude of in-situ snow depth within approximately 30 to 60 cm.

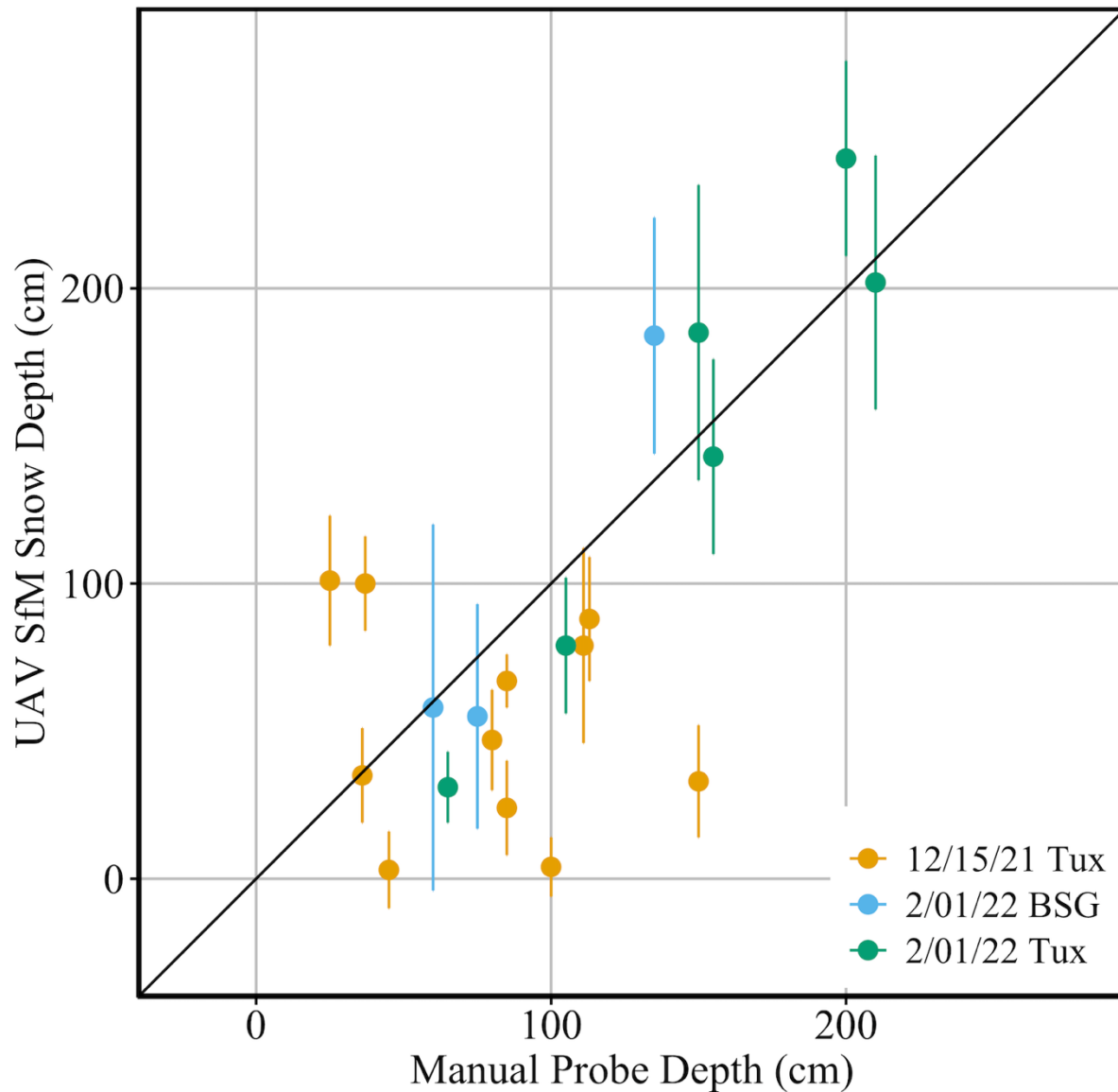


Figure 13: Comparison of UAV SfM Snow Depth to Avalanche Probe Snow Depth by Date and Location e.g., Tuckerman Ravine (Tux) and Boott Spur Gullies (BSG). Vertical Lines are \pm One Standard Deviation of the Three m Buffer Area SfM Snow Depth Values About Each Manual Probe Location.

4.3 UAV SfM Snow Depth

This section explores the 2021-2022 winter snow accumulation in Tuckerman Ravine and BSG study areas as mapped using UAV SfM. There were 13 and 11 campaigns in Tuckerman Ravine and BSG, respectively. Although this was a lower-than-average snow year, the snowfall was steady throughout the winter. The maximum snow depth in Tuckerman Ravine occurred on 4/25/22 and had an average depth of 2.50 m. In BSG, the maximum snow depth occurred on 3/30/22, with a much lower average depth of 0.90 m. Generally, gullies accumulated more snow than open, rocky, or heavily vegetated areas.

4.3.1 Tuckerman Ravine

The snow depth across the Tuckerman Ravine study area had large variability in space and time (Figure 14). That variability increased as the total snow depth increased. Gullies such as Left Gully, Chute, and Chicken Rock Gully consistently had deep snowpacks throughout the season. Isolated areas of deep snow accumulation are also visible within the Headwall area in Figure 14. These relatively small areas are situated in the shadow of steep terrain features. The UAV SfM does an excellent job of mapping these features and their extreme accumulation patterns as well as the contrasting exposed, less sheltered regions. Examples of exposed areas that have limited total snow accumulation are the Lunch Rocks and the area separating Left Gully and Chute. The UAV SfM approach was also able to distinguish the distinct snow depth differences between gullies and scour areas. Both the snow depth patterns showing the deep snow in isolated areas and gullies are consistent in all snow depth maps.

The high degree of spatial variability of snow in Mount Washington avalanche terrain is clearly evident through the AOI to POI comparisons. Figure 15 shows that snow depth consistently

increases throughout the entire season in all AOIs and POIs except Lunch Rocks. The average snow depth in the Lunch Rocks area was less than 0.54 m throughout the entire winter. This contrasts with the deepest snow in the study area, which was observed in Chicken Rock Gully. Although only 30 m away from the Lunch Rocks, the snow depth in the Chicken Rock Gully AOI exceeded 6 m on 3/30/22 (Table 2). Some areas in this gully had local snow depths greater than 16 m (Table 3). The other gullies, Chute, Left Gully, and Headwall also had relatively deep snow with approximately 3.6 m of snow late in the season. In contrast to these steady increases found in most AOIs, the Scour Area rapidly increased in depth until January but then ceased to accumulate more snow. The SfM maps capture this area's accumulation and redistribution of snow to lower-elevation gullies and terrain from westerly winds. As shown in Figure 15, the Scour Area snow depth increased and decreased, as expected throughout the season.

Four POIs, Headwall, Chute, Left Gully, and Chicken Rock Gully, have depths that are consistently greater than the cumulative snowfall depth. This is likely due to wind deposition from the scour of snow in adjacent upwind areas such as the Bigelow Lawn. A differential of up to 10 m is present between area and point snow depth measurement in the case of Chicken Rock Gully. Close inspection of individual snow depth maps in Figure 14 shows a high level of depth variation within the named AOIs.

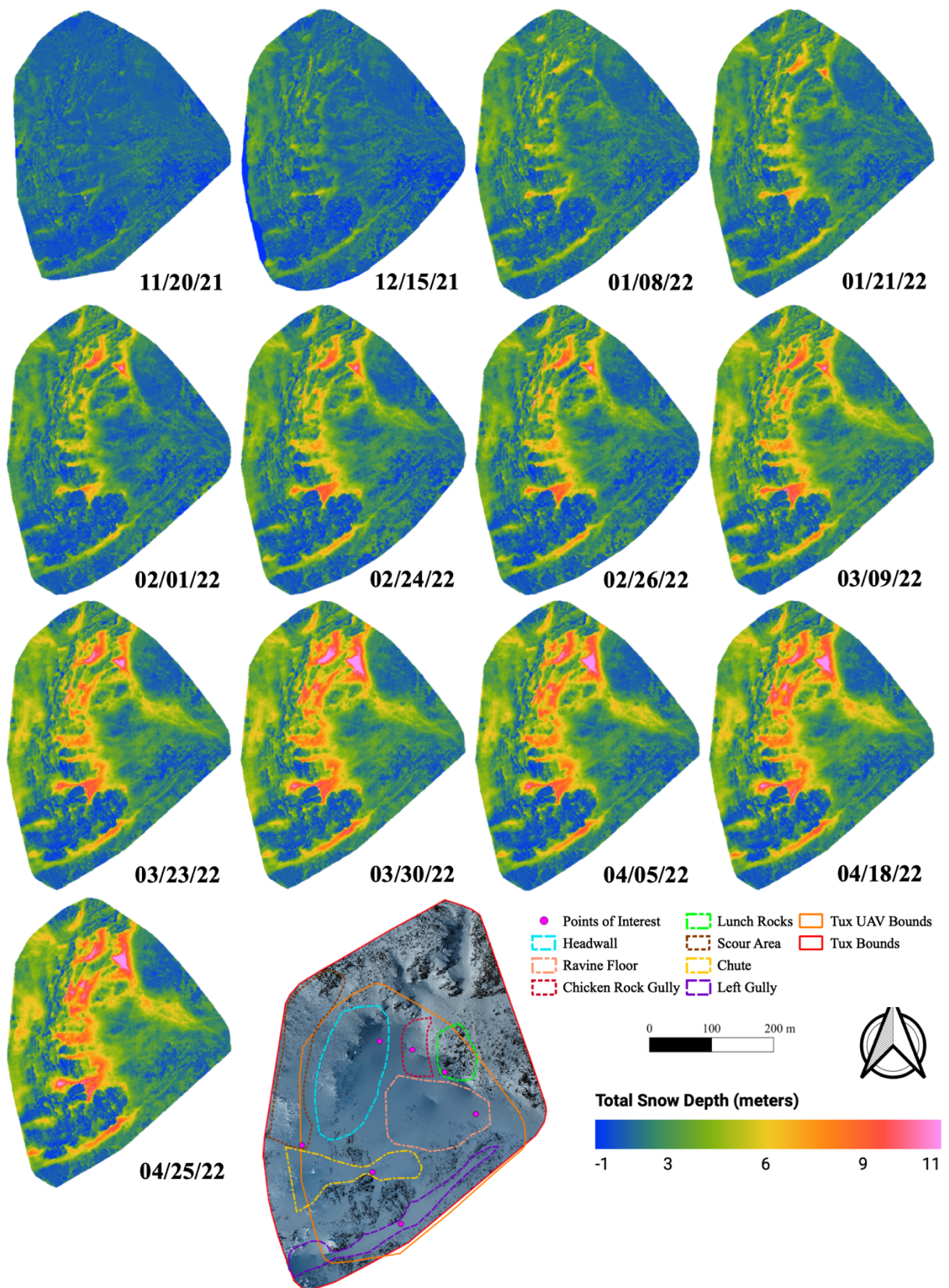


Figure 14: Tuckerman Ravine Snow Depth Time Series. Note Each Date's Extent is Based on the 10/29/21 Baseline Extent. AOI Map (Figure 5) Outlines Orange "Tux UAV Bounds" To Show Where Extents Above Reside with Areas of Interest and Points of Interest.

Table 2: Tuckerman Ravine (Tux) Average Snow Depth (m) for the Areas of Interest (AOI) by Date

Survey Date	MWOBS Cumulative Snowfall	Location							
		Chicken Rock Gully	Headwall	Lunch Rocks	Ravine Floor	Scour Area	Chute	Left Gully	Tux Avg
11/20/21	0.75	0.23	0.35	0.15	0.45	0.77	0.54	0.73	0.33
12/15/21	1.72	0.41	0.94	0.14	0.45	-0.37	0.48	1.06	0.45
1/8/22	2.32	0.97	1.67	0.33	0.85	2.10	1.62	1.52	1.06
1/21/22	2.84	1.94	1.83	0.34	0.92	2.89	1.86	1.71	1.48
2/1/22	3.11	2.92	1.97	0.30	0.86	1.97	1.80	1.62	1.24
2/24/22	3.58	3.43	2.28	0.25	1.52	2.28	2.62	2.15	1.56
2/26/22	3.77	3.47	2.32	0.28	1.48	2.12	2.56	2.12	1.54
3/9/22	4.31	3.92	2.92	0.54	1.95	3.00	3.25	2.47	2.08
3/23/22	4.79	4.53	3.12	0.31	1.97	2.98	3.29	2.48	2.10
3/30/22	5.00	6.63	3.50	0.44	2.17	3.12	3.58	2.91	2.44
4/5/22	5.17	6.31	3.30	0.25	2.14	2.90	3.32	2.57	2.21
4/18/22	5.70	6.21	3.58	0.29	2.49	2.89	3.51	2.81	2.40
4/25/22	5.88	6.37	3.60	0.28	2.53	3.09	3.66	3.01	2.50

Table 3: Tuckerman Ravine (Tux) Snow Depths (m) for the Points of Interest (POI) by Date

Survey Date	MWOBS Cumulative Snowfall	Location							
		Chicken Rock Gully	North Headwall	Lunch Rocks	Ravine Floor	Scour Area	Chute	Left Gully	Tux Avg
11/20/21	0.75	2.00	0.37	0.12	0.28	0.48	2.37	1.79	0.33
12/15/21	1.72	3.39	1.62	0.09	0.50	0.69	4.37	3.38	0.45
1/8/22	2.32	6.32	2.23	0.09	1.45	1.80	5.10	3.33	1.06
1/21/22	2.84	9.94	4.01	0.06	1.54	1.32	7.14	5.10	1.48
2/1/22	3.11	11.74	6.17	-0.05	1.42	1.54	7.25	5.37	1.24
2/24/22	3.58	12.00	7.12	0.02	1.93	1.66	9.07	6.34	1.56
2/26/22	3.77	12.16	7.31	0.02	2.60	2.07	8.78	6.27	1.54
3/9/22	4.31	12.33	7.42	0.22	3.64	2.51	9.16	6.43	2.08
3/23/22	4.79	13.86	8.05	0.02	3.65	2.55	9.52	6.63	2.10
3/30/22	5.00	16.03	10.47	0.17	3.59	2.67	9.45	8.41	2.44
4/5/22	5.17	16.09	7.76	0.06	4.65	2.52	8.89	7.64	2.21
4/18/22	5.70	16.11	7.46	0.05	4.91	2.28	8.84	7.48	2.40
4/25/22	5.88	16.11	7.99	-0.11	4.92	2.71	9.62	7.79	2.50

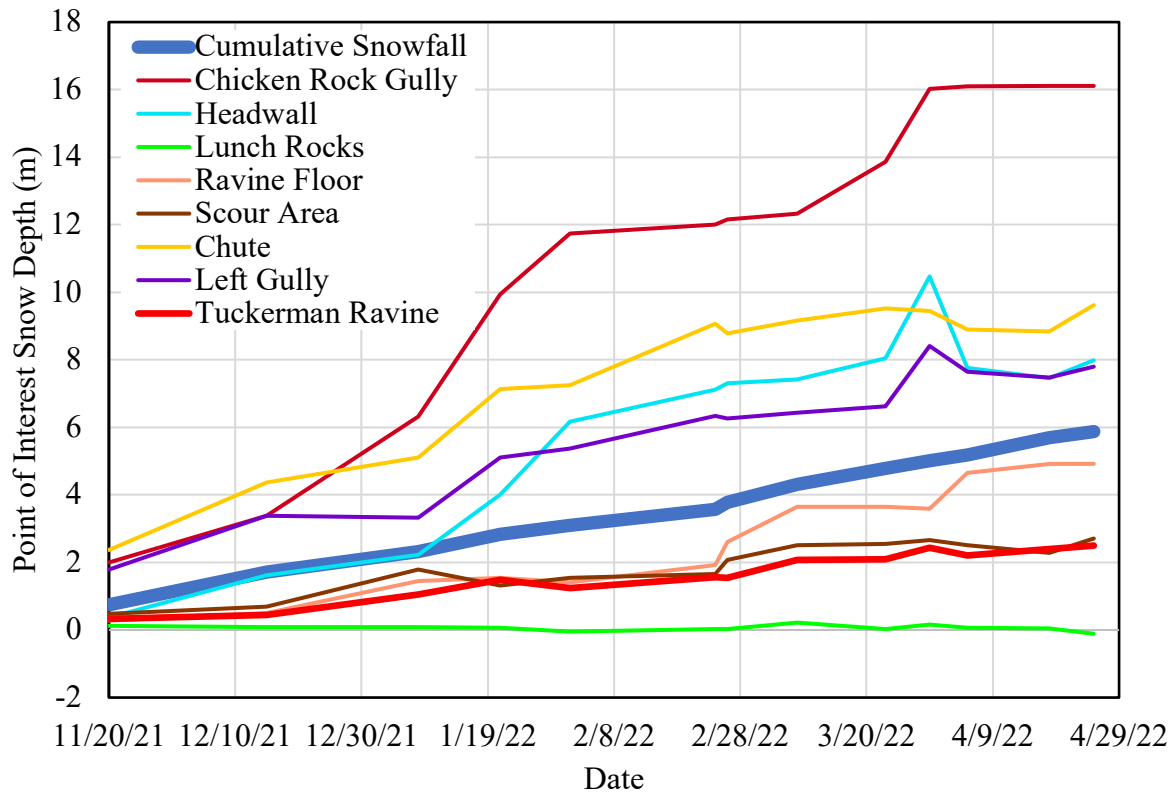
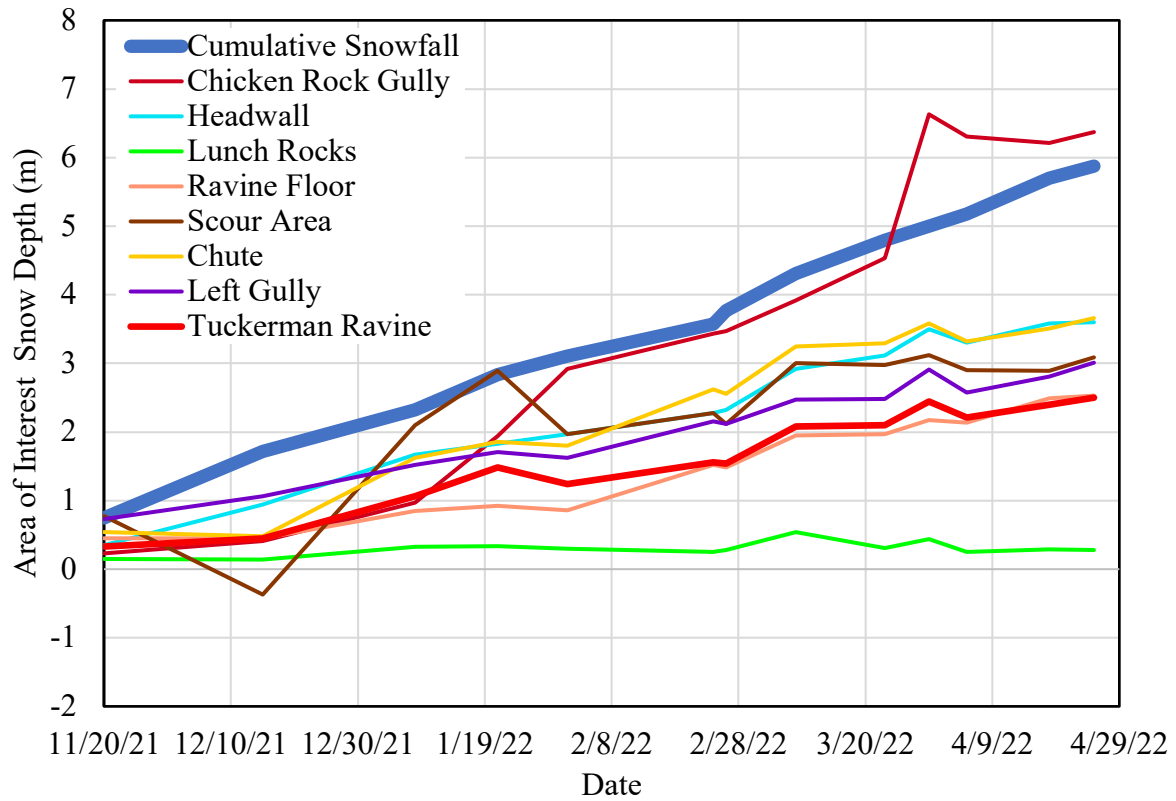


Figure 15: Tuckerman Ravine Snow Depth for the Areas of Interest (top) and Points of Interest (bottom) by Date

4.3.2 Boott Spur Gullies

The BSG snow depth time series illustrates which areas first accumulate snow and distinguishes between varying magnitudes of snow depth across the study area (Figure 16). BSG had less snow accumulation than Tuckerman Ravine with an average maximum depth of only 0.81 m compared to Tuckerman Ravine's 2.40 m (Table 4). Contrary to Tuckerman Ravine, no BSG AOIs or POIs exceeded the cumulative snowfall value throughout the season. This is likely due to the smaller quantity of wind-transported snow in this area throughout the season. Tuckerman Ravine had about one more meter of snow throughout the season compared to BSG (Figure 17).

Each of the three AOIs in BSG had a distinct snow accumulation pattern. The Hillman's Highway gully is where the deepest snow was found. The maximum average snow depth of 1.91 m was recorded on 4/18/22 in the Hillman's Highway AOI. The Hillman's Highway 3 (HH3) POI had a maximum snow depth of 3.67 m on 2/26/22 (Table 5). This gully area accumulates deeper snow depth because of its geomorphic shape. Although Tuckerman Ravine and BSG experience predominantly western winds, Nor'easter storm tracks bring eastern winds, and therefore the lee turns to the other side of the terrain. Gullies such as Hillman's Highway collect snow on both sides because of their opposingly sloped walls. Also, avalanche debris can fill the lower reaches of Hillman's Highway gully.

The Lower Snowfield area is made of up mostly deciduous shrubs and measured a modest accumulation of 2 m. In an average winter, this area will fill with enough snow to entirely cover the sparse deciduous vegetation. The average snow depth throughout the season in Lower Snowfield is comparable to Hillman's Highway with the snow depth on 4/18/22 being within 0.01 m (Table 4).

The Christmas Tree AOI and POI are clearly below the other areas in BSG. Even on high snow years, the Christmas Tree AOI is a tree line that remains visible with a distinct triangle shape. The Christmas Tree is clearly delineated in SfM snow depth maps (Figure 16) by predominantly blue areas signifying minimal snow accumulation. In this area, SfM shows little snow depth due to the tall height of vegetation which is incorrectly identified as the ground level in the baseline flight digital surface model (DSM) due to the dense canopy. Snow fills between the trees but does not extend above their tops which results in a consistent depth throughout the season. Negative depths correspond to periods when snow weighs down the trees' branches causing the region to appear to be lower than in the baseline DSM. Negative snow depth values occur for the Christmas Tree AOI and POI for several dates (Table 4 and Table 5), though these values are within the SfM detection limit.

The snow depth progression across each AOI and POI displays an upwards trend for all AOIs except the Christmas Tree (Figure 17). However, snow depth variations occur throughout the season and match observed widespread accumulation and ablation events. Such events will be explored further in section 4.6.

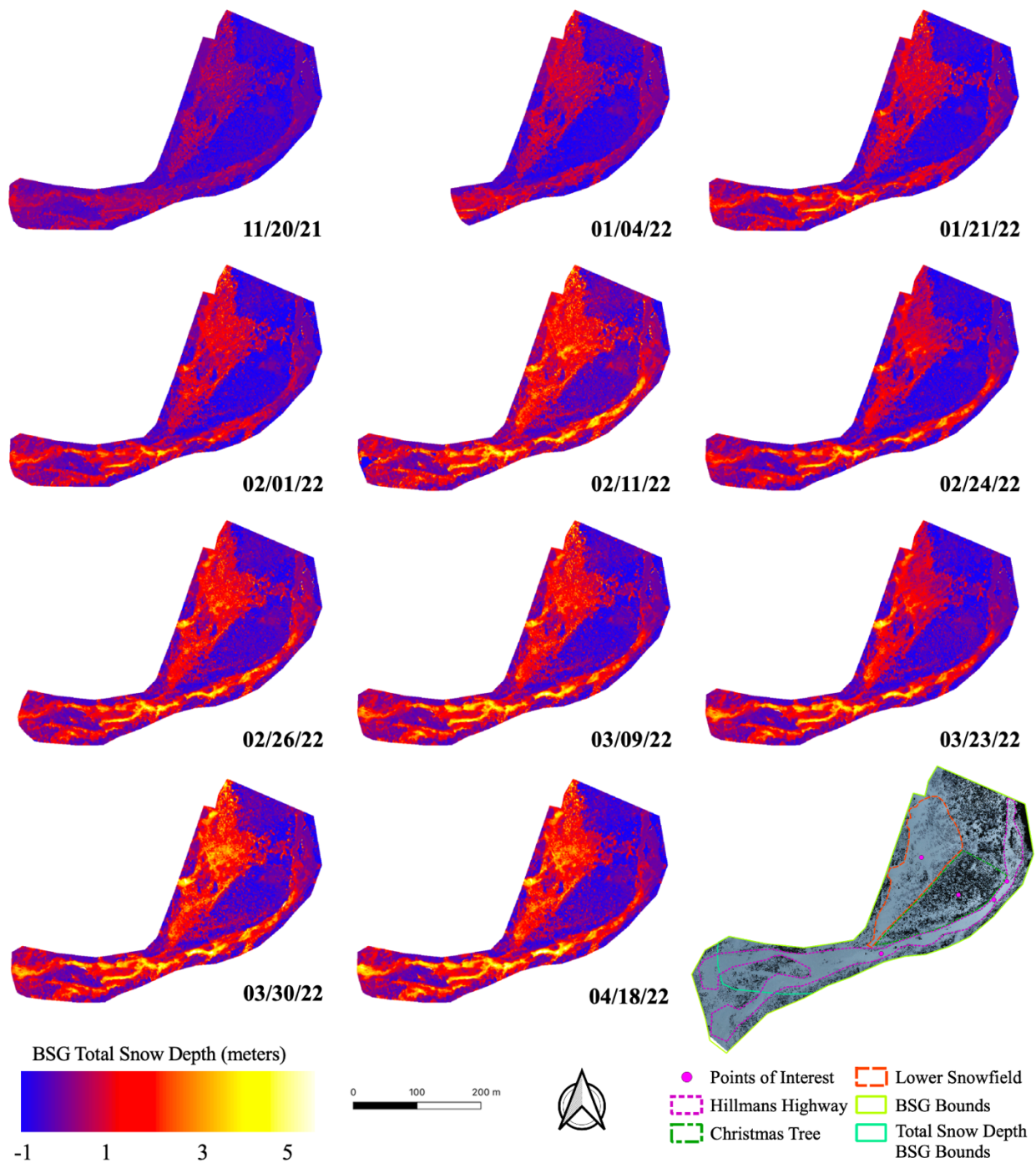


Figure 16: BSG Total Snow Depth Time Series Winter 2021-2022

Table 4: Boott Spur Gullies (BSG) Snow Depths (m) for the Areas of Interest (AOI) by Date

Survey Date	MWOBS Cumulative Snow	Location				
		Lower Snowfield	Christmas Tree	Hillman's Highway	BSG Avg	Tux Avg
11/20/21	0.75	0.25	-0.50	0.32	-0.09	0.33
1/4/22	2.15	0.60	-0.56	0.61	0.06	1.06
1/21/22	2.84	0.91	0.11	1.08	0.29	1.48
2/1/22	3.11	1.03	-0.44	1.08	0.32	1.24
2/11/22	3.49	1.77	0.05	1.47	0.84	1.38
2/24/22	3.58	0.94	-0.46	1.36	0.33	1.56
2/26/22	3.77	1.52	-0.14	1.64	0.67	1.54
3/9/22	4.31	1.55	-0.18	1.74	0.71	2.08
3/23/22	4.79	1.77	-0.26	1.64	0.51	2.10
3/30/22	5.00	2.00	0.24	1.87	0.90	2.44
4/18/22	5.70	1.90	-0.11	1.91	0.81	2.40

Table 5: Boott Spur Gullies (BSG) Snow Depths (m) for the Points of Interest (POI) by Date

Survey Date	MWOBS Cumulative Snow	Location						Tux Avg
		Lower Snowfield	Christmas Tree	HH 1	HH 2	HH 3	BSG Avg	
11/20/21	0.75	0.40	-0.27	0.22	0.12	0.26	-0.09	0.33
1/4/22	2.15	1.21	-0.49	0.72	0.30	1.12	0.06	1.06
1/21/22	2.84	1.33	-0.78	0.91	0.21	2.74	0.29	1.48
2/1/22	3.11	1.73	-0.83	0.88	0.29	2.88	0.32	1.24
2/11/22	3.49	3.55	-0.69	3.27	2.77	3.43	0.84	1.38
2/24/22	3.58	2.71	-0.73	2.36	0.54	2.73	0.33	1.56
2/26/22	3.77	3.12	-0.80	2.81	1.13	3.67	0.67	1.54
3/9/22	4.31	3.08	-0.63	2.22	0.62	3.38	0.71	2.08
3/23/22	4.79	2.81	-0.53	2.06	0.62	3.01	0.51	2.10
3/30/22	5.00	3.56	-0.70	2.12	2.57	3.26	0.90	2.44
4/18/22	5.70	3.47	-0.53	1.81	1.99	3.54	0.81	2.40

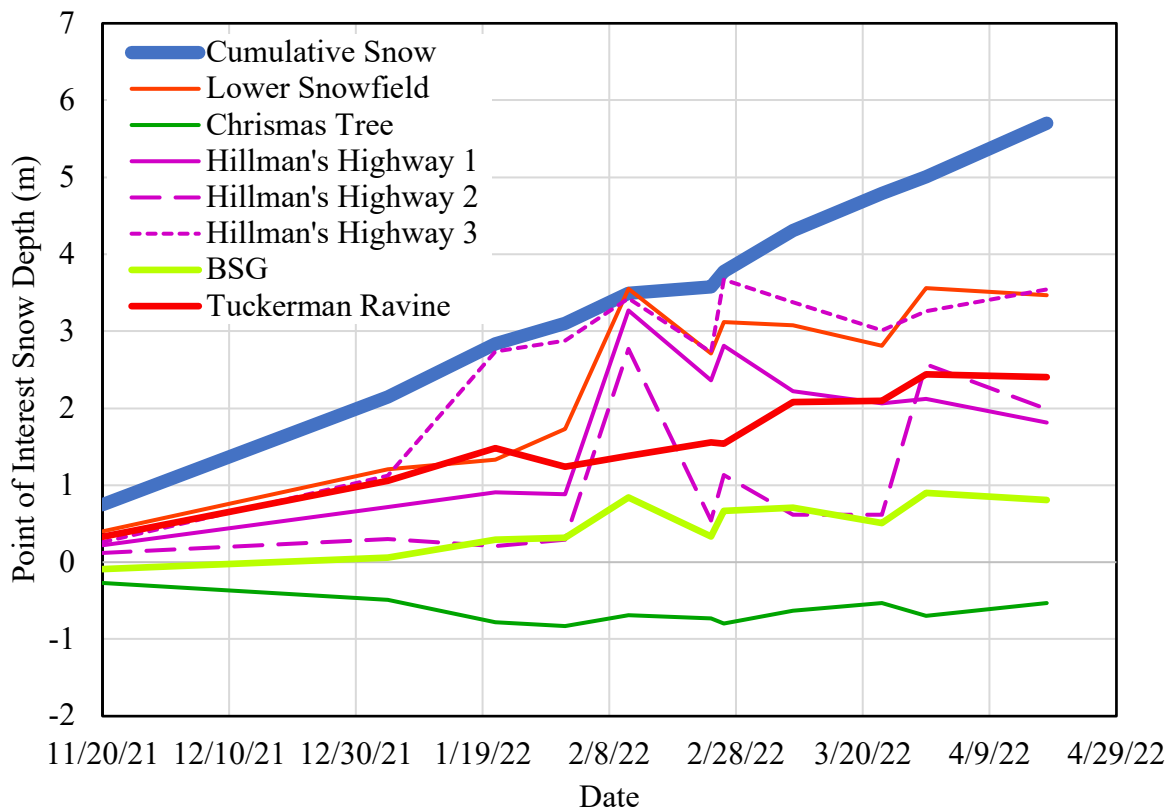
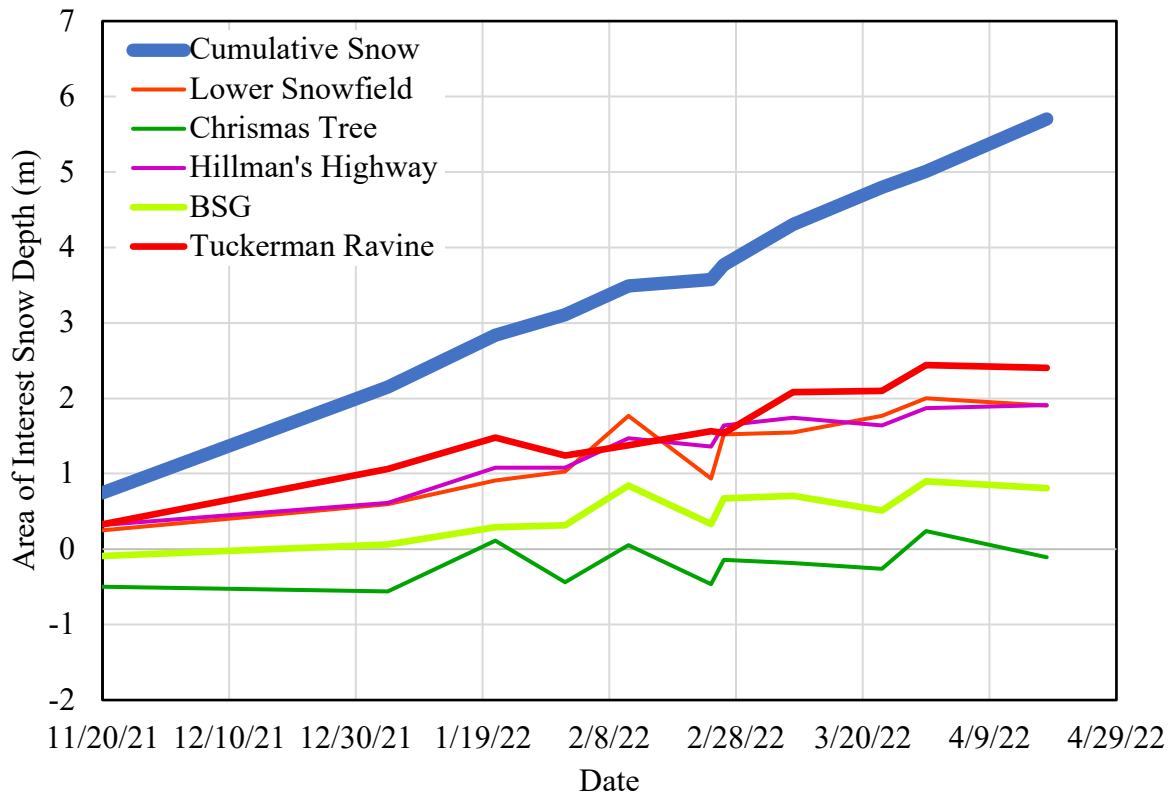


Figure 17: BSG Snow Depth for the Areas of Interest (top) and Points of Interest (bottom) by Date

4.4 UAV SfM Snow Depth Change

Non-uniform patterns of snow depth are primarily driven by wind redistribution of snow. To illustrate the 2021-2022 winter wind slab production and scouring process in Tuckerman Ravine and BSG, snow depth change between campaigns was analyzed. Sections 4.4.1 and 4.4.2 highlight areas in Tuckerman Ravine and BSG, respectively, with unique accumulation and ablation features.

4.4.1 Tuckerman Ravine

The spatial distribution and depth of wind-transported snow changes are highly variable within the 2021-2022 winter season (Figure 18). AOIs that accumulate the most snow (e.g., Chicken Rock Gully, Left Gully, Chute, and Headwall) typically have greater snow depth change than the overall Tuckerman Ravine snow depth change (Figure 19). Areas such as the Lunch Rocks are entirely below the 1:1 line which represents only a slight contribution to the overall Tuckerman Ravine snow depth change. The UAV SfM snow depths consistently increased when snowfall greater than 0.5 m occurred on these occasions: between 12/15/21 to 1/08/22, 2/26/22 to 3/09/22, and 4/05/22 to 4/18/22 (Table 2). Mapped snow depth changes for these periods are also predominantly blue indicating a snow depth increase across most of the ravine (Figure 18).

Areas having the greatest increases in snow depth are where wind slabs have formed. Wind slab production is evident in Left Gully, Chute, Headwall, and Chicken Rock Gully for these three time periods. Most of the wind slabs reside on eastern aspects of the AOIs because of snow transport from westerly winds. Even during periods when Tuckerman Ravine receives less snow, 1/08/22 to 1/21/22, 1/21/22 to 2/01/22, 3/09/22 to 3/23/22, and 3/23/22 to 3/30/22, snow depth is increasing in these same regions. The largest snow drifts are on the steep slopes of the Headwall.

These drifts share a similar spatial extent over time. Between 1/21/22 and 2/01/22, there was an accumulation of snow on the southeastern aspects rather than the western aspects. During this period, the prominent wind direction was from the northwest which transported snow to a different aspect than usual. There is also an unusually large accumulation of snow between 2/01/22 and 2/24/22 on the Ravine Floor. This accumulation is attributed to a series of natural avalanches along the Headwall. Section 4.6 explores this wind slab formation and subsequent avalanche in the Headwall area in greater detail.

Scour occurs most often in the study area's highest elevations. These scour changes are more modest than slab formation but occur over a larger area. Scour areas are apparent in the westernmost region of the study area adjacent to the edge of the Bigelow Lawn. The slope angle here (40°) is not as steep as the headwall zone (55°). The snow depth change map between 3/23/22 and 3/30/22 clearly shows this scour phenomenon. There is also a modest decrease in snow depth in the westernmost area of the Ravine. As shown in Figure 19, the Scour Area AOI has very different patterns of snow depth change throughout the winter than the other AOIs. Extreme values near the western edge of the study area are believed to be SfM processing artifacts that do not accurately represent the snow depth of a given day. These artifacts are seen on the 12/15/21 to 1/08/22, 1/08/22 to 1/21/22, 1/21/22 to 2/01/22, and 2/01/22 to 2/24/22 snow depth change maps (Figure 18). Since the Scour Area AOI is near the edge of the study area, the effects of these SfM artifacts impact the quantification of this area's snow depth. While scour is present in this region, the magnitude is likely less than that measured by the UAV.

Between most survey dates, snow depth decreases in areas that do not have wind deposition are caused by metamorphosis, compaction due to wind, and sublimation. This is seen with a slight red color showing up on areas surrounding dark blue drift features (Figure 18). More evident is

the significant widespread ablation and densification which occurred between March 30th and April 5th due to rain and consistently above-freezing air temperatures. During this period, snow depth decreased in almost every AOI and POI. Snow depth only increased in the Ravine Floor. This increase reflects the avalanche debris which was deposited from the Headwall slide. A very large decrease in snow depth occurs in this time period in the Headwall POI, which was the source of the avalanche.

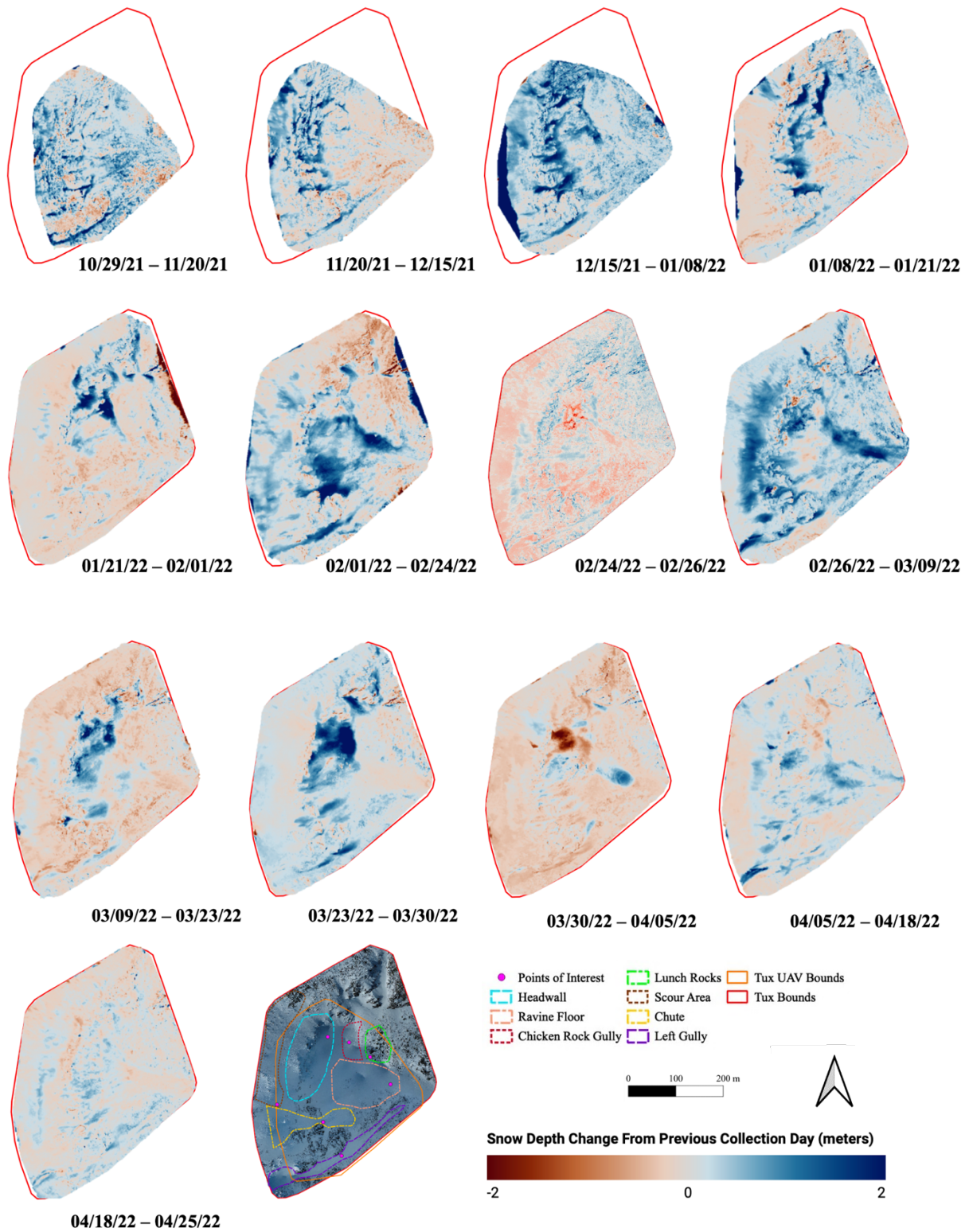


Figure 18: Tuckerman Ravine Snow Depth Change Time Series. Note Flights 10/29/21 – 1/21/22 Had a Smaller Flight Plan. A Red Outline Shows the Full Flight Plan That was Enacted on 2/1/22 and used for the Remainder of Data Collection.

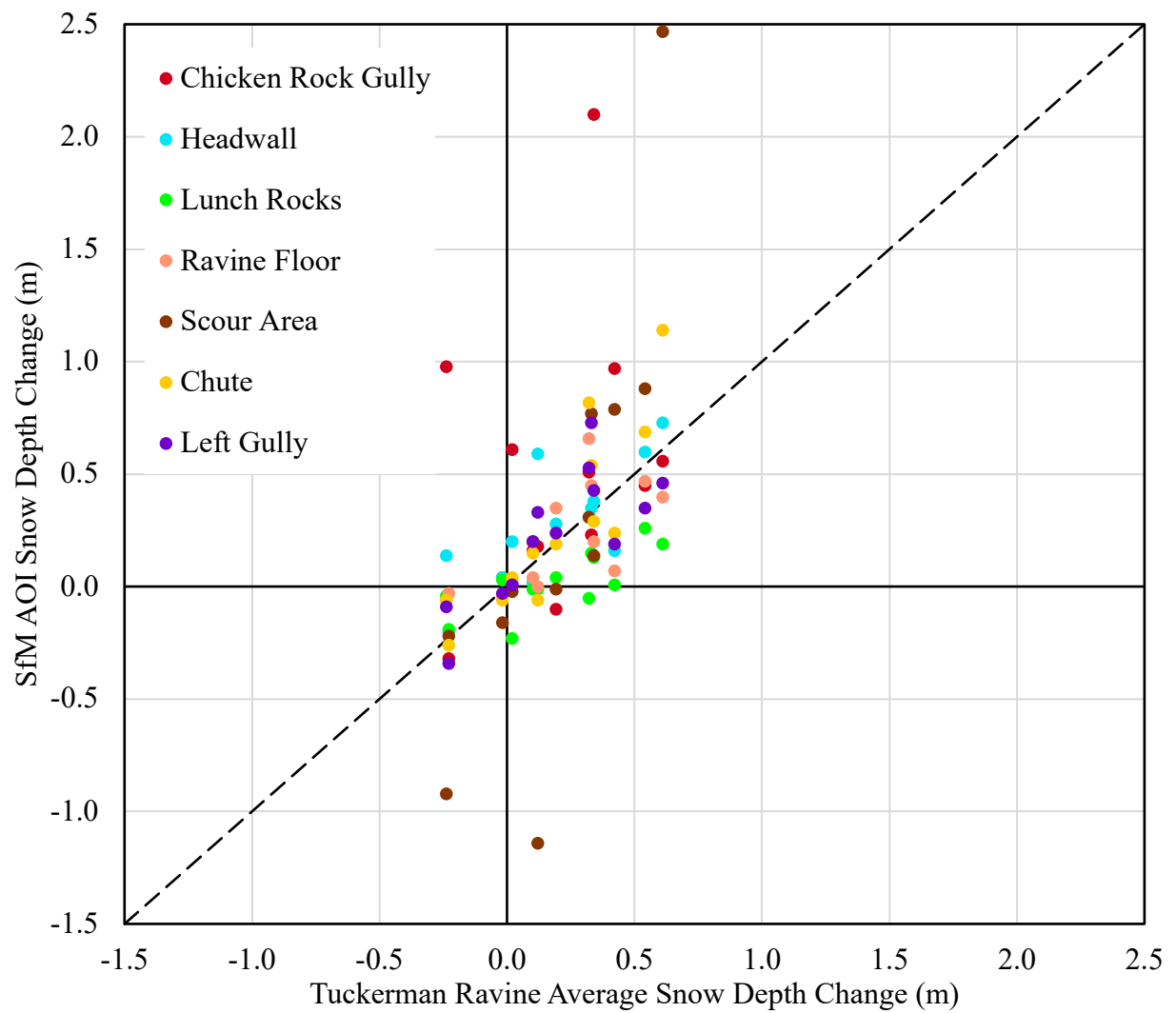


Figure 19: AOI Snow Depth Change Sensitivity to Tuckerman Ravine Snow Depth Change Scatterplot. The Dashed Line is the 1:1 Line.

4.4.2 Boott Spur Gullies

Most snow depth change maps in Figure 20 show accumulation in BSG's Lower Snowfield and Hillman's Highway gully. The Christmas Tree area exhibits limited accumulation throughout the season. This area often has snow depth decreases. This is attributed to the settling of coniferous vegetation by the weight of snow loading. A predominant red color throughout the entire study (e.g., 2/11/22 to 2/24/22, 3/09/22 to 3/23/22) in Figure 20 indicates when there were widespread ablation events. During these events, the only area that shows positive accumulation is the Christmas Tree, which is likely due to the vegetation in that area rebounding from snow unloading. Thus, the Christmas Tree AOI has an inverse relationship of snow depth change compared to the surrounding areas. When a positive snow depth change is observed in the Lower Snowfield and Hillman's Highway increase in snow depth, the Christmas Tree has a negative change and vice versa.

An abrupt increase in snow depth occurred between 2/01/22 and 2/11/22 followed by a rapid loss of snow between 2/11/22 and 2/24/22 (Figure 20). The Hillman's Highway 2 POI clearly shows this large ablation event. This event will be investigated further in section 4.6.

In contrast to Tuckerman Ravine, the three AOIs have readily discernable change features. There is a disproportional contribution to the snow depth change in BSG from AOIs within its bounds. The Lower Snowfield and Hillman's Highway make up the majority of the snow depth change average throughout BSG. In comparison, the Christmas Tree region has very little influence on BSG's overall snow depth change. While most of the Christmas Tree snow depth decreases during most periods, there is still a relationship between the overall BSG snow depth change and the Christmas Tree snow depth change (Figure 21).

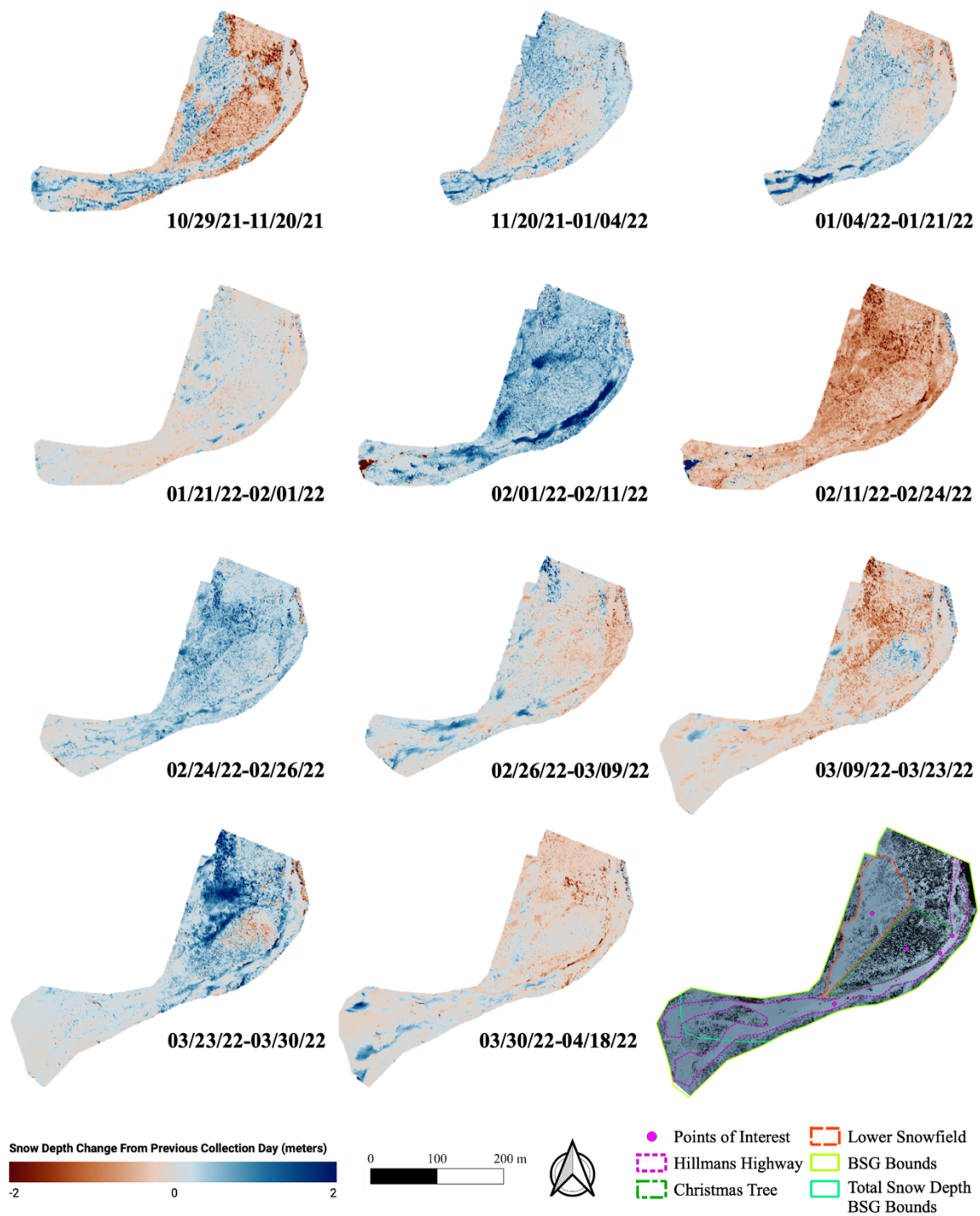


Figure 20: Boott Spur Gullies Snow Depth Change Time Series. Surveys from 10/29/21 Through 3/09/22 use a Slightly Smaller Flight Plan from the Three Remaining Flights (3/23/22 through 4/18/22). This Smaller Boundary is Shown in the Bottom Right Corner with a Teal Outline.

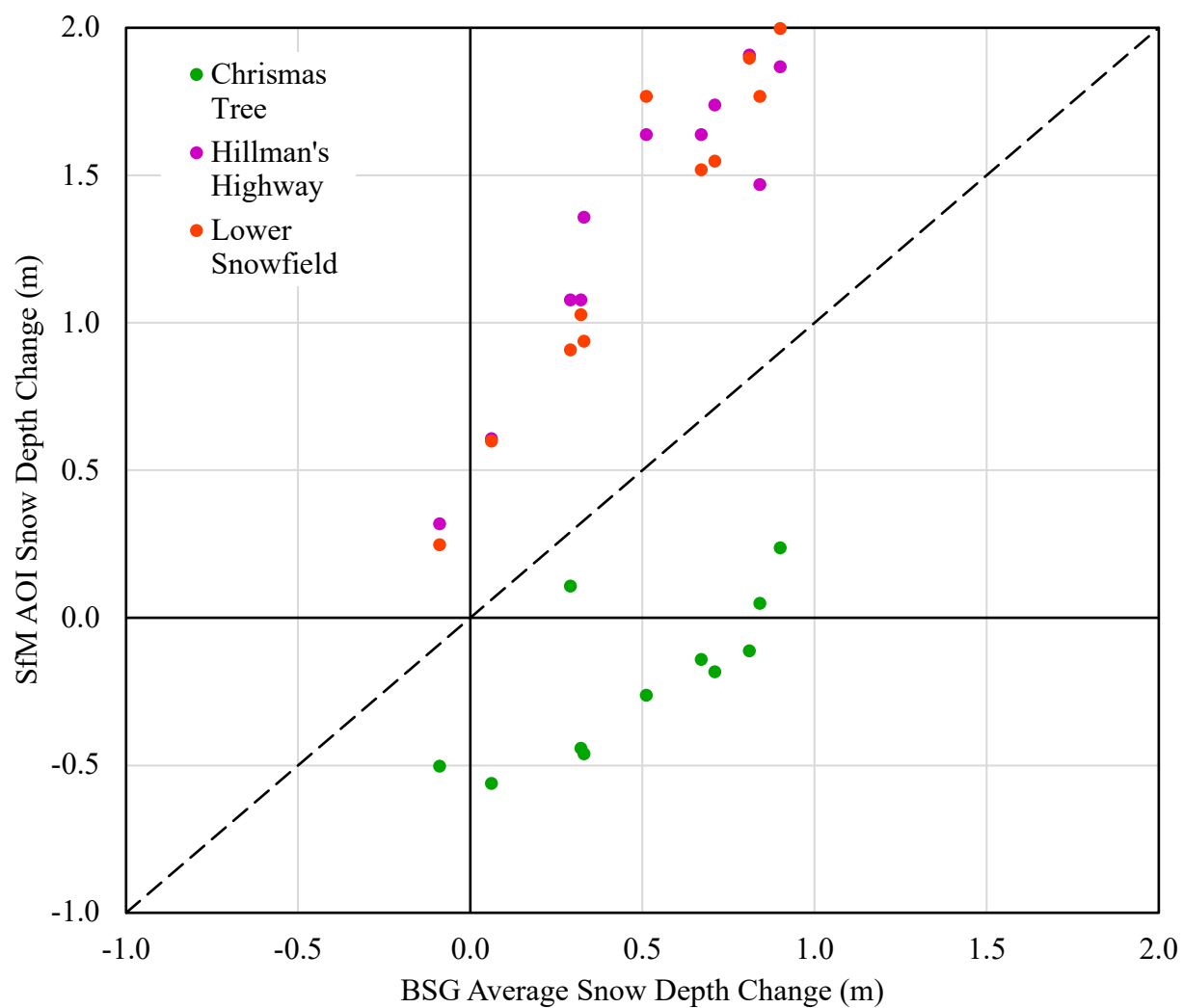


Figure 21: AOI Snow Depth Change Weighting on Boott Spur Gullies (BSG) Average Snow Depth Change. The Dashed Line is the 1:1 Line.

4.5 SnowModel Derived Snow Depth

SnowModel was implemented to understand if a physics-based model can estimate snow depth and depth change patterns over the Mount Washington study region. SnowModel snow depth time series coinciding with the Tuckerman Ravine and BSG UAV campaigns are explored in section 4.5.1. Performance statistics between SfM and SnowModel were calculated for AOIs and POIs and analyzed in section 4.5.2. These statistics quantify the agreement between the two snow depth estimation techniques. The UAV SfM serves as the validation dataset for SnowModel. Because of the large bias present in the SnowModel total snow depths, snow depth change is the primary comparison.

4.5.1 SnowModel Time Series

SnowModel redistributes snow from western to eastern aspects in a manner that agrees with typical patterns for the region (Figure 22). The deepest snowdrifts are on the eastern aspect of the Mount Washington summit cone. Although the snow depth in this area was not measured by UAV SfM, the eastern snowfield holds snow into late June and early July due to its considerable snow depth attributed to wind redistribution.

The UAV SfM snow depth evolution was captured in two relatively small areas in the SnowModel model domain. The general locations of observed drifts are represented well by the model. A large, 10 m drift is simulated by SnowModel in the upper elevations of Tuckerman Ravine (Figure 22). Drifting is evident early in the season and drifts build over time with accumulation and wind redistribution events. A drift is seen just above Tuckerman Ravine; specifically, where Bigelow Lawn begins losing elevation to the east. There is a slight convexity in this location which led the model to accumulate a snow drift. In reality, this area is not steep

enough to sustain a drift as simulated. Instead, the transported snow gets swept into the steep parts of Tuckerman Ravine.

At the end of the model run for April, SnowModel estimated a 5 to 7.5 m snow depth in the lower elevation forested terrain around the east and west edges of the study area. In-situ snow depth measurements record a much lower snow depth than that of SnowModel. The Hermit Lake SNOTEL site recorded 0.87 m (34 in) of snow depth on April 25th. This depth is much less when compared to SnowModel's 6.3 m of snow.

Average SnowModel snow depth values generally follow the trend of the cumulative snowfall values for the 2021-2022 season (Figure 23). The SnowModel average value at the end of April was about 1 m lower than the cumulative snowfall, but much higher than the observed values. This suggests that SnowModel underestimates ablation, sublimation, and/or densification throughout the study area. There was also a large difference present in the average Tuckerman Ravine and BSG snow depths between modeled and measured methods. SnowModel simulated approximately 3 m more snow than the UAV SfM in both study areas. However, SnowModel was able to capture Tuckerman Ravine snow depths as being deeper than those in BSG.

The average snow depth in the SnowModel maps was greater than the cumulative observed snowfall until 1/08/22. SnowModel inputs precipitation and uses a temperature threshold to differentiate between snow and rain. There were many days close to freezing temperatures. Additionally, because the model was run on a daily time step rather than hourly, the average daily temperature may not have accurately reflected the air temperature when precipitation was occurring. Diurnal temperature fluctuations lead to an inconsistency between measured and model precipitation states. Some incorrect snowfall occurred when there was measured rainfall. Shortly after the SnowModel simulation start date, a total of 13 cm of precipitation fell. For this period,

SnowModel simulated snow. However, MWOBS observations indicated rain and no snowpack was present after the event. This early snow caused a 129 cm bias relative to the UAV SfM that persisted throughout the season. The average SnowModel snow depth for the study area as of November 3rd, 2021 was 1.29 m. Because there was no snow on that date, a 1.29 m reduction in the average SnowModel snow depth was applied to subsequent dates.

Despite the large bias between SnowModel and the UAV SfM snow depths, Landsat 8 satellite data show that SnowModel captures the general trends of snow cover distribution on April 25th (Figure 24). The Landsat 8, at a 30 m spatial resolution, shows the snow cover over the model domain. Areas in the alpine zone, above 1,400 m ASL, have a darker hue that is most likely bare earth. Large snow drifts match snow cover extent on Mount Washington's Summit Cone Eastern Snowfield, Tuckerman Ravine, Boott Spur Gullies (excluding the Christmas Tree), and isolated parts of the Bigelow Lawn.

The normalized difference snow index (NDSI) (Hall et al., 2002; Riggs et al., 1994) calculated on bands 3 and 6 of the Landsat 8 defines a threshold of 0.2 to determine snow cover (Figure 25). Boxplots created using NDSI and average SnowModel snow depth within each 30 m pixel show modest increase in snow depth above 0.2 NDSI. While factors such as canopy cover and vegetation influence the NDSI's ability to classify snow in this area, there are many outliers having deep snow drifts with moderate NDSI values. NDSI value above 0.4 have a distinctly higher modeled snow depth than lower NDSI values. NDSI maps also indicate SnowModel's spatial redistribution of snow is quite coarse compared to observation and imperfectly captures scour and wind driven snow.

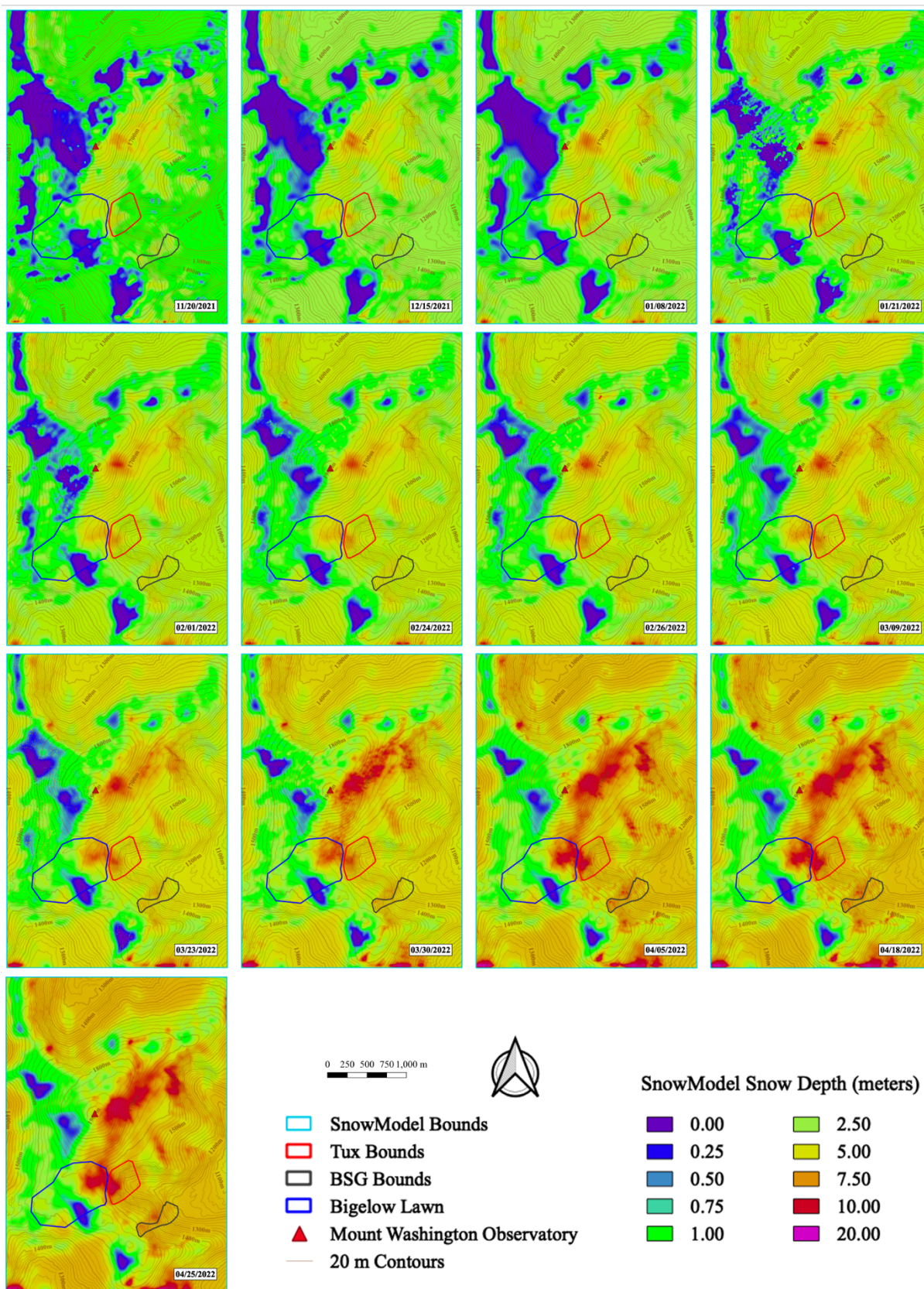


Figure 22: SnowModel Time Series Coinciding with UAV Flight Dates

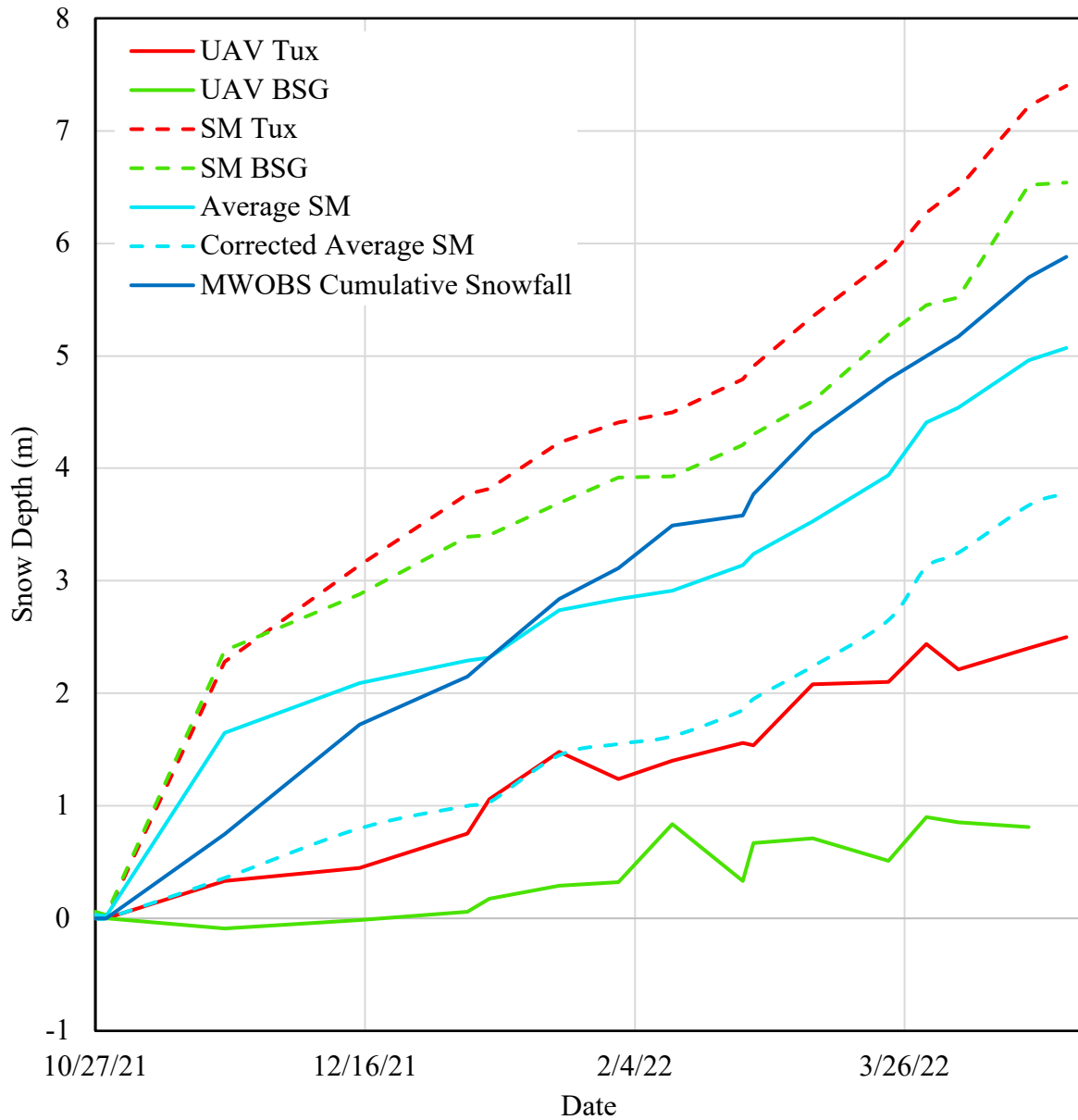


Figure 23: SnowModel (SM) and UAV Comparison Time Series. Corrected Average SM is 1.29 m Less Than the Average SM Data Due to an Early Season Rainstorm That SnowModel Simulated Snow.

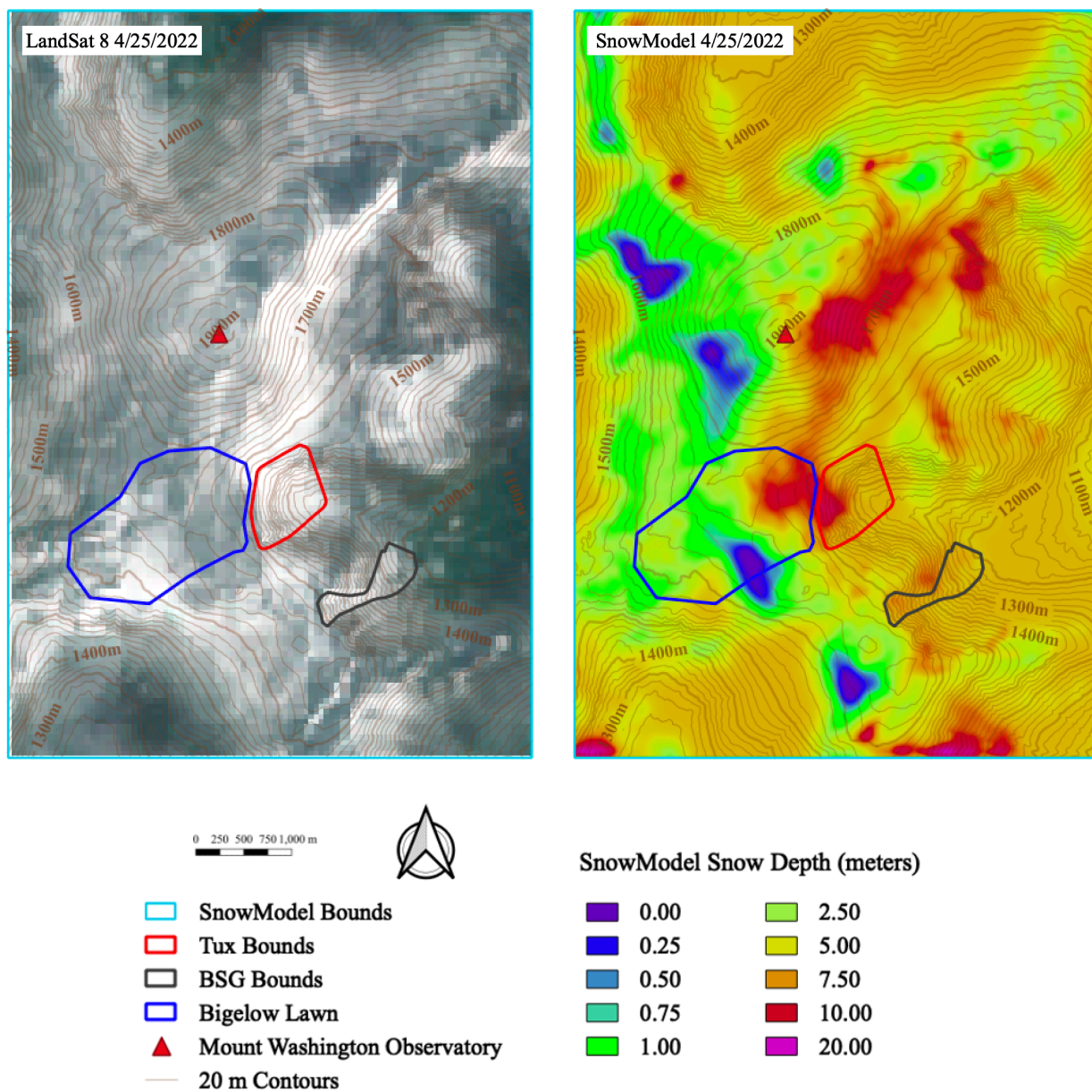


Figure 24: Landsat 8 and SnowModel Snow Cover Comparison of 4/25/2022

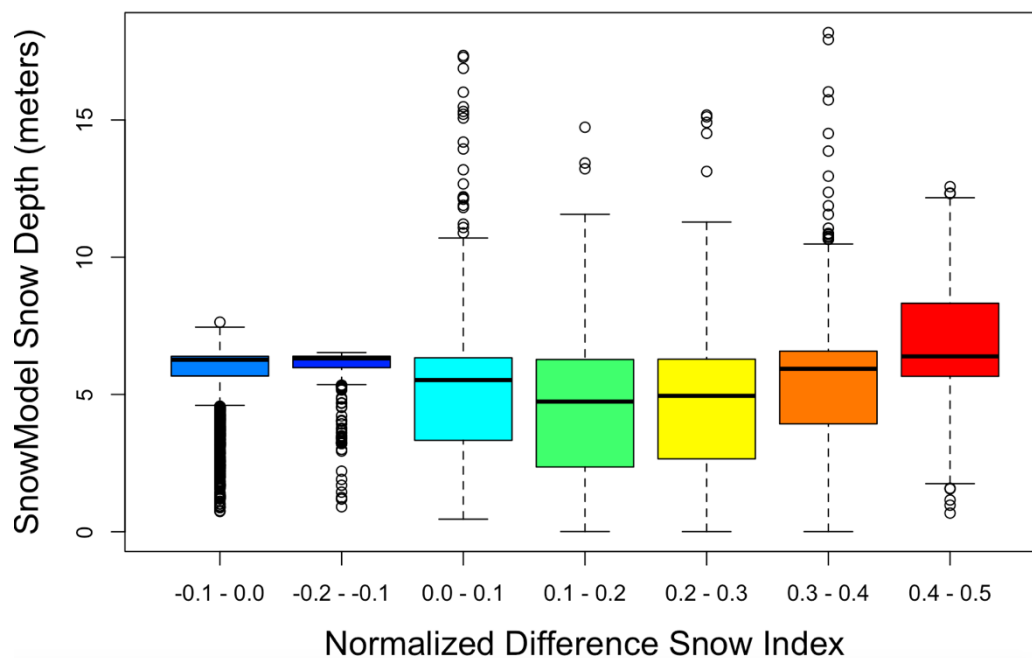
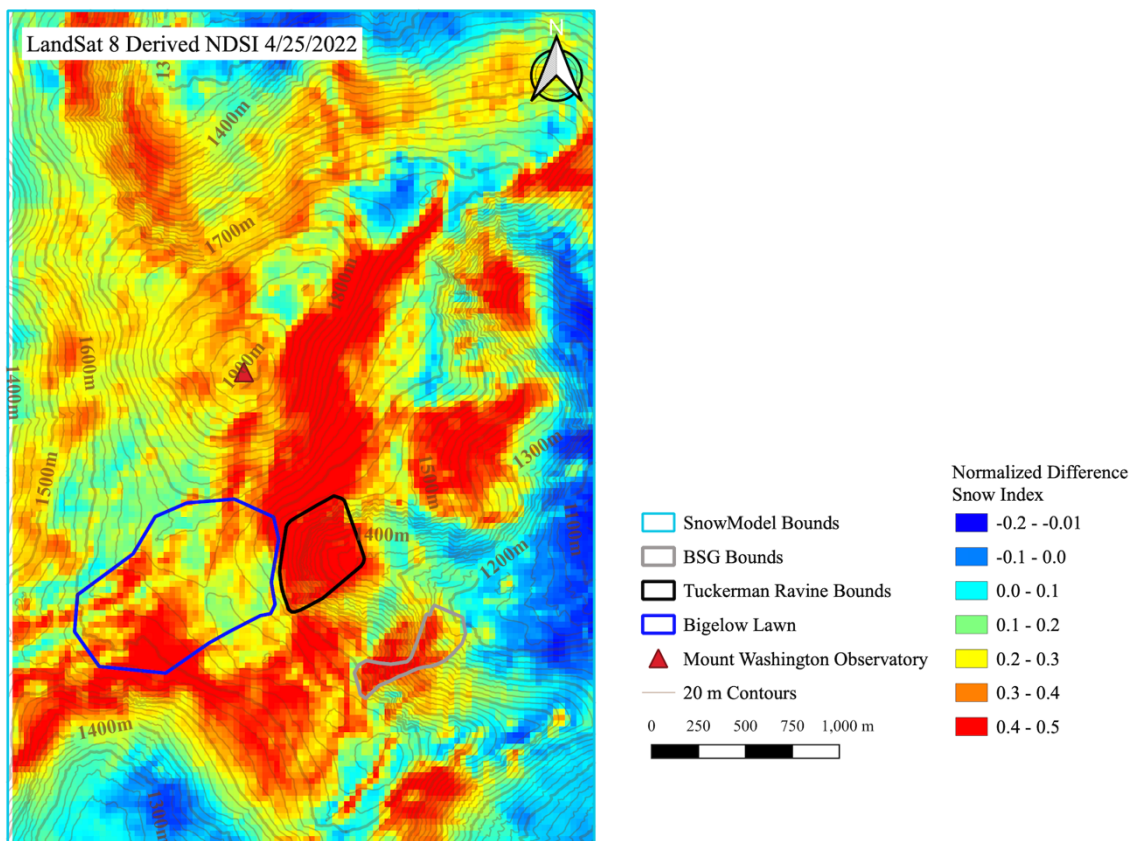


Figure 25: Normalized Difference Snow Index (NDSI) Derived from Landsat 8 Data Captured 4/25/2022. NDSI Map Above and Boxplots Showing SnowModel Snow Depth Below

4.5.2 SnowModel and UAV SfM Snow Depth Change Comparison

To compare UAV and SnowModel, Willmott statistics are calculated from UAV SfM and SnowModel AOIs and POIs (Table 6 and Table 7). Snow depth change was compared to test if SnowModel can replicate similar snow redistribution as the UAV SfM. The maximum R^2 values across all AOIs and POIs calculated are the Chute POI, Chicken Rock Gully POI, and Left Gully AOI with values of 0.40, 0.36, and 0.34 respectively. The Chute and Chicken Rock Gully POIs are located in a part of the respective gully that records the deepest snowpack. The model did a much better job of capturing increases and decreases in snow depth in locations that had relatively deep snow over the season. This may indicate that the model is not able to capture changes on the order of 10s of cm for this region, but that larger changes are possible.

The SnowModel mean is greater than that of the UAV SfM for all AOIs. This is shown in Figure 26 with the majority of points residing on the SnowModel side of the 1:1 line. Three of the areas with the deepest snow (Chicken Rock Gully, Headwall, and Chute) had a greater POI mean than SnowModel. Three RMSE values are greater than 1 m (Scour Area AOI, Headwall POI, and Scour Area POI). The lowest RMSE occurs in the Left Gully POI.

BSG's Willmott comparison to SnowModel resulted in similar values to those of Tuckerman Ravine. The largest RMSE was the Christmas Tree AOI with a value of 0.46. Seven out of the nine AOIs and POIs resulted in an R^2 value below 0.10. A very strong bias is present in all sampled AOIs and POIs with SnowModel resulting in much larger snow depth changes than the UAV SfM. This phenomenon is clear in Figure 27 with most of the points residing above the 1:1 line favoring SnowModel.

Visual comparison of snow depth change maps is useful in determining if transported snow extent is similar between methods. SnowModel produces a much courser map, but areas of snow

are still distinguishable. There is a clear signal pointing towards a new slab of snow in the headwall area in both maps in the 3/23/22 to 3/30/22 change (Appendix G). Although this slab is not identical in spatial extent, the location is similar, and the depth is comparable. The average depth of the SnowModel wind slab is 1.5 m while the UAV wind slab is 2 m. The discrepancy between these depths is likely due to SnowModel distributing more snow in the upper reaches of the study area and the Bigelow Lawn as well as the forest below. Overall, SnowModel is effective in determining the general extent of wind slabs when isolating snow accumulation and wind events comparable to that of UAV data.

Table 6: Tuckerman Ravine AOI SfM and SnowModel (SM) Willmott Statistics (meters)

Location	SfM Mean	SM Mean	SfM Std Dev	SM Std Dev	N	Slope	Intercept	RMS E	Bias	R ²
Chicken Rock Gully	0.39	0.49	0.43	0.40	13	0.45	0.12	0.54	-0.10	0.02
Chute	0.41	0.64	0.71	0.77	13	0.54	0.23	0.93	-0.23	0.05
Headwall	0.27	0.60	0.24	0.72	13	0.33	1.00	0.73	-0.33	0.11
Left Gully	0.21	0.52	0.28	0.49	13	0.30	1.02	0.49	-0.31	0.34
Lunch Rocks	0.03	0.48	0.13	0.39	13	0.46	0.87	0.58	-0.45	0.09
Ravine Floor	0.19	0.50	0.24	0.55	13	0.34	0.88	0.59	-0.32	0.15
Scour Area	0.55	0.64	1.54	0.89	13	0.61	0.05	1.65	-0.08	0.01
Tuckerman Ravine	0.19	0.54	0.27	0.56	13	0.44	0.56	0.64	-0.35	0.07

Table 7: Tuckerman Ravine POI SfM and SnowModel (SM) Willmott Statistics (meters)

Location	SfM Mean	SM Mean	SfM Std Dev	SM Std Dev	N	Slope	Intercept	RMSE	Bias	R ²
Chicken Rock Gully	0.54	0.50	0.94	0.44	13	0.33	0.32	0.71	0.04	0.36
Chute	0.58	0.55	0.82	0.51	13	0.32	0.19	0.68	0.16	0.40
Headwall	0.54	0.48	0.96	0.45	13	0.50	0.07	1.01	0.00	0.02
Left Gully	0.47	0.53	0.57	0.47	13	0.37	0.10	0.54	0.05	0.06
Lunch Rocks	-0.01	0.46	0.20	0.38	13	0.46	0.53	0.59	-0.47	0.08
Ravine Floor	0.33	0.49	0.45	0.42	13	0.42	0.27	0.53	-0.18	0.08
Scour Area	0.22	0.71	0.33	1.26	13	0.52	0.89	1.27	-0.50	0.06

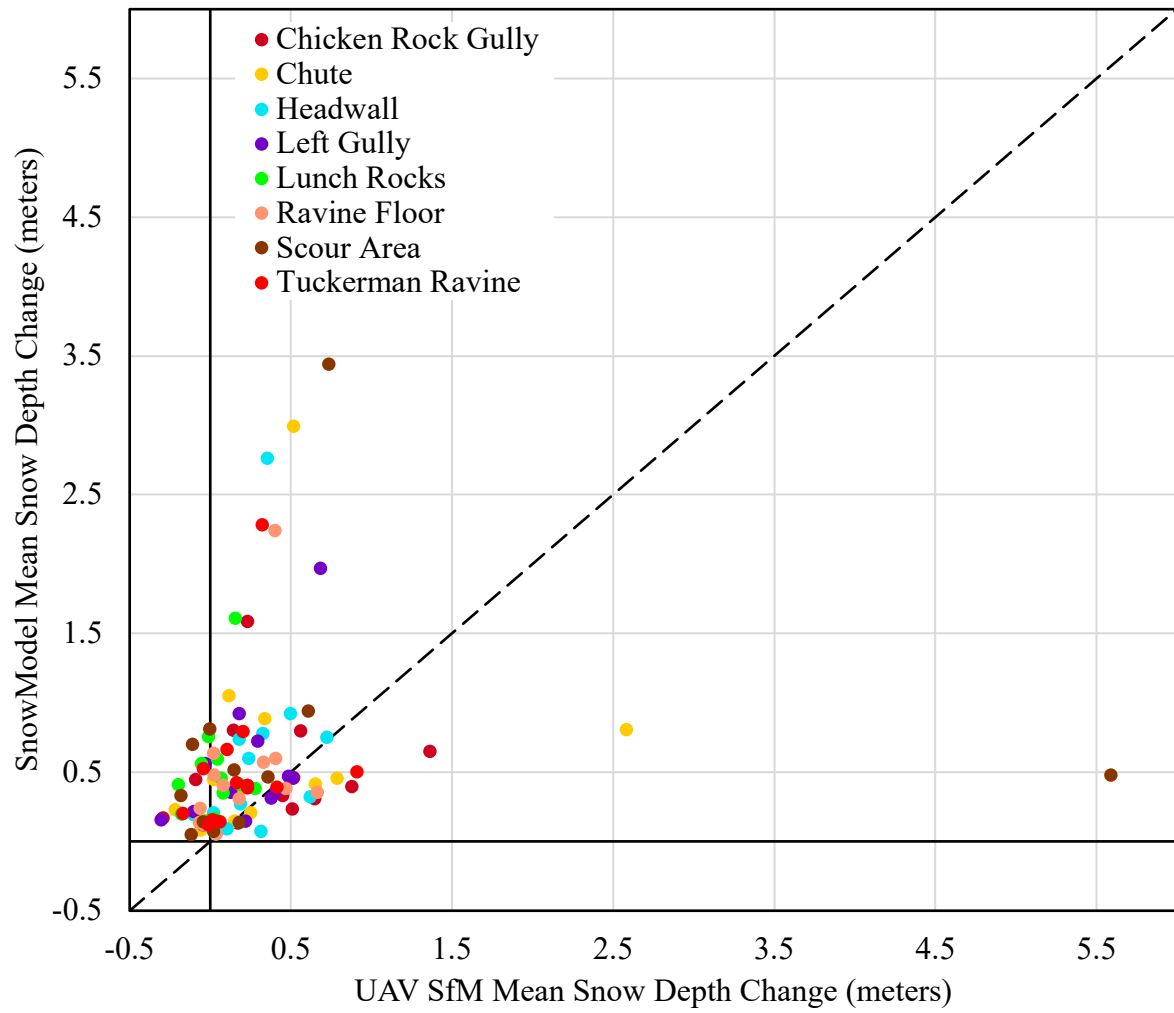


Figure 26: Tuckerman Ravine SnowModel and UAV SfM Snow Depth Change Comparison by AOI. The Dashed Line is the 1:1 Line.

Table 8: Boott Spur Gullies (BSG) AOI SfM and SnowModel (SM) Willmott Statistics (meters)

Location	SfM Mean	SM Mean	SfM Std Dev	SM Std Dev	N	Slope	Intercept	RMSE	Bias	R ²
BSG	0.08	0.60	0.31	0.69	11	0.65	-0.67	0.95	-0.52	0.09
Christmas Tree	0.00	0.55	0.31	0.70	11	0.55	-1.54	1.05	-0.55	0.46
Hillman's Highway	0.17	0.60	0.29	0.63	11	0.58	0.16	0.78	-0.44	0.01
Lower Snowfield	0.17	0.61	0.48	0.74	11	0.63	-0.15	0.98	-0.43	0.01

Table 9: Boott Spur Gullies (BSG) POI SfM and SnowModel (SM) Willmott Statistics (meters)

Location	SfM Mean	SM Mean	SfM Std Dev	SM Std Dev	N	Slope	Intercept	RMSE	Bias	R ²
Christmas Tree	-0.05	0.52	0.22	0.72	11	0.44	-1.49	0.99	-0.57	0.21
Hillman's Highway 1	0.16	0.56	0.85	0.65	11	0.58	-0.12	1.17	-0.40	0.03
Hillman's Highway 2	0.19	0.60	1.21	0.71	11	0.63	-0.14	1.53	-0.41	0.06
Hillman's Highway 3	0.30	0.57	0.61	0.61	11	0.64	-0.16	0.87	-0.14	0.02
Lower Snowfield	0.31	0.56	0.68	0.63	11	0.57	0.00	0.92	-0.26	0.00

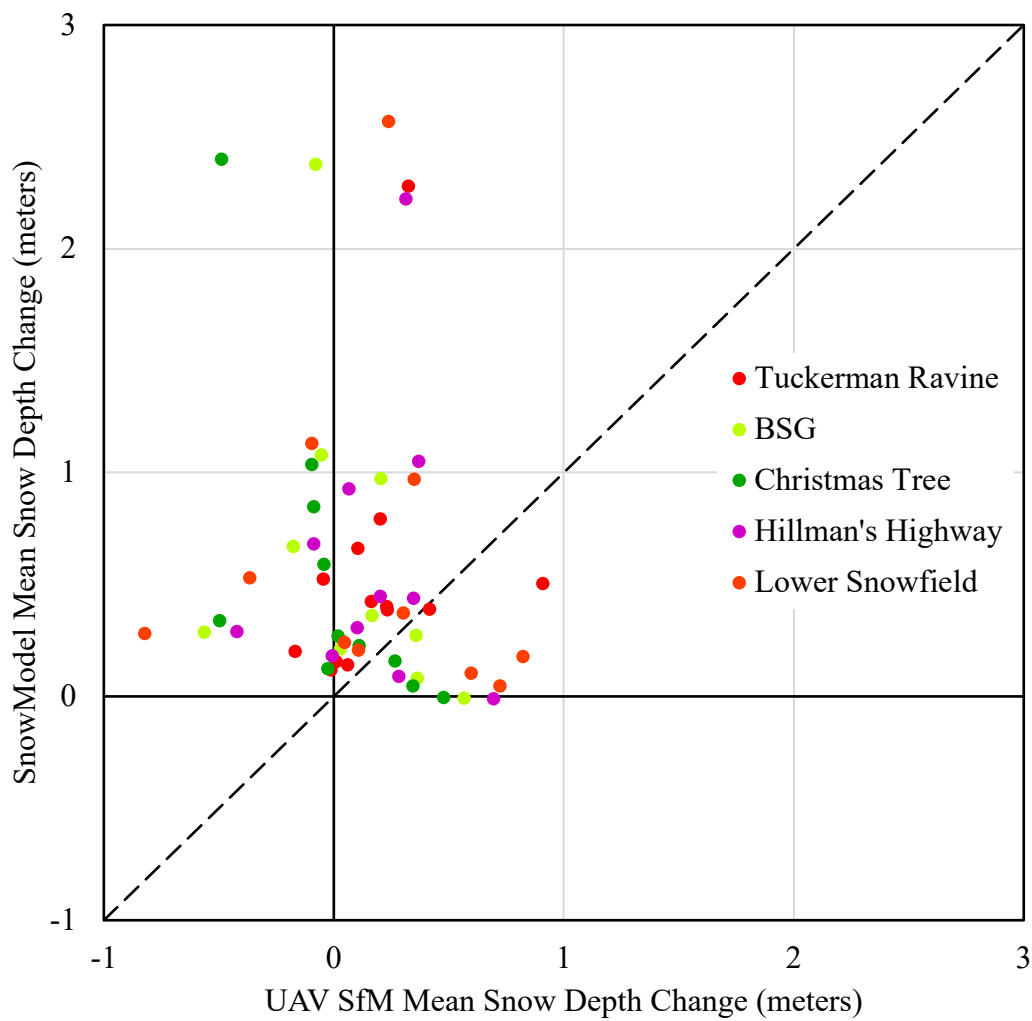


Figure 27: BSG SnowModel and UAV SfM Snow Depth Change Comparison by AOI. The Dashed Line is the 1:1 Line.

4.6 Winter 2021-2022 Case Studies

The winter of 2021-2022 on Mount Washington was unique because it had an uncharacteristic number of rain-on-snow events at all elevations. This section explores two events that demonstrate the value of UAV SfM snow depth change mapping for avalanches. Highly variable snow depth was found in the BSG study area during February because there was a large natural avalanche followed by a widespread rain-on-snow ablation event. These impacts were captured by the UAV SfM. This event is explored in greater detail in section 4.6.1. A substantial snow accumulation event followed by high westerly winds caused large wind slabs to form on steep Tuckerman Ravine terrain at the end of March 2022. The UAV SfM captures the depth and extent of spatially isolated wind slabs throughout the entire Tuckerman Ravine study area. A large natural avalanche also occurred on April 1st which is seen in the April 5th snow depth change map created on April 5th is studied. Section 4.6.2 analyzes this series of events.

4.6.1 February BSG Snow and Rain Event Case Study

Between 2/3/22 and 2/4/22, 21.3 cm (8.4 in) of new snow and 64.4 km/h (40 mph) average wind speeds were recorded by the MWOBS. This weather led to snowpack conditions that caused a large natural avalanche to occur on Hillman's Highway. The avalanche was estimated to have slid 305 vertical meters (1000 ft) which is roughly the entire length of the gully. Before the avalanche, the snowpack did not cover the large car-sized boulders in the lower reaches of the gully. The snow depth change map developed from UAV SfM flights on 2/1/22 and 2/11/22 (Figure 28) shows the location of the avalanche debris post-avalanche. A large positive flux of new snow, ranging from 1.5 to 2 m, is visible at the base of Hillman's Highway. Figure 28A shows this snow depth change. A camera image (courtesy of Brian Post) looking up to the crown line and

path (red outline) of the avalanche in Hillman's Highway is shown in Figure 28B. The avalanche debris, which is the primary contributor to the influx of snow depth increase is delineated. A comparison of orthomosaics from before and after the avalanche clearly shows the increase in snow that covered the large boulders and vegetation that were previously visible (Figure 28C-D).

After the avalanche, a series of minor snow events occurred between 2/11/22 and 2/17/22. On 2/17/22 and 2/18/22, the maximum temperatures were 1.11 °C and 3.33 °C respectively, and 17.78 mm (0.7 in) of rain fell with only 7.62 mm (0.3 in) of snow (MWOBS, 2022). This rapid warming and rain event led to dramatic snowmelt and meltwater channelization in prominent gullies. Excess liquid flow from the Boott Spur Ridge collected in the Hillman's Highway gully and resulted in a rapid snowpack collapse to the ground surface in an isolated pocket near the bottom of the gully. Between 2/11/22 and 2/24/22, which includes the warmup and rain, snowpack decreased across the entire study (Figure 29A). The areas that had the greatest decrease are in the 1220 to 1260 m elevations of the lower snowfield and an isolated area just below the 1260 m contour in Hillman's Highway. The lower region of Lower Snowfield also had more snow depth loss due to the collection of the upslope warm liquid runoff. Outside of the winter, Hillman's Highway is a streambed that typically freezes during the winter. This stream began flowing following rain on 2/17/22 and 2/18/22 which caused a large 2 m section of snow to release. By the 2/24/22 campaign, this stream had refrozen, but the snow void remained. This void is visible in the snow depth change map and camera image taken directly below the feature (Figure 29B).

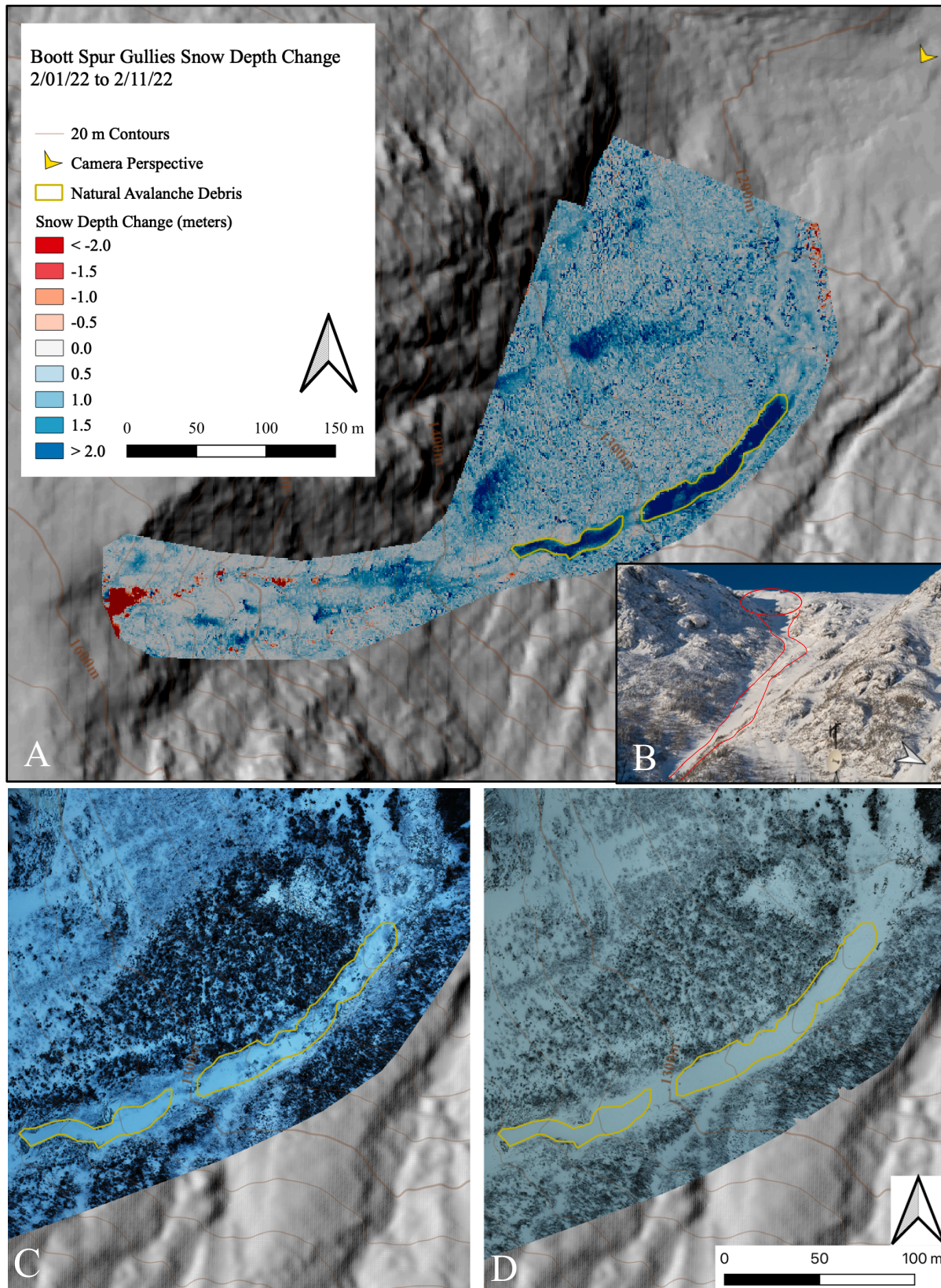


Figure 28: BSG Natural Avalanche Case Study. Snow Depth Change Map after Avalanche (A) Avalanche Crown Line in Hillman's Highway. Credit: Brian Post (B). Orthomosaic Comparison Captured 2/01/22 (C) and 2/11/22 (D) with Avalanche Debris Delineated.

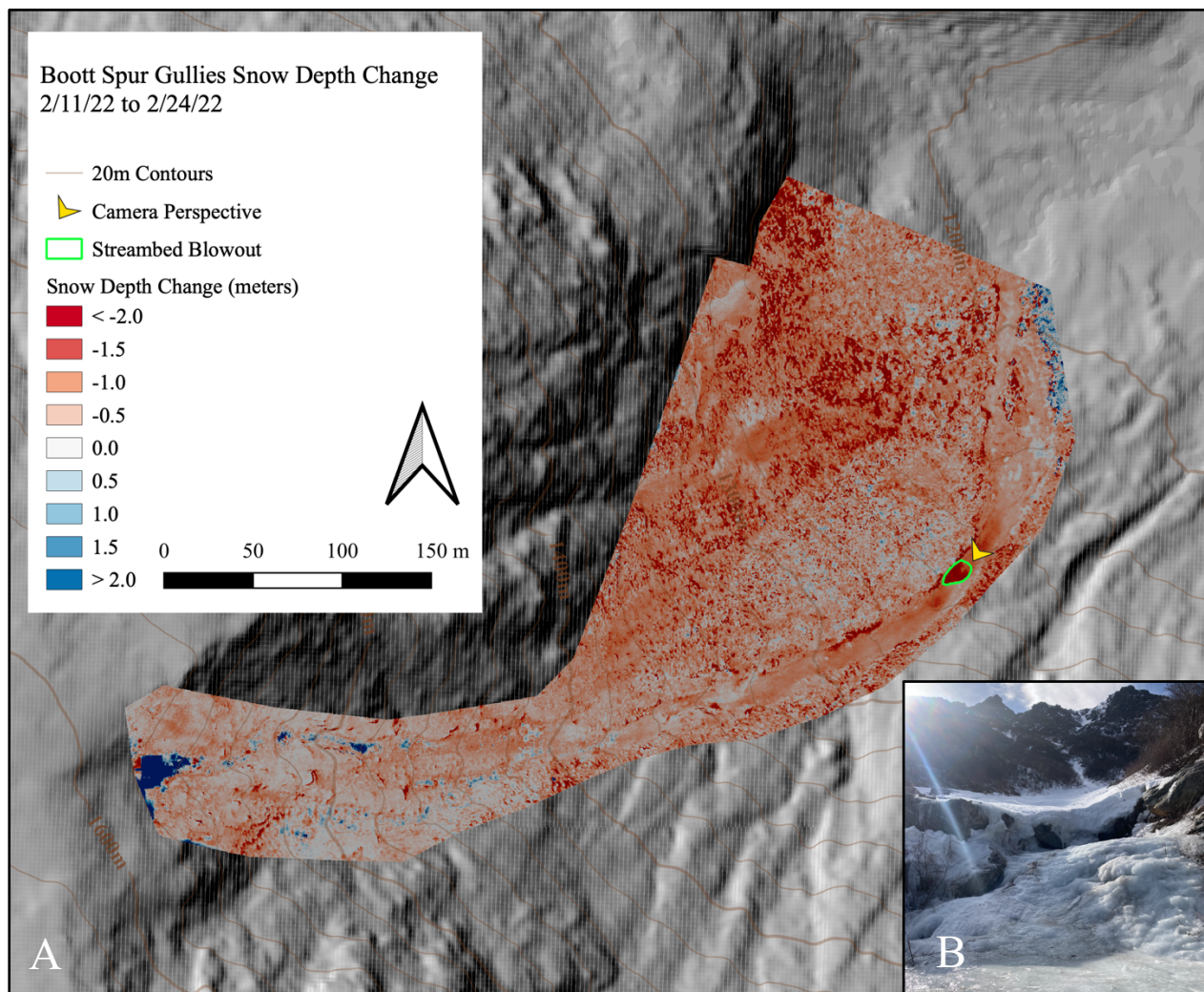


Figure 29: BSG Snow Depth Change After Rain-On-Snow Event (A) with Photograph Taken by Cameron Wagner on 2/24/22 of Extreme Ablation Feature (B)

4.6.2 Late March Tux Wind Slab Formation and 4/01/22 Avalanche Case Study

Wind slabs formed on steep eastern aspect terrain of Tuckerman Ravine in late March. On 3/27/22 there was 12.7 cm (5.0 in) snow accompanied by an average of 56.2 kph (34.9 mph) westerly wind. The slabs hardened and grew during the following three days when the wind gusted to 159.3 kph (99mph) from the west (MWOBS, 2022). The UAV SfM data on 3/23/22 and 3/30/22 isolates these newly formed slabs (Figure 30A). Distinct slabs ranging from 1 to 3 m in depth appear across the headwall area of Tuckerman Ravine. A spatially isolated slab can also be found in the lower section of Left Gully (Figure 30B). This wind slab was photographed from below on March 30th and can be easily distinguished by its color difference. The old surrounding snow surface has a darker shiny tint while the newly drifted wind slab is a bright matte white color. While ground measurements were not possible due to safety and time limitations, UAV SfM could map these wind slabs' depths and extents. An observation was posted to the MWAC website with the wind slab map and brief write-up to inform the public where these slabs reside (Appendix D).

A rain-on-snow event occurred on 3/31/22. This storm system dropped 15 mm (0.59 in) liquid precipitation and had an average temperature of 1.11 °C (34 °F) and a maximum temperature of 6.67 °C (44 °F) (MWOBS, 2022). The sudden warming and influx of liquid to the existing wind slabs created instability. A natural avalanche occurred during the night of 3/31/22 in the headwall area of Tuckerman Ravine. This avalanche was classified as D2 in destructive capability with a one-meter-deep crown line. The next weather window that allowed UAV data collection was 4/05/22. The snow depth change map before and after the avalanche is shown in Figure 31A with optical photographs of the avalanche crown line and debris pile in Figure 31B-C. Inspection of the 3/30/22 to 4/05/22 snow depth change map indicates that the warm precipitation caused widespread ablation resulting in a red hue across the study area. The snow depth change map also

reveals that the area of snow that slid coincides with the wind slab identified in the previous snow depth change map. The change map shows the overall loss of snowpack due to the widespread warm temperatures and rain. The avalanche source area is readily distinguishable as is the avalanche debris pile on the ravine floor (Figure 31A).

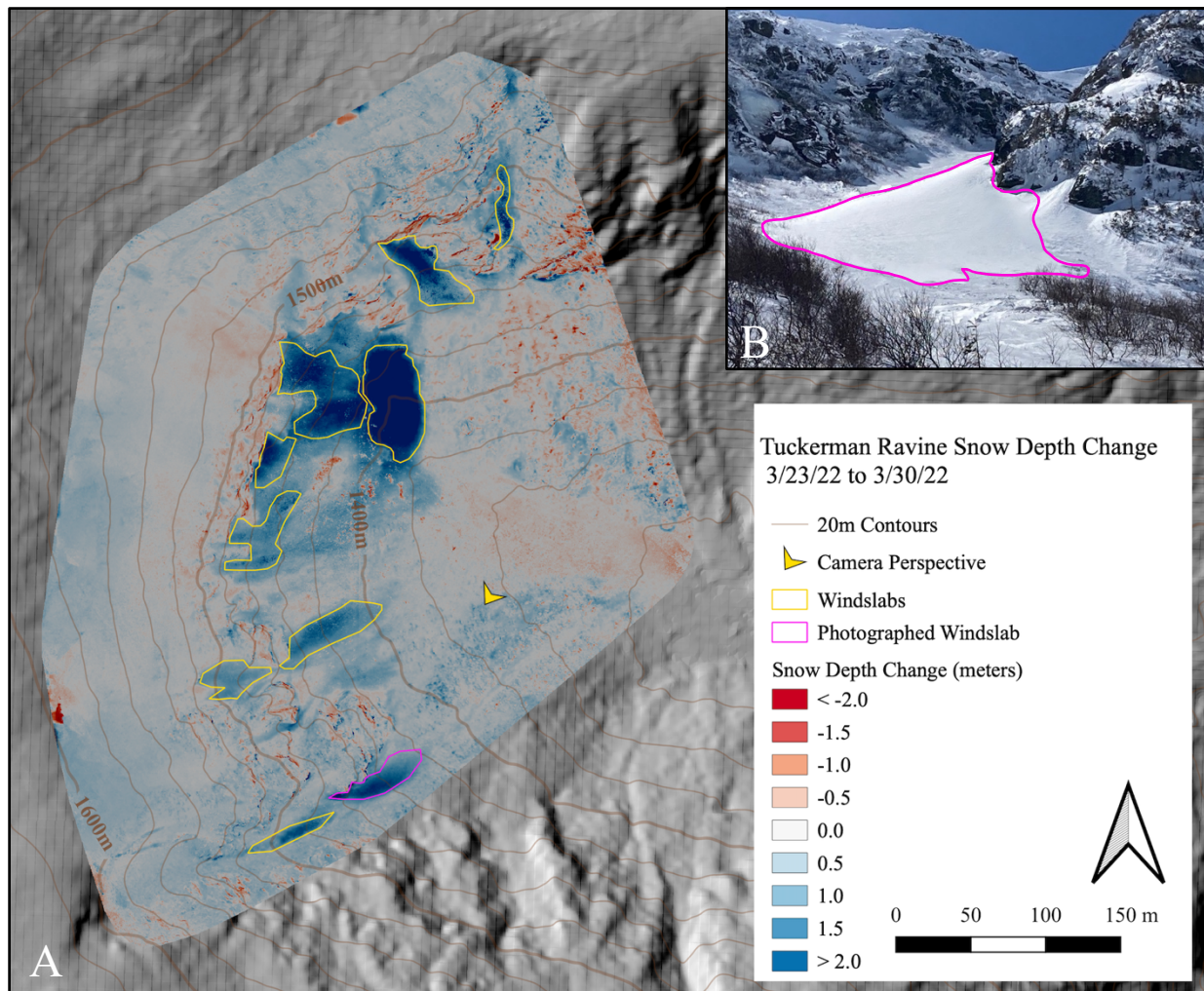


Figure 30: 3/23/22 to 3/30/22 Tuckerman Ravine Wind Slab Snow Depth Change with Delineated Wind Slabs (A) Visual Observation and Delineation of a Wind Slab in the Runout of Left Gully (B) Credit: Cameron Wagner

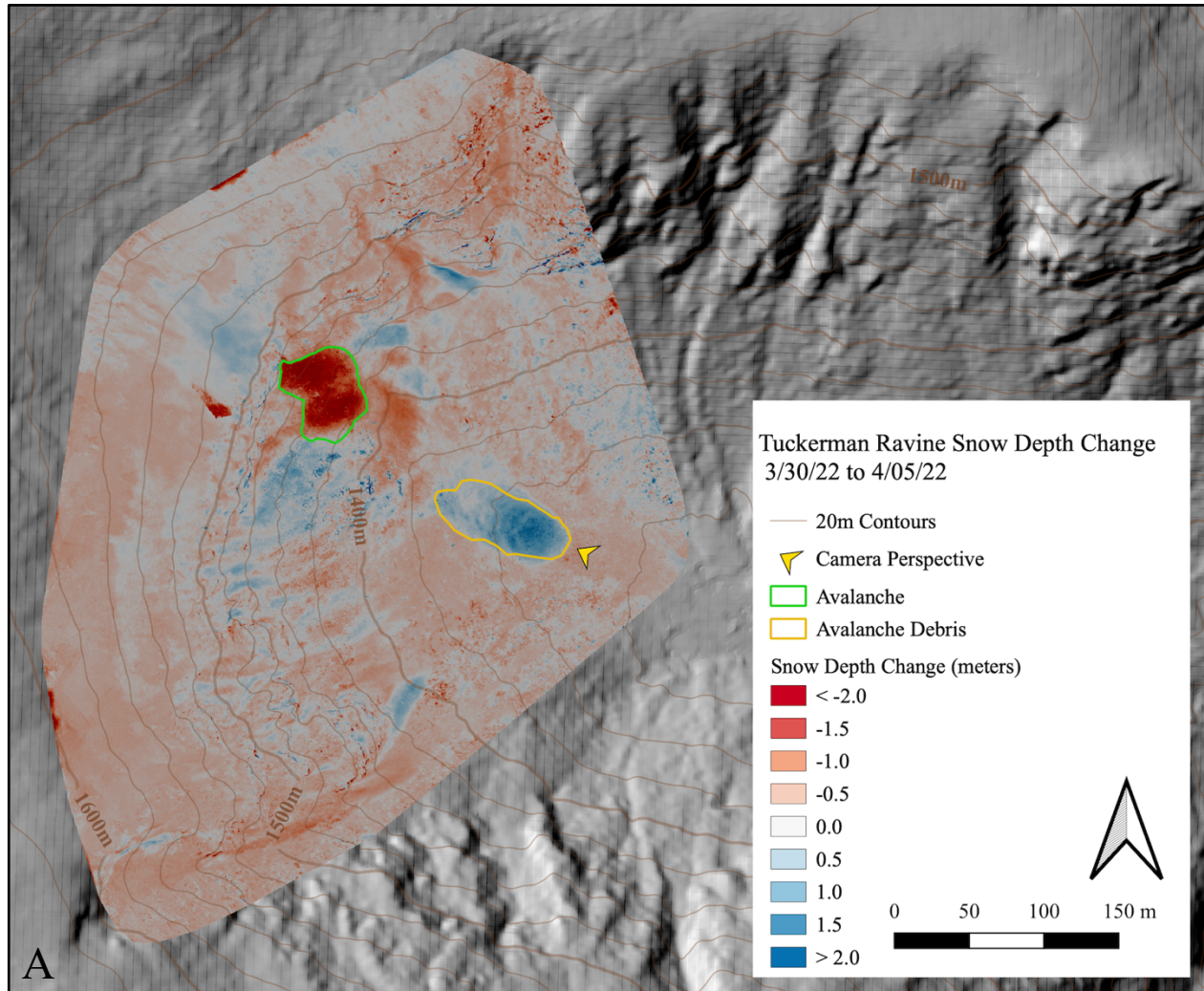


Figure 31: Post-Avalanche Snow Depth Change Map (A) with Camera Images of Avalanche Debris (B) and Avalanche Crown Line (C) Credit: Ryan Lewthwaite (MWAC)

5 CHAPTER 5 – DISCUSSION

5.1 Snow Accumulation Patterns in Tuckerman Ravine and Boott Spur Gullies

Mount Washington's notoriously high winds contribute to large and widespread wind slab production throughout the winter. The aspect and steep geomorphic character of Tuckerman Ravine and Boott Spur Gullies promote wind slab creation mainly from predominant westerly winds. Gullies such as Left Gully, Chute, Chicken Rock Gully, and Hillmans Highway receive the most snow transport due to their shape. The Tuckerman Ravine POI with the deepest observed snow depth, Chicken Rock Gully, has three times more snow than what the MWOBS recorded fell for the study period. This extremely high factor shows how dominant snow transport is in this region. Areas that display the lowest snow depth are highly vegetated areas and talus piles (i.e., Christmas Tree, and Lunch Rocks). Although nearly 6 m of snow was observed to have fallen on the Mount Washington summit, these areas have minimal if not negative snow depths throughout the season. This is likely due to the combination of scouring and the process of filling in the gap between rocks and vegetation. SfM DSMs are accurate to the ground surface and in these regions, obstructions to the true ground depth are present. Filtering to eliminate vegetation and or large rocks would provide a more accurate sense of how much snow is on the ground. For this project, DSMs were selected for analysis in order to study wind slabs, an avalanche problem that is visible on the surface of the snowpack rather than below a vegetation layer.

5.2 UAV and SnowModel Snow Redistribution

The goal of this study was to identify Mount Washington wind slab depth and extent with two novel methodologies: UAV structure from motion (SfM) and SnowModel. SfM is a proven method for measuring snow depth in large open areas with deep snowpacks. Although this study lacked a full ground validation campaign, UAV SfM-derived total snow depth values had a reasonable comparison to manual probing values. RMSE values observed in this study of ~30 cm are similar to those observed in similar UAV SfM snow depth studies with RMSE errors in the range of 8.5 to 115 cm (Avanzi et al., 2018; Harder et al., 2016; Lendzioch et al., 2019; Miller, 2021; Miller et al., 2022). The spatial extent of wind-deposited snow matched visual observations (Figure 30 and Figure 31). A 30 cm error is about 24% of the average depth from delineated wind slabs on 3/30/22 (Figure 30) and only 12% of the average snow depth in Tuckerman Ravine on April 25th (Table 2). This indicates that SfM mapping of wind slab extent is possible, but that depth of wind slabs may be less reliable. Although measuring wind slab area in the field would be an effective means of ground validation of spatial extent, such an effort was not included in this study due to challenging conditions. Regardless, future validation in this region is recommended but should avoid conditions where probing through vegetation is likely to occur as observed on 12/15/21.

SnowModel generated wind slabs by transporting snow from west to east and creating drifts of similar magnitude to the deepest points of Tuckerman Ravine. The widespread snow accumulation and transport patterns of Mount Washington are represented in the model. The deepest drifts reside in areas that are known to remain snow-covered latest into the summer on the mountain. However, local snow depth spatial variations are not well represented by SnowModel. While SnowTran-3D helped to capture the wind redistribution of snow, it was not able to capture

finer details and hyper-local weather variations. In the region with the largest SnowModel snow accumulation, visual observations from the ground show considerable scouring and a lack of snow drift. SnowModel was not able to reconstruct the isolated wind drifts (wind slabs) that exist in Tuckerman Ravine which has rapid shifts in wind and precipitation (Joosen, 2008). The daily meteorological data used to force SnowModel were not able to represent these conditions. Overall, SnowModel does a good job of modeling widespread scour and drift magnitude and extent due to the regions extremely high winds, but it struggles to simulate highly variable surface conditions as observed in situ and by the UAV SfM.

An important limitation of SnowModel for avalanche forecasting is that the model is not able to simulate avalanches and their redistribution of snow. Avalanche slab release and debris piles can cause notable snow depth changes as seen in the UAV snow depth maps. The ability to collect UAV SfM data pre- and post-avalanche could provide training data for SnowModel to identify problem areas or potentially be assimilated into the model for subsequent snow evolution.

5.3 Experimental Error

In the Mount Washington region, meteorologic conditions, and access limit routine UAV data collection. High winds, freezing temperatures, and low cloud ceilings inhibit the routine use of UAVs to map snow. Only 9% of days (17 days) in the 2021 – 2022 winter (181 days) had conditions permitting UAV flights. Other constraints are access and time. The combination of travel time to the trailhead, Pinkham Notch, and a two-hour hike to and from the study areas led to long field days. Flights in the Tuckerman Ravine and BSG study areas take 1.5 hours and 1 hour, respectively. With minimal daylight in the winter (~10 hours), the ability to collect other

observations such as ground-truthing measurements is limited. Because in situ and UAV efforts are both technically and practically challenging, improved snow modeling capabilities in such areas may be a more viable means to categorize conditions.

The UAV-collected SfM produced high-resolution (5 cm) snow depth maps with less than 10 cm GPS error (Table 1). These snow depth maps can readily distinguish where large drifts of snow reside as well as their magnitude without the need to manually measure and be exposed to avalanche risk. The orthomosaic output is useful for visually inspecting surface conditions and identifying avalanche activity (Eckerstorfer & Bühler, 2015; Eckerstorfer et al., 2016). UAV data collection and subsequent SfM outputs are limited by meteorological conditions (i.e., wind, temperature, and cloud cover) as well as UAV flight parameters. The 30 m resolution of the SRTM data used for the base map to enable terrain-following was quite coarse for this study area. Tuckerman Ravine is extremely steep and drops nearly 170 m in elevation over a length of 150 m. Additionally, the SRTM data was captured in February 2000, a time of year that likely had a significant snowpack in this study's area (Farr et al., 2007). The presence of snow when this data was collected would cause a positive bias when compared to a snow-off baseline. When the terrain-following the flight plan was generated with this coarse 30 m resolution base map, the UAV flew much higher above the ground than instructed. This was likely due to the highest elevation in a 30 m grid cell dictating the UAV's height. To combat this and to enable desirable flight elevations of 45 m AGL, the overlap was decreased from 80% to 70%. The lower heights could then be flown at faster speeds. Flying lower has the benefit of greater image resolution and lower ground sampling distance (GSD) (Frey et al., 2018).

An integral part of UAV snow surveying is the element of ground truthing. Manual snow depth measurements distributed across the study area serve as SfM snow depth map validation.

Several limitations prevented carrying out an extensive ground truthing campaign in this study. The first limitation is safety. Traveling and working in avalanche terrain is inherently dangerous and poses a risk while taking snow depth measurements. The next limitation is the presence of thick ice crust layers and extremely dense snow, making probing into the ground difficult if not impossible. Similarly, in order to ground truth snow depth change maps, new snow must be discerned between existing bed surface snow. Upon digging a snow pit on 2/01/2022, newly wind-deposited snow was not distinguishable from the other snow layers within the profile. Although this is not true for all transported snow depositional features, this trial snow pit's location and date were not useful. Finally, depths greater than 3 m are difficult to gather due to conventional avalanche probe lengths only extending to 3 m.

Even for ground observations collected at the study site, a few limitations persist. First, the GPS location of each measurement has a ± 2 m positional error. Second, probe angle in steep terrain can skew the measured depth. To reduce error, the probe was inserted as vertically as possible, but this was not always possible. Last, the presence of sub-snow surface vegetation and impenetrable ice crust layers resulted in both over-probing and under-probing (McGrath et al., 2019; Proulx et al., 2022; Sturm & Holmgren, 2018). When baseline conditions were collected, the digital surface model was created based on the top of all vegetation. When snow falls and compacts this vegetation surface, the surface level appears to decrease according to the total snow depth map. When the vegetation is fully buried, there is still potential to probe through the snowpack and measure deeper to the actual ground surface. While this is an accurate snow depth measurement, the UAV SfM snow depth model will not match this value due to the vegetation surface collected during the baseline. Additionally, rain on snow (ROS) events create a highly saturated snow layer which, when temperatures inevitably drop, becomes a very hard ice crust

layer. ROS events were observed a few times throughout the winter of 2021-2022, with the most notable event on 2/17/22 and 2/18/22. These ice crust layers make probing to ground level difficult, if not entirely impossible.

5.4 SnowModel

The landcover dataset SnowModel uses to determine snow holding depth is the North American Land Change Monitoring System's 2015 30 m dataset (Latifovic et al., 2012). SnowModel assigns a constant snow-holding depth value to each 30 by 30 m grid cell in the study area. Once SnowModel's simulated snow exceeds this snow holding depth value for a given grid cell, the new snow in this grid cell is available for redistribution by the wind. Mount Washington has highly variable land cover which cannot be accurately described at a 30 m resolution. A higher-resolution (<10 m) land cover dataset generated by high-resolution snow-off areal or satellite imagery would likely be more effective in representing this study area's snow-holding characteristics.

SnowModel is typically implemented on large grid cells over large areas such as the catchment or regional scale (Liston et al., 2018; Litherland, 2013; Pedersen et al., 2021; Reynolds et al., 2021; Sawyer, 2007). These studies have validated SnowModel's snow depth output with either in-situ ground measurements, Airborne Snow Observatories (ASO) data, or with other modeled snow depth results. Errors between model and observed snow depth values fluctuate from having an R^2 value of 0 to 0.87 (Litherland, 2013; Pedersen et al., 2021). Willmott statistics between SnowModel and UAV SfM AOIs and POIs resulted in a range of R^2 values from 0 to 0.46 which is in line with the literature. This study's UAV validation data does not share the entire

model domain. Instead, Landsat 8 imagery was used as a comparison for the study region. The NDSI derived from Landsat 8 data showed a substantial difference in SnowModel snow depth present in pixels with NDSI values greater than 0.4. SnowModel can be used on a much larger scale than UAV data without the need for in-situ data collection. This means that snow depth models can be generated for large study areas anywhere in the world. The main disadvantage of SnowModel compared to UAV data is the resolution and accuracy. UAV SfM provides a direct measurement of snow depth in an area while SnowModel produces a model product. Even with the best parameterization, errors and deviations from observed values are inevitable. Fine-scale applications such as wind slab depth and extent for avalanche forecasting, will challenge a model's capabilities and are unlikely to reliably capture these features. The greatest source of error is likely due to the incorrect interpolation of meteorological variables across the domain. Another source of error is due to SnowModel's inability to model snow density as it exists in reality.

SnowModel simulates snow density in several ways. Melt, calculated by the sub-model EnBal (Figure 8), results in liquid in the snowpack and subsequently increases density. Fresh snow is assigned a density value based on the current wet-bulb temperature (Anderson, 1976). Compaction then increases density based on wind speed and current snow density. A wind-related density offset is applied to the temperature-dependent density when wind speeds are greater than 5 m/s (Liston et al., 2007; Liston & Sturm, 1998). Because wind speeds are almost always above 5 m/s in the Mount Washington study area, the snow was simulated to be quite dense (550 kg/m^3). This study did not measure density in-situ to validate density outputs.

SnowModel is highly dependent on meteorological forcing data to determine snow depth and redistribution. Temperature determines if precipitation is liquid or solid. Wind speed is responsible for transporting snow. Precipitation produces snow across the study area. The sub-

model MicroMet (Glen E Liston & Kelly Elder, 2006) uses the Barnes objective analysis scheme to interpolate irregularly spaced input weather station data across a study area. In this study, a single weather station at the highest elevation in the study domain was used for the SnowModel runs. Most previous studies use meteorologic stations at lower elevations than the study domain high point. With only a single station, interpolation will likely be inaccurate when linear lapse rates are applied. Singular value lapse rates are not effective in representing a micro-climate such as Mount Washington because of the highly inconsistent weather patterns. The addition of the Hermit Lake snotel station would provide a second weather station. The Hermit Lake snotel is located at the base of both the Tuckerman Ravine and the Boott Spur Gullies areas (Figure 5). The sub-alpine location of this weather station would provide contrast to the high-elevation, alpine data collected at the MWOBS and likely improve the interpolation of meteorological conditions across the model domain.

5.5 Future Directions

This study is the first to quantify snow depth change and spatial extent of wind-deposited snow on Mount Washington. Additionally, this is the first study attempting to compare modeled snow depth values with those derived from UAV SfM. Based on the findings, there are several areas for improvement. First, a more robust ground truthing campaign should be conducted to validate UAV and SnowModel measurements. The use of permanent snow depth stakes situated around the study area could provide snow measurements without digging snow pits as well as providing high-accuracy GPS locations of sample sites. A high-resolution base map should be uploaded to the DJI flight planning software so that the UAV follows the terrain at a more

consistent elevation. This could be accomplished with an initial baseline digital surface model collected before the snow on flights. Similarly, testing the minimum overlap between photos and maximum flight height and speed to achieve a usable resolution of snow depth products would be useful in decreasing flight times and the resultant temporal burden on the processing workflow due to less input photos.

Further technological advancement in UAV weather resilience (i.e., wind and freezing temperature resistance) will improve the ability to collect routine data in mountainous regions. While this study proved SfM's efficacy, other sensors such as LiDAR, ground penetrating radar (GPR), and synthetic aperture radar (SAR) have been proven to be comparable if not better than SfM in measuring snow (Deems et al., 2013; Jacobs et al., 2021; Proulx et al., 2022; Rott & Mätzler, 1987; Verfaillie et al., 2022; Vergnano et al., 2022). Comparing LiDAR and SfM proves that LiDAR produces high-resolution snow depth maps more effectively (Verfaillie et al., 2022). LiDAR has the advantage of being able to make observations under cloudy conditions, which is useful where there is limited visibility.

There are several ways to improve SnowModel using UAV snow depths. The UAV-gathered snow surface could be used as the snow-surface input for subsequent time step runs. Due to the snow surface depth having a high degree of change, and the inability of SnowModel to completely move drifts when wind speed is above a certain threshold, this could update the model for subsequent drift simulation. While SnowModel is capable of redistributing large amounts of snow in complex terrain, specific customization of this model for specific study areas would help it simulate snow depth closer to actual conditions. For example, to better represent observed snow depths, customization of built-in SnowTran-3D snow transport and accumulation parameters and physics responsible for drifting snow into steep terrain should be explored.

In order to help the Mount Washington Avalanche Center (MWAC) in their avalanche forecast generation, creating a workflow to automatically generate snow depth change maps with SnowModel given weather forecasts distributed by the National Weather Service (NWS) or Mount Washington Observatory (MWOBS) would provide numerical snow depth data. This study proves how useful UAV SfM snow depth data can be for Tuckerman Ravine. To gather visual and snow depth information to add quantitative data in forecast generation, the MWAC should pursue routine UAV flights. Numerical spatial data is also a great resource to share with the public that travels in this terrain.

For those pursuing the modeling of snow in complex alpine terrain with extreme weather, the need for multiple meteorologic stations for model forcing is integral. Reliably capturing the range of weather conditions in the model domain is paramount in effective snow modeling. Additionally, a thorough sensitivity analysis of all parameters that influence snow drift formation and evolution should be carried out to achieve accurate drift placement. Last, high-resolution validation data should be collected for the most accurate model validation for the entire study domain.

6 CHAPTER 6 – CONCLUSION

This research tested the efficacy of UAV SfM-generated total snow depth and snow depth change maps to identify wind slabs' spatial extent and depth in Mount Washington avalanche terrain. A total of 17 UAV campaigns, conducted across two study areas, Tuckerman Ravine, and Boott Spur Gullies, provided 5 cm resolution snow depth maps. Total snow depth maps described widespread accumulation patterns. Snow depth change maps were able to distinguish wind slabs and scour areas. The UAV SfM captured an isolated extreme ablation in the BSG main gully due to a rain-on-snow event. The snow depth change map identified this region with an extreme 2 m loss of snow depth. In Tuckerman Ravine, when 12.7 cm of snowfall occurred during strong 44.7 m/s westerly wind gusts, the SfM snow depth change maps revealed large wind slabs, then depletion after a natural avalanche. The natural avalanche recorded on April 1st shared nearly the same extent and depth as a measured wind slab from the previous UAV SfM snow depth change map.

The collection of UAV SfM data was intended to provide a high-resolution spatially distributed validation dataset for SnowModel. These two snow depth mapping techniques complement each other. To produce wind-transported snow maps, SnowModel, a numerical snow evolution model that uses topography, landcover, and daily meteorological data was employed to reproduce the snow depth maps for the same period as the UAV SfM observation. SnowModel proved to be useful in simulating large-scale snow accumulation features and transport trends on Mount Washington. Model parameterization and refinement are needed to achieve resolution and detail to capture the scour and slab formation revealed using UAV-derived snow depths.

This study piloted UAV data collection on Mount Washington for quantifying wind-distributed snow in avalanche terrain. An effective UAV data collection workflow in hostile alpine environments was developed, tested, and refined. SfM was highly effective in quantifying wind slab depth and extent at high resolutions in highly spatially variable avalanche terrain. SnowModel is a powerful model that is capable of simulating large-scale depositional snow features, but its off-the-shelf use is not recommended for direct wind slab quantification.

LIST OF REFERENCES

- Adams, M. S., Bühler, Y., & Fromm, R. (2018). Multitemporal Accuracy and Precision Assessment of Unmanned Aerial System Photogrammetry for Slope-Scale Snow Depth Maps in Alpine Terrain. *Pure and Applied Geophysics*, 175(9), 3303-3324. <https://doi.org/10.1007/s00024-017-1748-y>
- Allen, K.-U. (2000). AVALANCHE TERRAIN AND CONDITIONS IN THE PRESIDENTIAL RANGE, NEW HAMPSHIRE, USA. Proceedings ISSW,
- Anderson, E. A. (1976). *A point energy and mass balance model of a snow cover*. Stanford University.
- Avanzi, F., Bianchi, A., Cina, A., De Michele, C., Maschio, P., Pagliari, D., Passoni, D., Pinto, L., Piras, M., & Rossi, L. (2018). Centimetric Accuracy in Snow Depth Using Unmanned Aerial System Photogrammetry and a MultiStation. *Remote Sensing*, 10(5), 765. <https://www.mdpi.com/2072-4292/10/5/765>
- Bliss, L. C. (1963). Alpine plant communities of the presidential range, New Hampshire. *Ecology*, 44(4), 678-697.
- Bruland, O., Liston, G. E., Vonk, J., Sand, K., & Killington, A. (2004). Modelling the snow distribution at two high arctic sites at Svalbard, Norway, and at an alpine site in central Norway. *Hydrology Research*, 35(3), 191-208. <https://doi.org/10.2166/nh.2004.0014>
- Brun, E., Martin, E., Simon, V., Gendre, C., & Coleou, C. (1989). An energy and mass model of snow cover suitable for operational avalanche forecasting. *Journal of Glaciology*, 35(121), 333-342.
- CAIC. (2023). *Statistics and Reporting*. Colorado Avalanche Information Center. Retrieved March 25th from <https://avalanche.state.co.us/accidents/statistics-and-reporting>
- CalTopo. (2019). CalTopo. In (Vol. Mobile App). Apple App Store: <http://www.apple.com/itunes/>.
- Crane, P. (2021). *Avalanche Deaths a Tragic Part of Mount Washington History*. Retrieved March 23rd from <https://www.mountwashington.org/windswept/avalanche.aspx>

- Deems, J. S., Painter, T. H., & Finnegan, D. C. (2013). Lidar measurement of snow depth: a review. *Journal of Glaciology*, 59(215), 467-479. <https://doi.org/10.3189/2013JoG12J154>
- Eckerstorfer, M., & Bühler, Y. (2015). Remote Sensing of Snow Avalanches.
- Eckerstorfer, M., Bühler, Y., Frauenfelder, R., & Malnes, E. (2016). Remote sensing of snow avalanches: Recent advances, potential, and limitations. *Cold Regions Science and Technology*, 121, 126-140. <https://doi.org/https://doi.org/10.1016/j.coldregions.2015.11.001>
- Farr, T. G., Rosen, P. A., Caro, E., Crippen, R., Duren, R., Hensley, S., Kobrick, M., Paller, M., Rodriguez, E., Roth, L., Seal, D., Shaffer, S., Shimada, J., Umland, J., Werner, M., Oskin, M., Burbank, D., & Alsdorf, D. (2007). The Shuttle Radar Topography Mission. *Reviews of Geophysics*, 45(2). <https://doi.org/https://doi.org/10.1029/2005RG000183>
- Frey, J., Kovach, K., Stemmler, S., & Koch, B. (2018). UAV Photogrammetry of Forests as a Vulnerable Process. A Sensitivity Analysis for a Structure from Motion RGB-Image Pipeline. *Remote Sensing*, 10(6), 912. <https://www.mdpi.com/2072-4292/10/6/912>
- Gauer, P. (2001). Numerical modeling of blowing and drifting snow in Alpine terrain. *Journal of Glaciology*, 47(156), 97-110. <https://doi.org/10.3189/172756501781832476>
- Gauthier, D., Conlan, M., & Jamieson, B. (2014). Photogrammetry of fracture lines and avalanche terrain: Potential applications to research and hazard mitigation projects. Proceedings, International Snow Science Workshop, Banff,
- Grant, A. N., Pszenny, A. A. P., & Fischer, E. V. (2005). The 1935–2003 Air Temperature Record from the Summit of Mount Washington, New Hampshire. *Journal of Climate*, 18(21), 4445-4453. <https://doi.org/https://doi.org/10.1175/JCLI3547.1>
- Greene, E., Atkins, D., Birkeland, K., Elder, K., Landry, C., Lazar, B., McCammon, I., Moore, M., Sharaf, D., Sterbenz, C., Tremper, B., & Williams, K. (2010). *Snow, Weather, and Avalanches: Observational Guidelines for Avalanche Programs in the United States*.
- Greene, E., Birkeland, K., Elder, K., Johnson, G., Landry, C., McCammon, I., Moore, M., Sharaf, D., Sterbenz, C., & Tremper, B. (2015). New Observation Guidelines for Avalanche Programs in the United States. In: Citeseer.

- Greene, E. M. (1999). *Simulation of Alpine snow distributions in the Northern Colorado Rocky Mountains using a numerical snow-transport model* [Colorado State University].
- Hall, D. K., Riggs, G. A., Salomonson, V. V., DiGirolamo, N. E., & Bayr, K. J. (2002). MODIS snow-cover products. *Remote Sensing of Environment*, 83(1), 181-194.
[https://doi.org/https://doi.org/10.1016/S0034-4257\(02\)00095-0](https://doi.org/https://doi.org/10.1016/S0034-4257(02)00095-0)
- Hammond, J. C., Sexstone, G. A., Putman, A. L., Barnhart, T. B., Rey, D. M., Driscoll, J. M., Liston, G. E., Rasmussen, K. L., McGrath, D., Fassnacht, S. R., & Kampf, S. K. (2023). High Resolution SnowModel Simulations Reveal Future Elevation-Dependent Snow Loss and Earlier, Flashier Surface Water Input for the Upper Colorado River Basin. *Earth's Future*, 11(2), e2022EF003092.
<https://doi.org/https://doi.org/10.1029/2022EF003092>
- Harder, P., Schirmer, M., Pomeroy, J., & Helgason, W. (2016). Accuracy of snow depth estimation in mountain and prairie environments by an unmanned aerial vehicle. *The Cryosphere*, 10(6), 2559-2571. <https://doi.org/10.5194/tc-10-2559-2016>
- Hiemstra, C. A., Liston, G. E., & Reiners, W. A. (2006). Observing, modelling, and validating snow redistribution by wind in a Wyoming upper treeline landscape. *Ecological Modelling*, 197(1), 35-51. <https://doi.org/https://doi.org/10.1016/j.ecolmodel.2006.03.005>
- Jacobs, J. M., Hunsaker, A. G., Sullivan, F. B., Palace, M., Burakowski, E. A., Herrick, C., & Cho, E. (2021). Snow depth mapping with unpiloted aerial system lidar observations: a case study in Durham, New Hampshire, United States. *The Cryosphere*, 15(3), 1485-1500. <https://doi.org/10.5194/tc-15-1485-2021>
- Joosen, C. (2008). The importance of micro-scale avalanche forecasting in Mount Washington's Tuckerman and Huntington Ravines. Proceedings of the 2008 international snow science workshop, September,
- Latifovic, R., Homer, C., Ressler, R., Pouliot, D. A., Hossian, S., Colditz, R., Olthof, I., Chandra, G., & Victoria, A. (2012). North American Land Change Monitoring System. *Remote Sensing of Land Use and Land Cover: Principles and Applications*, 303-324.
<https://doi.org/10.1201/b11964-24>
- Lehning, M., Bartelt, P., Brown, B., Russi, T., Stöckli, U., & Zimmerli, M. (1999). SNOWPACK model calculations for avalanche warning based upon a new network of weather and snow stations. *Cold Regions Science and Technology*, 30(1-3), 145-157.

- Lendzioch, T., Langhammer, J., & Jenicek, M. (2019). Estimating Snow Depth and Leaf Area Index Based on UAV Digital Photogrammetry. *Sensors*, 19(5), 1027.
<https://www.mdpi.com/1424-8220/19/5/1027>
- Liston, G. E., & Elder, K. (2006). A Distributed Snow-Evolution Modeling System (SnowModel). *Journal of Hydrometeorology*, 7(6), 1259-1276.
<https://doi.org/10.1175/jhm548.1>
- Liston, G. E., & Elder, K. (2006). A meteorological distribution system for high-resolution terrestrial modeling (MicroMet). *Journal of Hydrometeorology*, 7(2), 217-234.
- Liston, G. E., Haehnel, R. B., Sturm, M., Hiemstra, C. A., Berezovskaya, S., & Tabler, R. D. (2007). Simulating complex snow distributions in windy environments using SnowTran-3D. *Journal of Glaciology*, 53(181), 241-256.
<https://doi.org/10.3189/172756507782202865>
- Liston, G. E., Polashenski, C., Rösel, A., Itkin, P., King, J., Merkouriadi, I., & Haapala, J. (2018). A Distributed Snow-Evolution Model for Sea-Ice Applications (SnowModel). *Journal of Geophysical Research: Oceans*, 123(5), 3786-3810.
<https://doi.org/https://doi.org/10.1002/2017JC013706>
- Liston, G. E., & Sturm, M. (1998). A snow-transport model for complex terrain. *Journal of Glaciology*, 44(148), 498-516. <https://doi.org/10.3189/S0022143000002021>
- Litherland, T. (2013). *Snow Redistribution Modelling in Alpine Norway: Validation of SnowModel for a wet, high mountain climate*
- Lowe, D. G. (1999, 20-27 Sept. 1999). Object recognition from local scale-invariant features. Proceedings of the Seventh IEEE International Conference on Computer Vision,
- Masný, M., Weis, K., & Biskupič, M. (2021). Application of Fixed-Wing UAV-Based Photogrammetry Data for Snow Depth Mapping in Alpine Conditions. *Drones*, 5(4), 114.
<https://www.mdpi.com/2504-446X/5/4/114>
- McClung, D. M. (2002). The Elements of Applied Avalanche Forecasting, Part II: The Physical Issues and the Rules of Applied Avalanche Forecasting. *Natural Hazards*, 26(2), 131-146. <https://doi.org/10.1023/A:1015604600361>

- McGrath, D., Webb, R., Shean, D., Bonnell, R., Marshall, H.-P., Painter, T. H., Molotch, N. P., Elder, K., Hiemstra, C., & Brucker, L. (2019). Spatially Extensive Ground-Penetrating Radar Snow Depth Observations During NASA's 2017 SnowEx Campaign: Comparison With In Situ, Airborne, and Satellite Observations. *Water Resources Research*, 55(11), 10026-10036. <https://doi.org/https://doi.org/10.1029/2019WR024907>
- Miller, Z. S. (2021). *Quantifying snow depth distributions and spatial variability in complex mountain terrain* Montana State University - Bozeman, College of Letters & Science].
- Miller, Z. S., Peitzsch, E. H., Sproles, E. A., Birkeland, K. W., & Palomaki, R. T. (2022). Assessing the seasonal evolution of snow depth spatial variability and scaling in complex mountain terrain. *The Cryosphere*, 16(12), 4907-4930. <https://doi.org/10.5194/tc-16-4907-2022>
- Mock, C. J., & Birkeland, K. W. (2000). Snow Avalanche Climatology of the Western United States Mountain Ranges. *Bulletin of the American Meteorological Society*, 81(10), 2367-2392. [https://doi.org/10.1175/1520-0477\(2000\)081<2367:Sacotw>2.3.Co;2](https://doi.org/10.1175/1520-0477(2000)081<2367:Sacotw>2.3.Co;2)
- Morin, S., Horton, S., Techel, F., Bavay, M., Coléou, C., Fierz, C., Gobiet, A., Hagenmuller, P., Lafayse, M., Ližar, M., Mitterer, C., Monti, F., Müller, K., Olefs, M., Snook, J. S., van Herwijnen, A., & Vionnet, V. (2020). Application of physical snowpack models in support of operational avalanche hazard forecasting: A status report on current implementations and prospects for the future. *Cold Regions Science and Technology*, 170, 102910. <https://doi.org/https://doi.org/10.1016/j.coldregions.2019.102910>
- MWOBS. (2022). *Monthly F6 Reports*. Mount Washington Observatory Retrieved March, 30th from <https://www.mountwashington.org/experience-the-weather/mount-washington-weather-archives/monthly-f6.aspx>
- MWOBS. (2023). *Normal, Means, and Extremes*. Mount Washington Observatory. Retrieved March 24th from <https://www.mountwashington.org/experience-the-weather/mount-washington-weather-archives/normals-means-and-extremes.aspx>
- Olefs, M., Schöner, W., Suklitsch, M., Wittmann, C., Niedermoser, B., Neururer, A., & Wurzer, A. (2013). SNOWGRID—A new operational snow cover model in Austria. International Snow Science Workshop Grenoble—Chamonix Mont-Blanc,
- Pedersen, S. H., Bentzen, T. W., Reinking, A. K., Liston, G. E., Elder, K., Lenart, E. A., Prichard, A. K., & Welker, J. M. (2021). Quantifying effects of snow depth on caribou winter range selection and movement in Arctic Alaska. *Movement Ecology*, 9(1), 1-24.

- Peitzsch, E. H., Hendrikx, J., & Fagre, D. B. (2016). Using structure from motion photogrammetry to examine glide snow avalanches. Proceedings of the International Snow Science Workshop, Breckenridge, Colorado, USA,
- Proulx, H., Jacobs, J. M., Burakowski, E. A., Cho, E., Hunsaker, A. G., Sullivan, F. B., Palace, M., & Wagner, C. (2022). Comparison of in-situ snow depth measurements and impacts on validation of unpiloted aerial system lidar over a mixed-use temperate forest landscape. *The Cryosphere Discuss.*, 2022, 1-20. <https://doi.org/10.5194/tc-2022-7>
- Reynolds, D. S., Pflug, J. M., & Lundquist, J. D. (2021). Evaluating Wind Fields for Use in Basin-Scale Distributed Snow Models. *Water Resources Research*, 57(2), e2020WR028536. <https://doi.org/10.1029/2020WR028536>
- Riggs, G. A., Hall, D. K., & Salomonson, V. V. (1994). A snow index for the Landsat thematic mapper and moderate resolution imaging spectroradiometer. Proceedings of IGARSS'94-1994 IEEE International Geoscience and Remote Sensing Symposium,
- Rott, H., & Mätzler, C. (1987). Possibilities and Limits of Synthetic Aperture Radar for Snow and Glacier Surveying. *Annals of Glaciology*, 9, 195-199. <https://doi.org/10.3189/S0260305500000604>
- Saloranta, T. (2012). Simulating snow maps for Norway: description and statistical evaluation of the seNorge snow model. *The Cryosphere*, 6(6), 1323-1337.
- Sawyer, A. E. (2007). *Snowpack depletion modeling using Fast All-season Soil STrength (FASST) and SNOWMODEL in a high-elevation, high relief catchment in the central Rocky Mountains* Colorado State University].
- Schweizer, J., Jamieson, B., & Schneebeli, M. (2003). Snow avalanche formation. *Reviews of Geophysics*, 41, 1016. <https://doi.org/10.1029/2002RG000123>
- Schweizer, J., & Jamieson, J. B. (2001). Snow cover properties for skier triggering of avalanches. *Cold Regions Science and Technology*, 33(2), 207-221. [https://doi.org/10.1016/S0165-232X\(01\)00039-8](https://doi.org/10.1016/S0165-232X(01)00039-8)
- Seidel, T. M., Weihrauch, D. M., Kimball, K. D., Pszenny, A. A. P., Soboleski, R., Crete, E., & Murray, G. (2009). Evidence of Climate Change Declines with Elevation Based on Temperature and Snow Records from 1930s to 2006 on Mount Washington, New Hampshire, U.S.A. *Arctic, Antarctic, and Alpine Research*, 41(3), 362-372. <https://doi.org/10.1657/1938-4246-41.3.362>

- Smith, A. A. (1982). The Mt. Washington Observatory Celebrates 50 Years of the: "Worst Weather in the World". *Weatherwise*, 35(4), 164-168.
- Stempfhuber, W., & Buchholz, M. (2012). A PRECISE, LOW-COST RTK GNSS SYSTEM FOR UAV APPLICATIONS. *Int. Arch. Photogramm. Remote Sens. Spatial Inf. Sci.*, XXXVIII-1/C22, 289-293. <https://doi.org/10.5194/isprsarchives-XXXVIII-1-C22-289-2011>
- Sturm, M., & Holmgren, J. (2018). An Automatic Snow Depth Probe for Field Validation Campaigns. *Water Resources Research*, 54(11), 9695-9701. <https://doi.org/https://doi.org/10.1029/2018WR023559>
- Verfaillie, M., Cho, E., Dwyre, L., Khan, I., Wagner, C., Jacobs, J. M., & Hunsaker, A. G. (2023). *UAS Remote Sensing Applications to Cold Region Weather Disasters* [Review].
- Verfaillie, M., Cho, E., Jacobs, J. M., Hunsaker, A., Sullivan, F., Palace, M. W., Burakowski, E., & Wagner, C. (2022). *Fine scale characterization of snowpack evolution using unpiloted aerial system lidar and SfM photogrammetry*.
- Vergnano, A., Franco, D., & Godio, A. (2022). Drone-Borne Ground-Penetrating Radar for Snow Cover Mapping. *Remote Sensing*, 14(7), 1763. <https://www.mdpi.com/2072-4292/14/7/1763>
- Westoby, M. J., Brasington, J., Glasser, N. F., Hambrey, M. J., & Reynolds, J. M. (2012). 'Structure-from-Motion' photogrammetry: A low-cost, effective tool for geoscience applications. *Geomorphology*, 179, 300-314. <https://doi.org/https://doi.org/10.1016/j.geomorph.2012.08.021>

APPENDIX A – USDA WMNF RESEARCH PERMIT



United States
Department of
Agriculture

Forest
Service

White Mountain National Forest

71 White Mountain Drive
Campton, NH 03223
603-536-6100

File Code: 4080
Date: December 8, 2021

Cameron Wagner
1 Church St. Apt 2
Newmarket, NH 03857

Dear Cameron,

Thank you for contacting us regarding your request to research the use of Unmanned Aerial Vehicles (UAV) to map snowpack dynamics in the Tuckerman Ravine and Boott Spur gullies sections of Mount Washington. This letter will serve to authorize your research proposal to use a DJI Phantom 4 RTK UAV to collect images of the project area to process and create 3D snow elevation maps that can be used for gaining knowledge of how snow accumulates in the area. This data collection technique will be used in conjunction with other field measurement techniques and historical data. Ground truthing measurements will be taken with a digital snow penetrometer, and avalanche probe. The project entails the following:

- Develop flight plan to map area of interest using DJI proprietary software.
- Survey ground control points for georeferencing during post processing with RTK GPS.
- Conduct flight to gather images.
- Conduct second flight to visually inspect slope for possible failure points.
- Return to project site after snowfall.
- Repeat flights and survey to compare to baseline conditions.
- Collect snow depth measurements in a variety of locations to prove accuracy of generated model.

Your research proposal is approved with the following stipulations:

- Per Federal Aviation Administration (FAA) regulations, The UAV operator must be licensed with the FAA.
- Minimize any landing of the UAV in the alpine zone or near any structures.
- Limit impacts to sensitive alpine vegetation when traveling within and between study sites by walking on rocks when possible, avoiding trampling of exposed vegetation in winter, avoiding impacts on wet or moist sensitive soils and vegetation that is exposed as snow melts, and avoiding reinforcement of bootleg trails within the study area. A high concentration of rare plants occurs in ravines and gullies that skiers frequent and are also likely plant-host locations for the White Mountain Fritillary and White Mountain Butterfly.



Caring for the Land and Serving People

Printed on Recycled Paper



- If possible, avoid flying the UAV between May 15 and August 15 during Bicknell's Thrush nesting season. If flying is necessary, avoid flying close to the tops of spruce-fir vegetation.
- UAV may not be used in any areas designated as Wilderness. The South Snowfields track, near the Glen Boulder track, is near the Dry River-Presidential Range Wilderness. Overflight into any designated Wilderness is prohibited.

The landing of a UAV within the alpine zone or within ¼ mile of trails, trailheads, shelters, cabins, and developed recreation sites is prohibited under Forest Supervisor Order R9-22-19-01, unless specific permission is granted. This research approval letter serves as your permission to allow research UAV flights only and must be carried with you while using the UAV.

This permit is valid through December 31, 2022. Should you require an extension or change to the activities listed above please contact us.

We look forward to reviewing your results. Please forward to us any future publications that involve this research. We appreciate your efforts, and any information you can provide us will help us make better decisions on forest management in the future.

You assume any risks associated with your work. During the current pandemic, you must ensure your operations are consistent with the applicable Centers for Disease Control and Prevention guidelines and comply with applicable state and local requirements. Before operating, you are asked to develop and implement COVID-19 best practices for your work consistent with applicable federal, state and local requirements. These best practices do not need to be submitted for approval or acceptance.

Feel free to contact Landon Gryczkowski, Forest Hydrologist (landon.gryczkowski@usda.gov), or Erica Roberts, Ecologist and Forest Research Coordinator (erica.roberts@usda.gov), if you have any further questions.

Sincerely,

X DEREK
IBARGUEN

Digitally signed by
DEREK IBARGUEN
Date: 2021.12.08
08:25:31 -05'00'

DEREK J.S. IBARGUEN
Forest Supervisor

Figure A.1: United States Forest Service White Mountain National Forest Research Permit

APPENDIX B – GROUND SAMPLING LOCATIONS

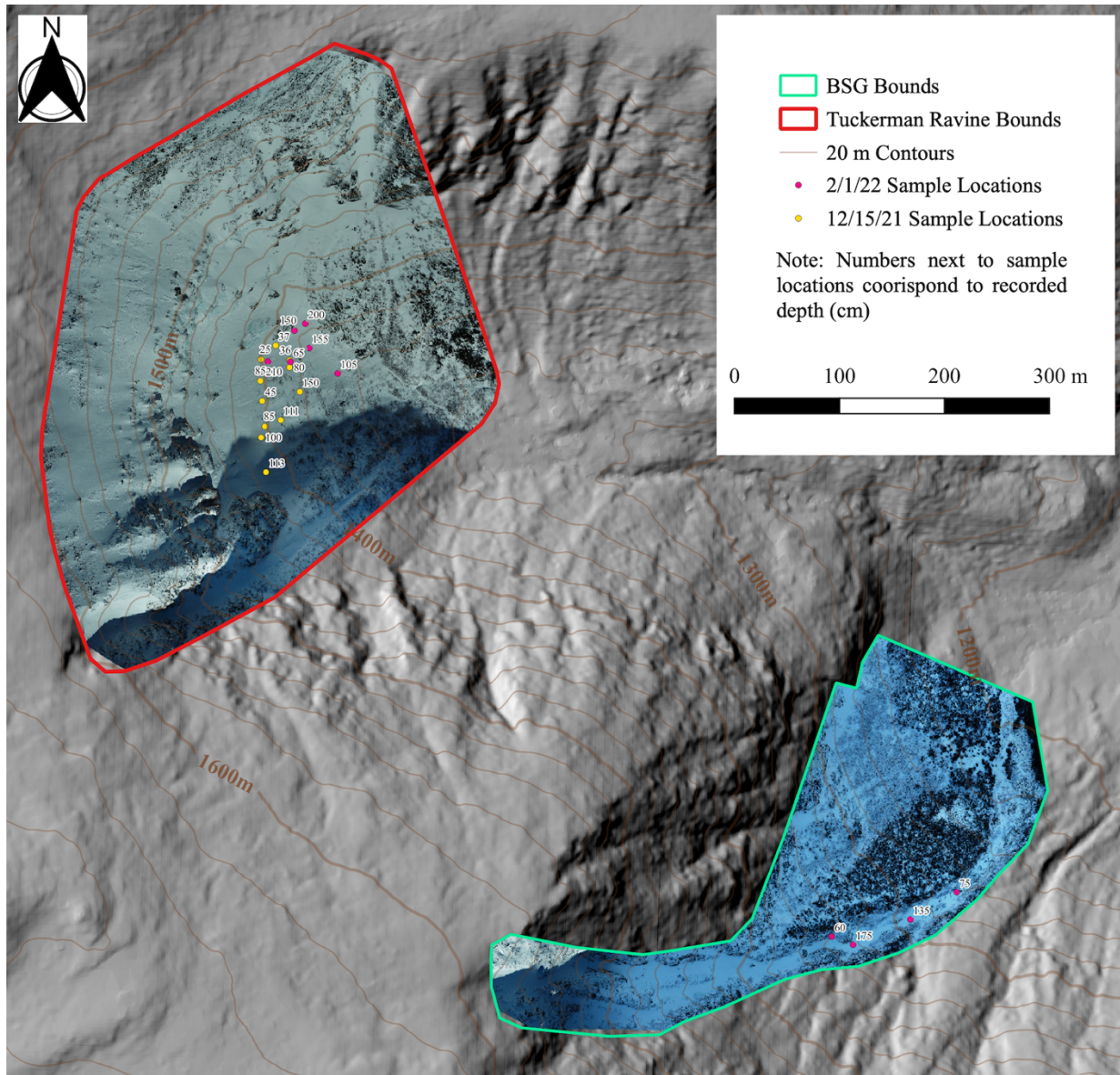


Figure A.2: Ground Sampling Campaign Locations by Date

APPENDIX C – WEB ODM REPORT AND SETTINGS FOR TUX MARCH 9TH

ODM Quality Report

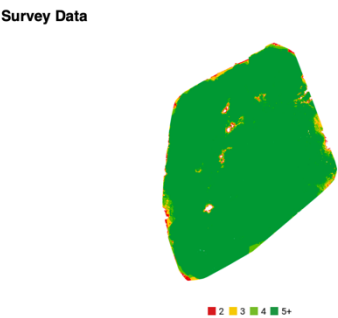
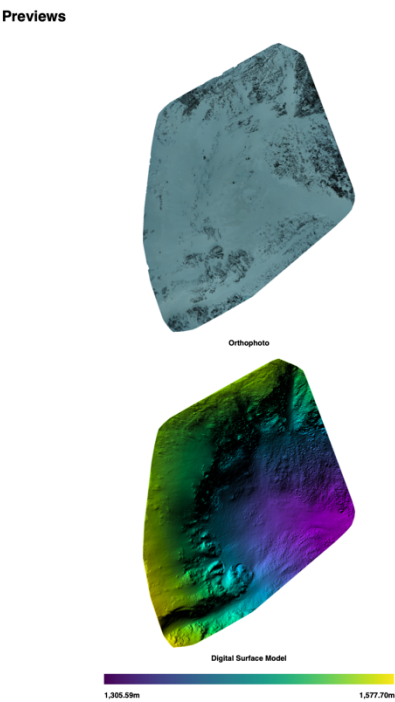
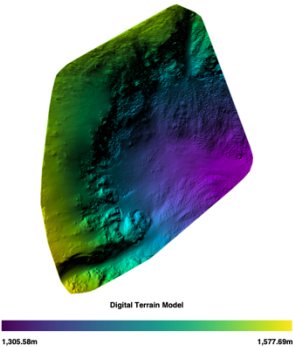
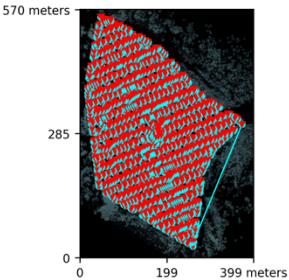
Processed with ODM version 2.6.7

Dataset Summary

Date	14/03/2022 at 06:14:39
Area Covered	0.186834 km²
Processing Time	6.0h:17.0m:12.0s
Capture Start	09/03/2022 at 10:41:27
Capture End	09/03/2022 at 12:14:31

Processing Summary

Reconstructed Images	1470 over 1470 shots (100.0%)
Reconstructed Points (Sparse)	1673540 over 1746506 points (95.8%)
Reconstructed Points (Dense)	165,970,853 points
Average Ground Sampling Distance (GSD)	2.5 cm
Detected Features	10,573 features
Reconstructed Features	7,109 features
Geographic Reference	GPS
GPS errors	0.03 meters



GPS/GCP/3D Errors Details

GPS	Mean	Sigma	RMS Error
X Error (meters)	-0.001	0.014	0.014
Y Error (meters)	0.000	0.012	0.012
Z Error (meters)	0.002	0.025	0.025
Total			0.027

3D	Mean	Sigma	RMS Error
X Error (meters)	0.117	0.258	0.283
Y Error (meters)	0.136	0.276	0.308
Z Error (meters)	0.250	0.461	0.525
Total			0.332

	Absolute	Relative
Horizontal Accuracy CE90 (meters)	0.029	0.597
Vertical Accuracy LE90 (meters)	0.037	0.629

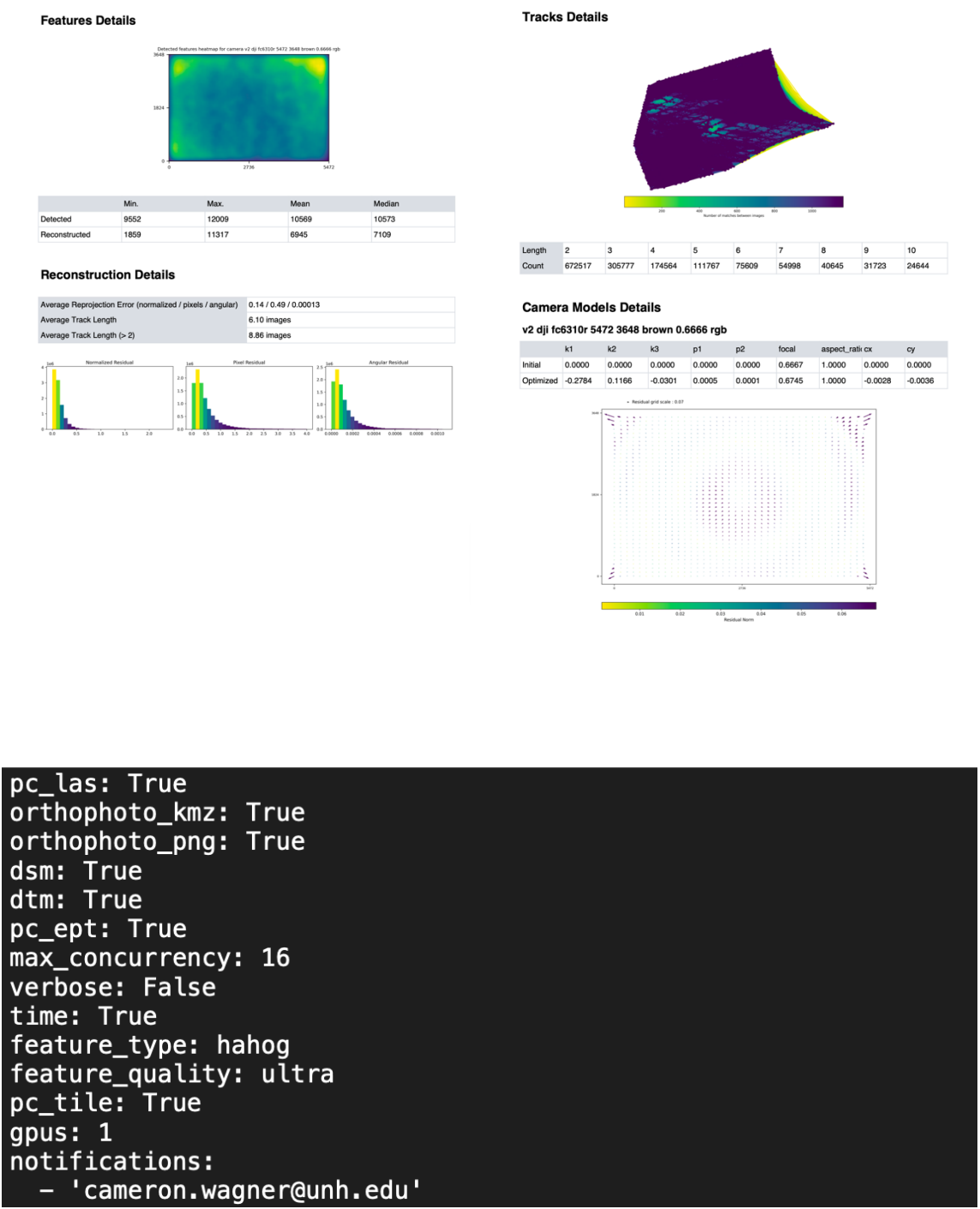


Figure A.3: Open Drone Map Sample Processing Report and Input Parameters

APPENDIX D – PUBLIC OUTREACH AND MOUNT WASHINGTON AVALANCHE CENTER (MWAC) INVOLVEMENT

Mount Washington is home to the only US-based avalanche center east of the Rocky Mountains. The Mount Washington Avalanche Center (MWAC) is a division of the United States Forest Service's Androscoggin Ranger District based in Gorham, New Hampshire. The MWAC is responsible for providing daily avalanche forecasts for the public who access Mount Washington avalanche terrain. The team of snow rangers makes frequent trips into the forecast area to make snowpack and weather observations that help guide forecast generation.

Wind slab depth and extent maps were shared with avalanche forecasters to help supplement field observations and generate successive avalanche forecasts. Similarly, these maps will be posted to the MWAC public observations website where the public can view and use the maps as another tool in their backcountry travel decision-making process.

An app was created in the Google Earth Engine code editor to share this data with the public in an intuitive manner. Google Earth Engine is an open-source coding platform that specialized in geospatial data representation and analysis. The first step in creating a Google Earth Engine app for the public to view is to upload data as an asset. Google Earth Engine requires the naming convention to go without spaces. Assets must be made available to share with everyone in the settings so that anyone can view the file. A Google Earth Engine app example code called forest change viewer served as a great reference point for the early workings of this project. Similarly, Lab 13 in Dr. Michael Palace's remote sensing class provided a framework for the split panel maps. In total four apps have been created to distribute photogrammetry data. The first of these maps show the total snow depth across the two study areas. This map has a consistent visualization parameter so that straightforward comparison can occur between subsequent models.

The next app is the snow depth change visualizer. This app is equipped with a date change selector to toggle between different dates with available data. Other features included with this, and the total snow depth map are an inspector tool to find exact point measurements, opacity sliders to compare with the satellite base map, and a 100 ft contour line toggle button. These features help the viewer get a context of what the terrain is around the study area. The last two apps made for this project are orthophoto viewer programs that utilize a slider to visually compare collection dates to one another.

LINK: <https://cameronwagner521.users.earthengine.app/view/mount-washington-east-total-snow-depth-visualizer>

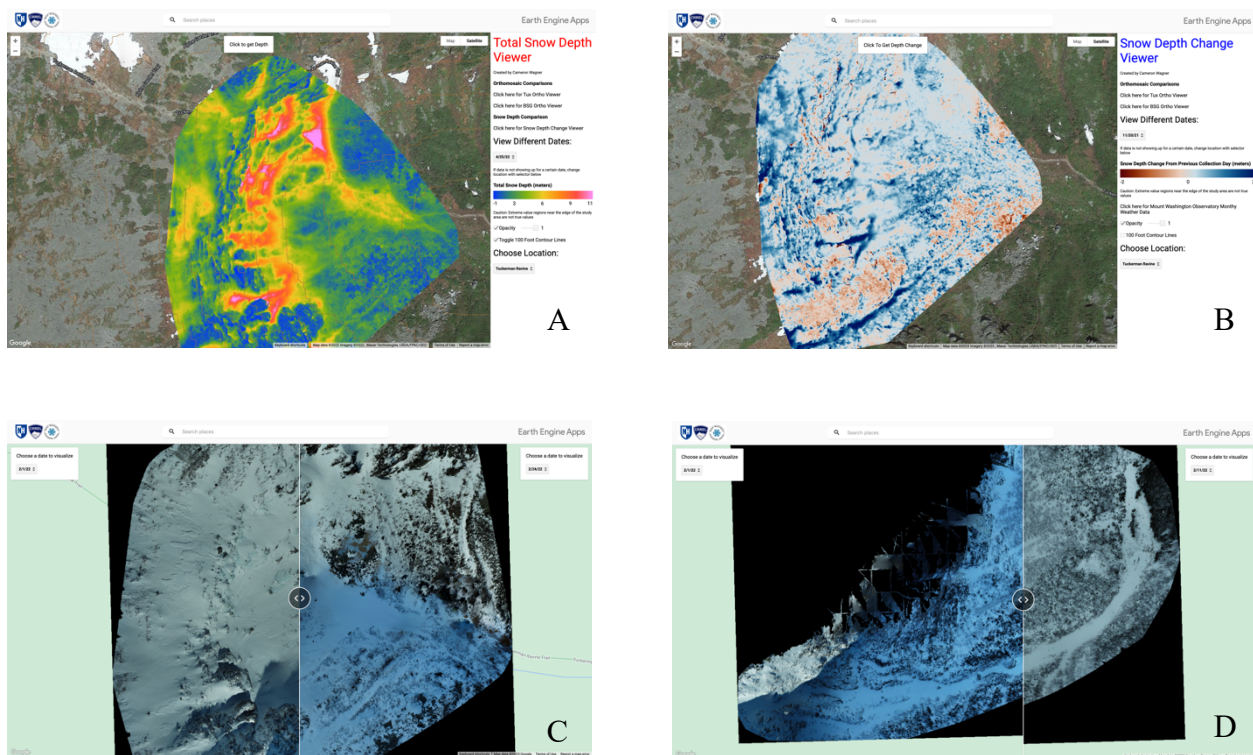



Figure A.4: GEE Products A. Total Snow Depth Viewer B. Snow Depth Change Viewer C. Tux Ortho Viewer D. BSG Ortho Viewer






Mount Washington

Avalanche Center

[Forecasts](#)
[Weather](#)
[Observations](#)
[Learn](#)
[News](#)
[About](#)

[Donate](#)

Q

OBSERVATIONS

Tuckerman Ravine Wind Slab Depth as of March 30, 2022

March 31, 2022 at 1:00 PM

Name: [Cameron Wagner](#) | [University of New Hampshire](#)

Location: Tuckerman Ravine Wind Slab Depth as of March 30, 2022

The past two Wednesday's have offered optimal conditions to collect photogrammetry data. Attached is the snow depth change map in meters from March 23rd to 30th. The six inches of recently accumulated snow from this past Sunday was heavily wind affected and formed large dense windslabs shown in blue in the depth map. These slabs vary in depth but are typically at least 3 feet thick where the map is the darkest blue.

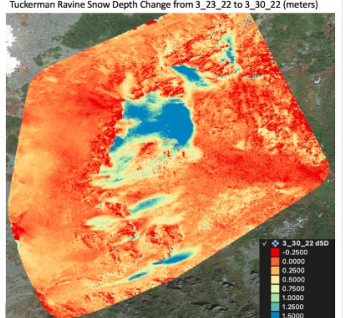
The aim of this data is to be used as yet another tool in backcountry travelers' decision making. Due to the difference in surface appearance between rotten frozen ice/snow and fresh windslab, problem areas can be defined easily in the field. This is the first attempt at quantifying the exact spatial extent and depth of these slabs remotely, something that would be quite difficult on the ground. I plan on incorporating a numerical model that simulates snow transport and accumulation so that given input MWOBs meteorological values, similar models can be made without the need to fly a drone.

Thank you for all who have stopped to talk when I am flying at connection cache.

Feel free to reach out to me with any further questions or comments.
cameron.wagner@unh.edu

Special thanks to ERDC CRREL for web based structure from motion processing workflow.

Tuckerman Ravine Snow Depth Change from 3_23_22 to 3_30_22 (meters)



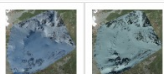


Figure A.5: Wind Slab Notification Observation Posted to the MWAC's Public Observation Website on March 31st, 2022.






Figure A.6: Backpack with UAV Data Collection Gear Backpack Mounted (A) and USFS Snowmobile Mounted (B)

97

APPENDIX E – SNOWMODEL PARAMETERS

```

snowmodel.par
nx =      3028
ny =      4310
deltax =   1.00000000
deltay =   1.00000000
xmn =  314960.69799999997
ymn =  4902030.7039999999
dt =   86400.0000
iyear_init =      2021
imonth_init =      10
iday_init =       27
xhour_init =  12.0000000
max_iter =      181
isingle_stn_flag =      1
igrads_metfile =      0
met_input_fname =      met/stations/mk_micromet_input_file/met_station_daily.dat
undef = -9999.00000
ascii_topoveg =   0.00000000
topoveg_fname = topo_vege/NoAm_30m/topo_vege.gdat
topo_ascii_fname = xxxxxx
veg_ascii_fname = xxxxxx
veg_shd_25 =  0.100000001
veg_shd_26 =  0.100000001
veg_shd_27 =  0.100000001
veg_shd_28 =  0.100000001
veg_shd_29 =  0.100000001
veg_shd_30 =  0.100000001
const_veg_flag =   0.00000000
iveg_ht_flag =      0
xlat =  45.1199989
lat_solar_flag =      0
UTC_flag =   0.00000000
run_micromet =   1.00000000
run_enbal =   1.00000000
run_snowpack =   1.00000000
run_snowtran =   1.00000000
irun_data_assim =      0
ihrestart_flag =      -2
i_dataassim_loop =      1
ihrestart_inc =      0
i_tair_flag =      1
i_rh_flag =      1
i_wind_flag =      1
i_solar_flag =      1
i_longwave_flag =      1
i_prec_flag =      1
ifill =      1
iobsint =      0
dn =   1.00000000
barnes_lg_domain =   0.00000000
n_stns_used =      4
snowmodel_line_flag =   0.00000000
check_met_data =   1.00000000
curve_len_scale =  300.000000
slopetw =  0.579999983
curvetw =  0.419999987
curve_lg_scale_flag =   0.00000000
windspd_min =  0.100000001
lapse_rate_user_flag =      0
iprecip_lapse_rate_user_flag =      0
iprecip_scheme =      1
snowfall_frac =   3.00000000
wind_lapse_rate =  100.000000
calc_subcanopy_met =   1.00000000
gap_frac =  0.200000003
cloud_frac_factor =   1.00000000

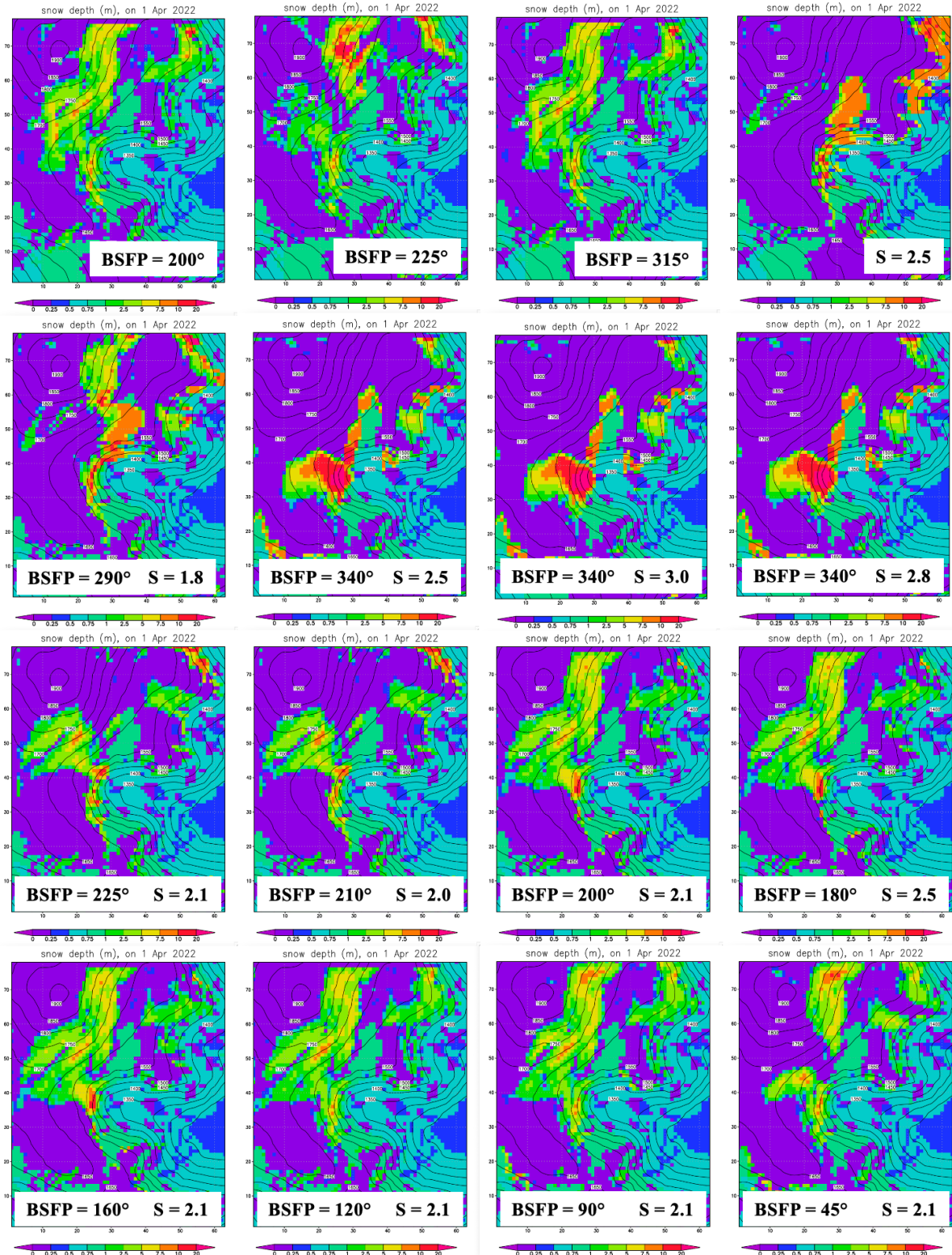
```

```

use_shortwave_obs = 0.00000000
use_longwave_obs = 0.00000000
use_sfc_pressure_obs = 0.00000000
cf_precip_flag = 0.00000000
Utau_t_flag = 1.00000000
Utau_t_const = 0.25000000
subgrid_flag = 1.00000000
tabler_dir = 140.000000
slope_adjust = 2.09999990
twolayer_flag = 1.00000000
bc_flag = 0.00000000
ht_windobs = 10.0000000
ht_rhobs = 10.0000000
ro_snow = 300.000000
snow_d_init_const = 0.00000000
topoflag = 1.00000000
icond_flag = 0
albedo_snow_forest = 0.449999988
albedo_snow_clearing = 0.600000024
albedo_glacier = 0.400000006
sfc_sublim_flag = 1.00000000
multilayer_snowpack = 0
tsls_threshold = 24.0000000
max_layers = 1
dz_snow_min = 1.00000005E-03
izero_snow_date = 90100
seaice_run = 0.00000000
print_micromet = 0.00000000
micromet_output_fname = outputs/micromet.gdat
print_snowtran = 0.00000000
snowtran_output_fname = outputs/snowtran.gdat
Tabler_1_flag = 1.00000000
tabler_sfc_path_name = outputs/
Tabler_2_flag = 0.00000000
print_enbal = 0.00000000
enbal_output_fname = outputs/enbal.gdat
print_snowpack = 0.00000000
snowpack_output_fname = outputs/snowpack.gdat
print_multilayer = 0.00000000
multilayer_output_fname = outputs/multilayer.gdat
print_user = 1.00000000
print_inc = 1.00000000
output_path_wo_assim = outputs/wo_assim/
output_path_wi_assim = outputs/wi_assim/

```

APPENDIX F – BLOWING SNOW FLUX ADJUSTMENT PARAMETER AND TABLER SLOPE ADJUSTMENT SCALING FACTOR TESTING



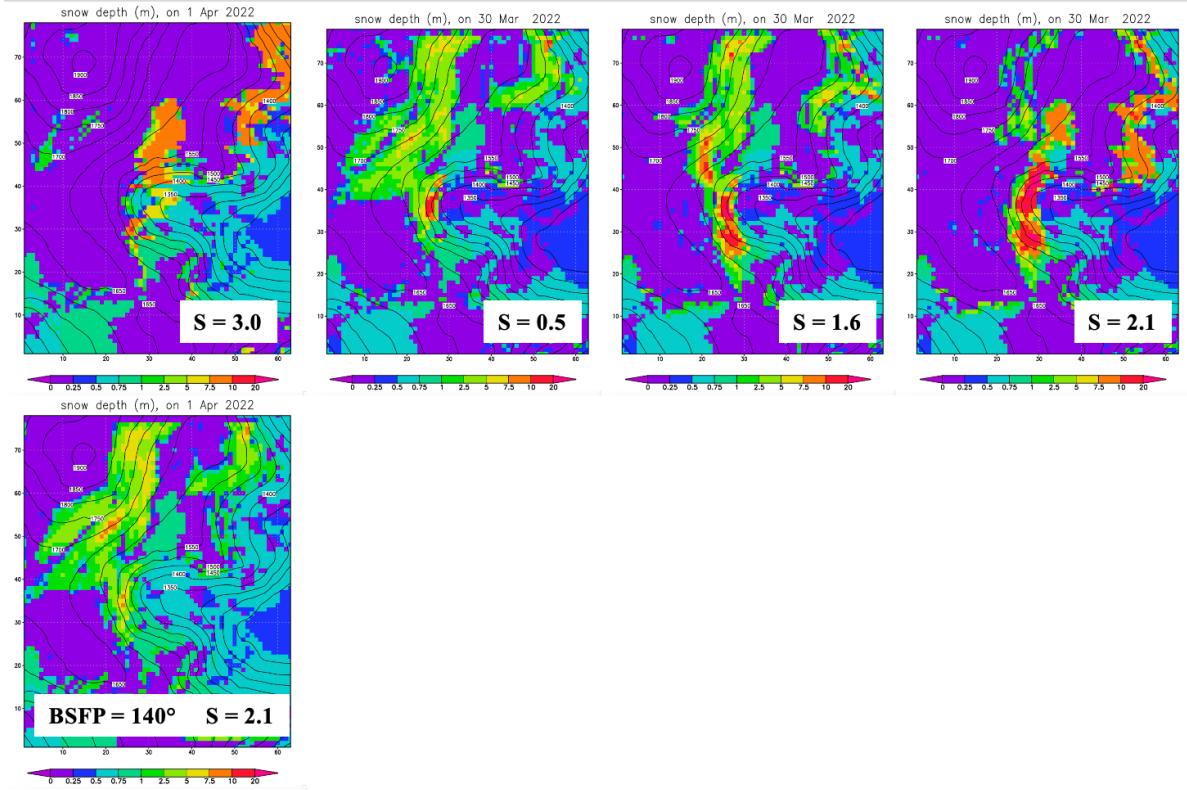
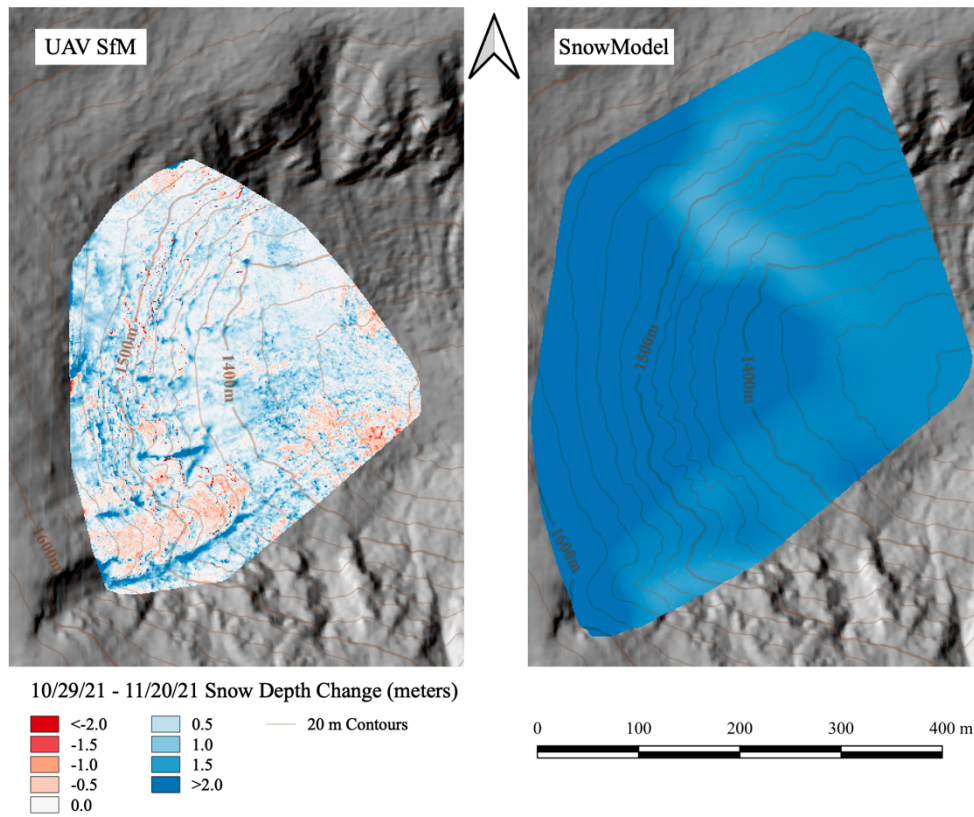
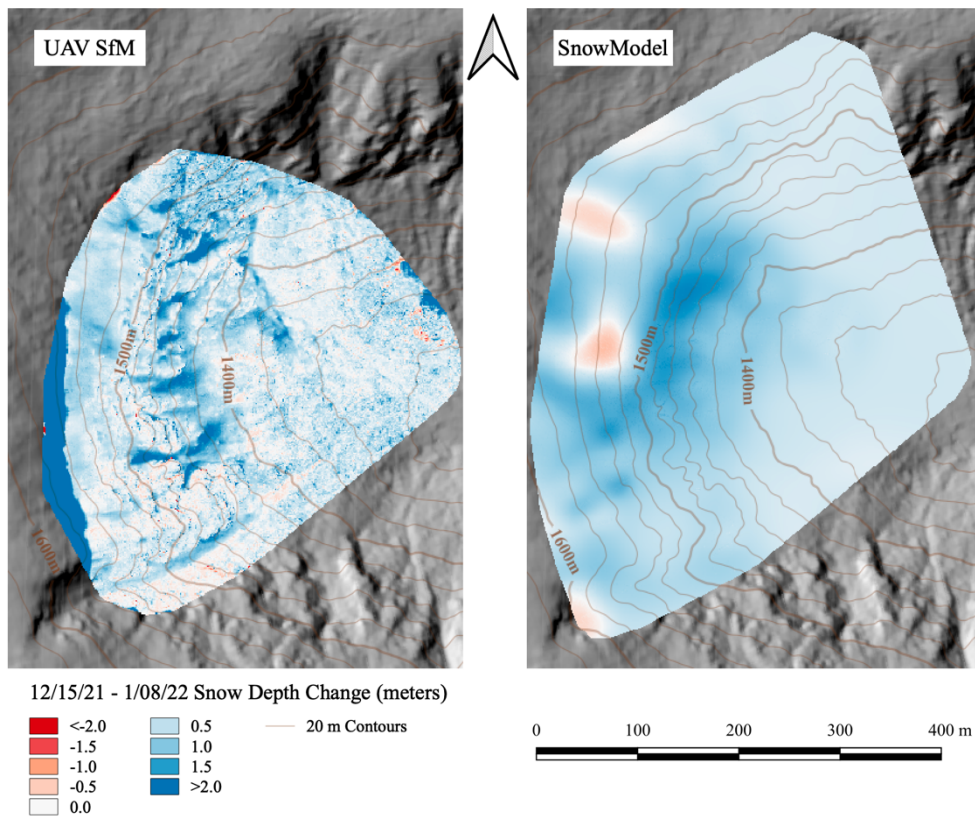
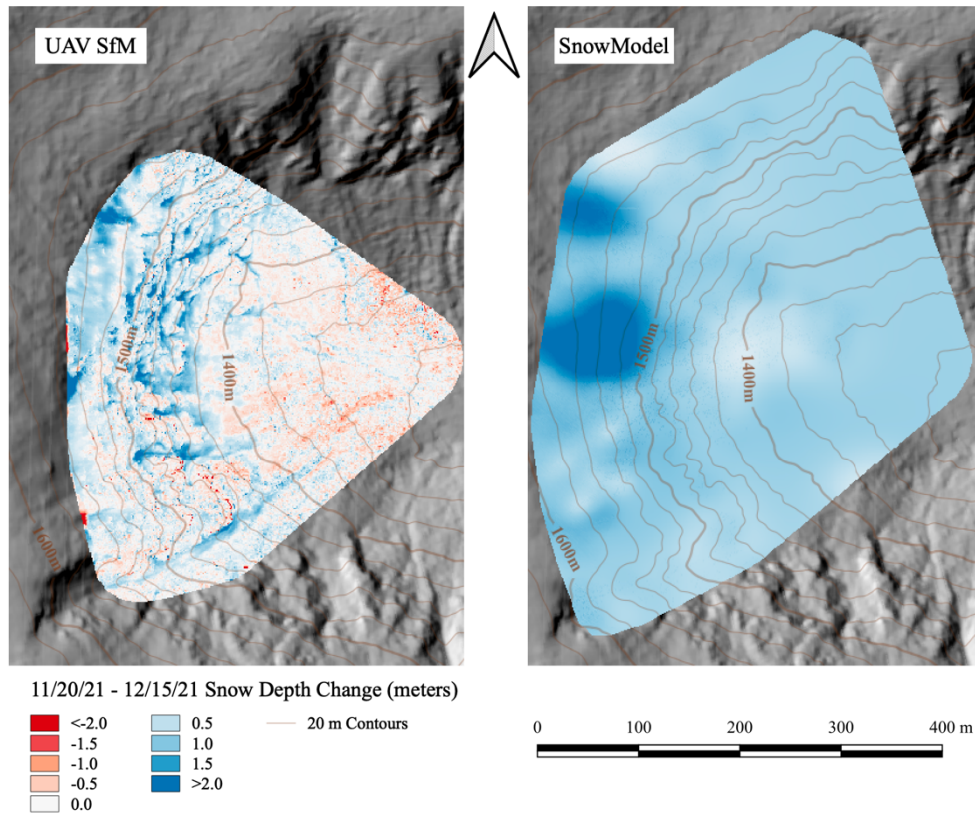
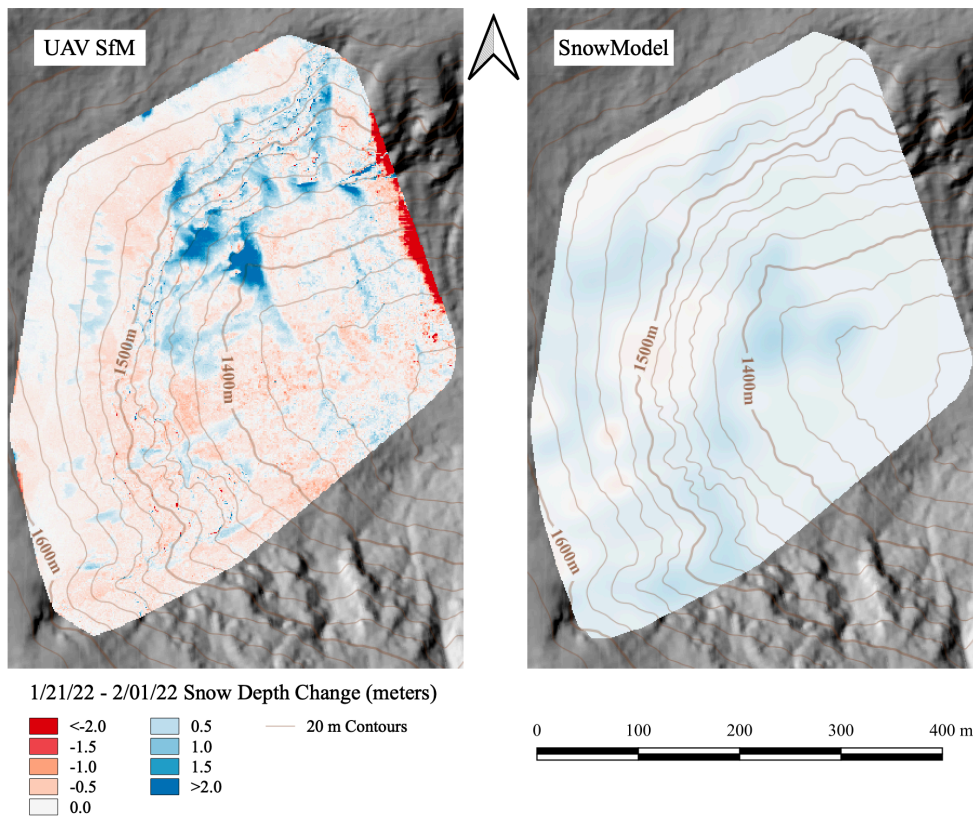
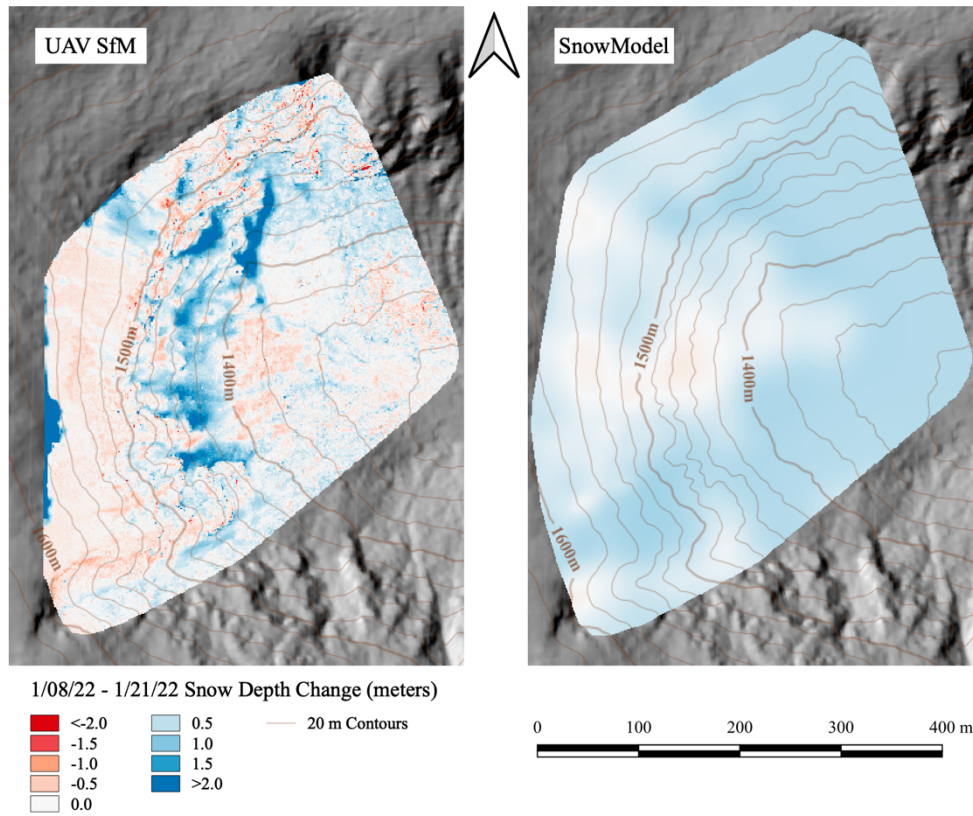


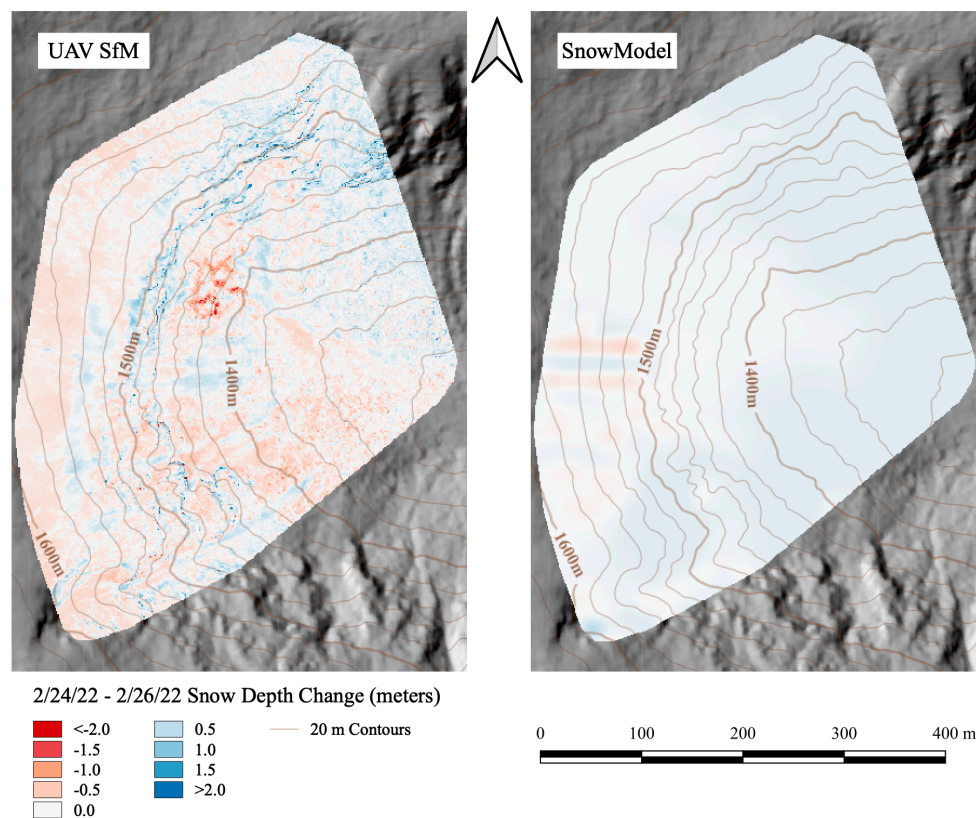
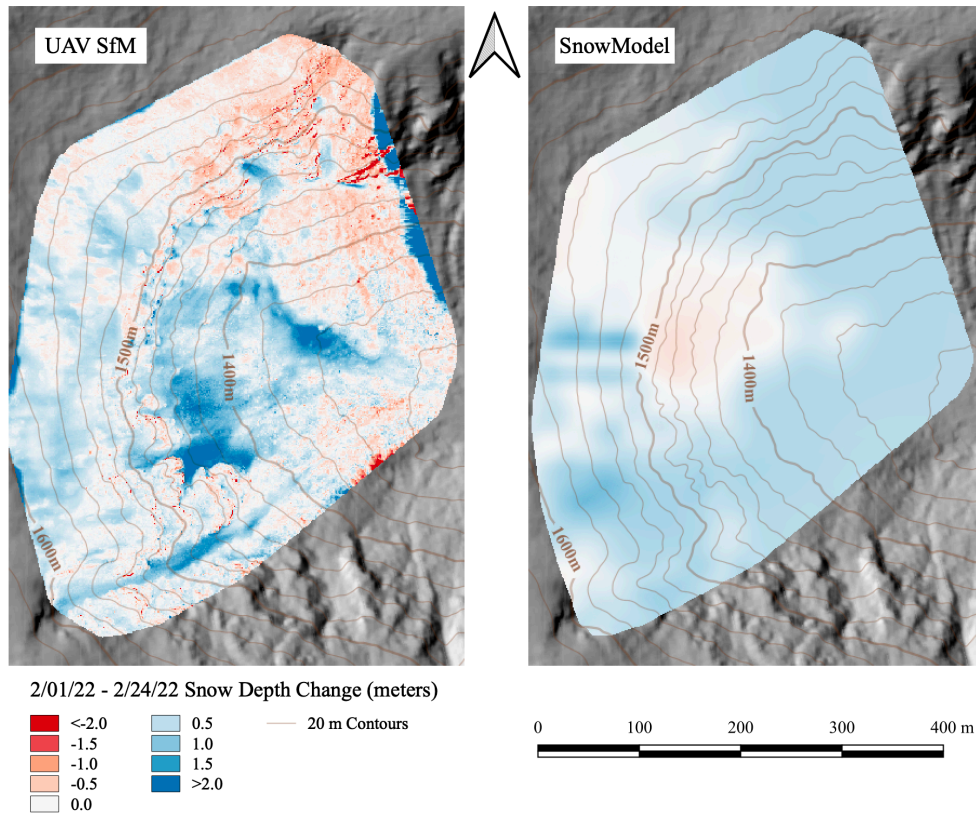
Figure A.7: Blowing Snow Flux Adjustment Parameter (BSFP) and Tabler Adjustment Scaling Factor (S) Testing on 30 m Resolution SnowModel Grid

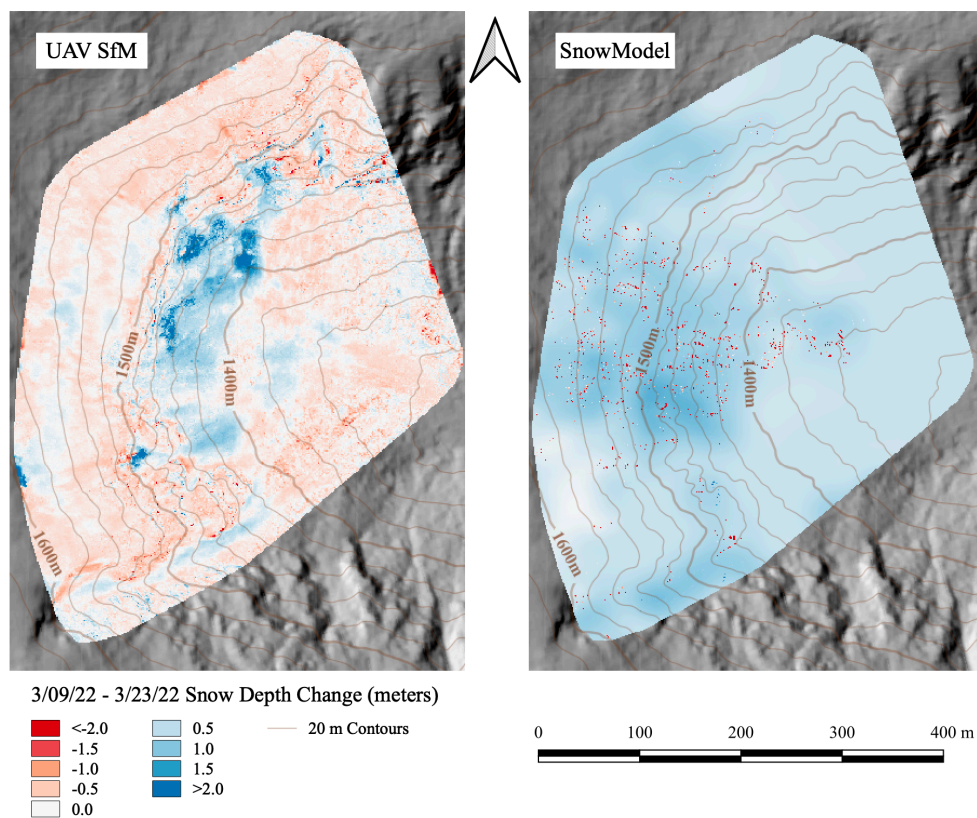
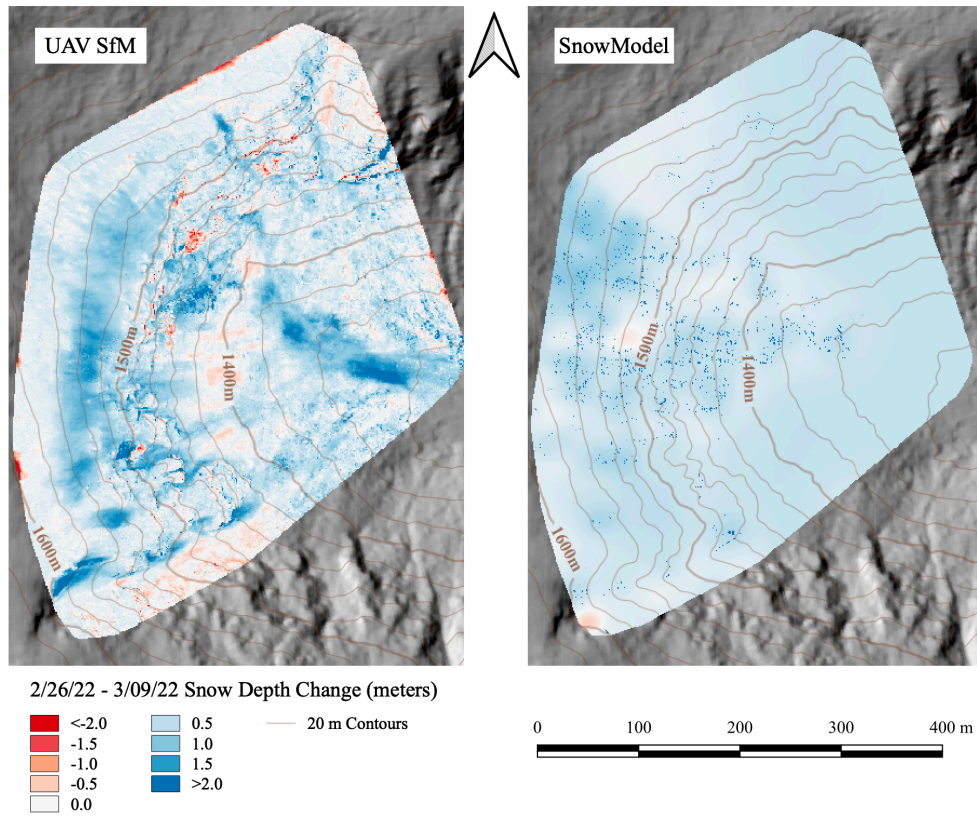
APPENDIX G – UAV SfM AND SNOWMODEL SNOW DEPTH CHANGE COMPARISON MAPS

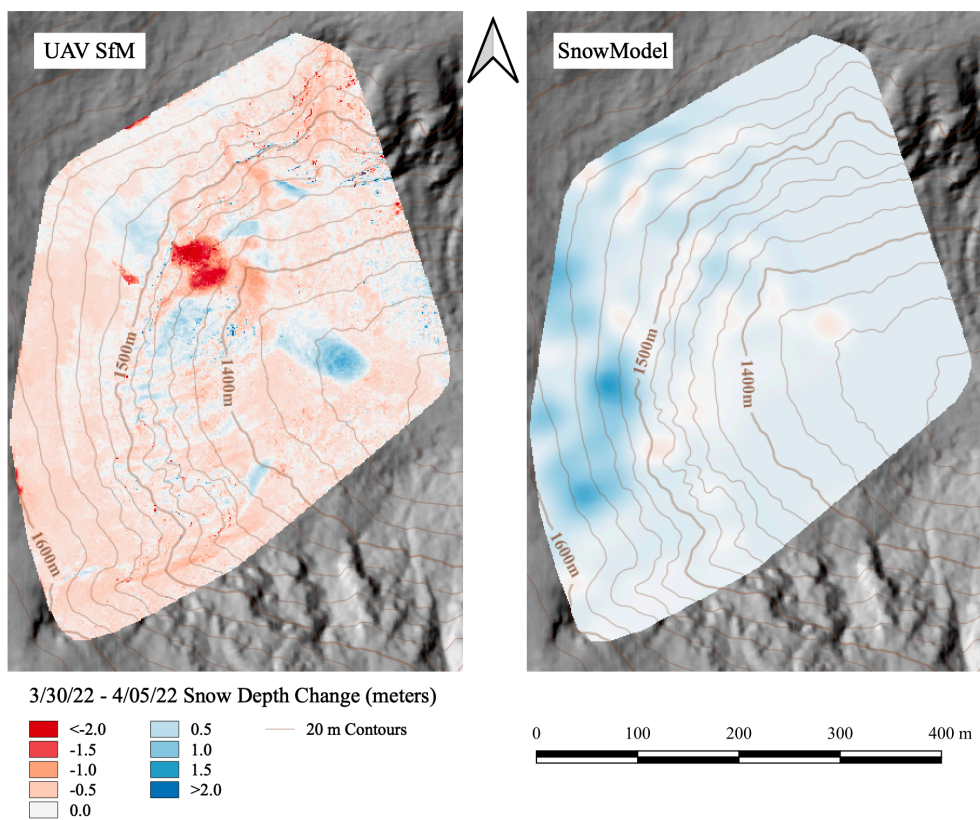
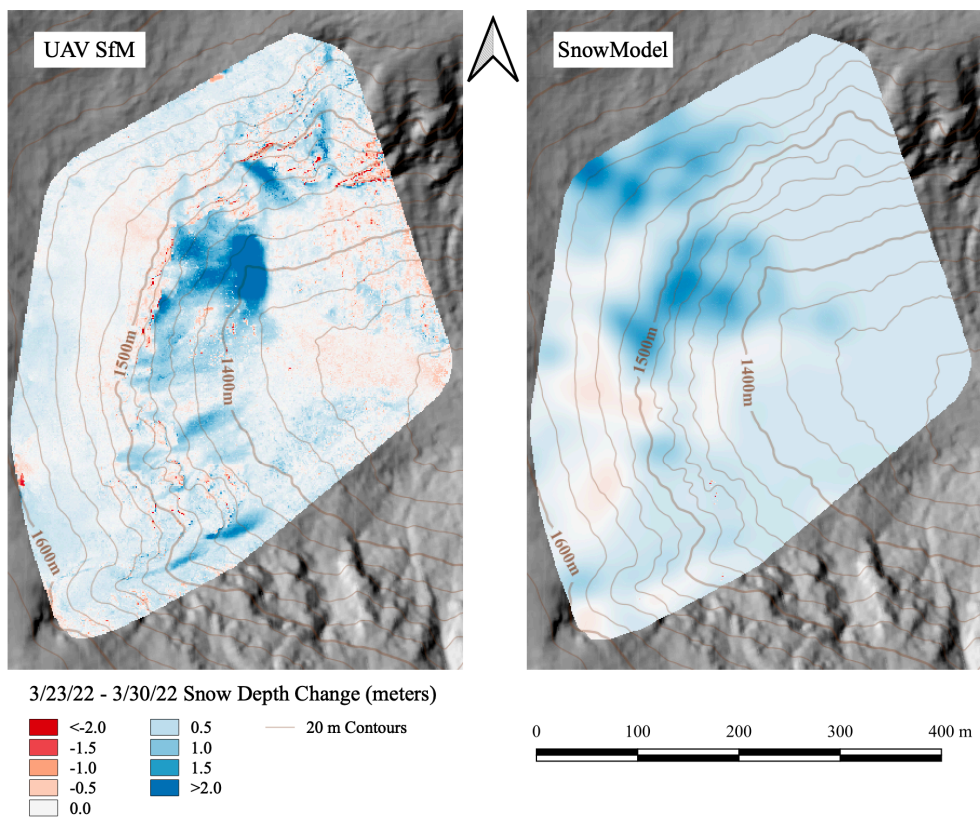












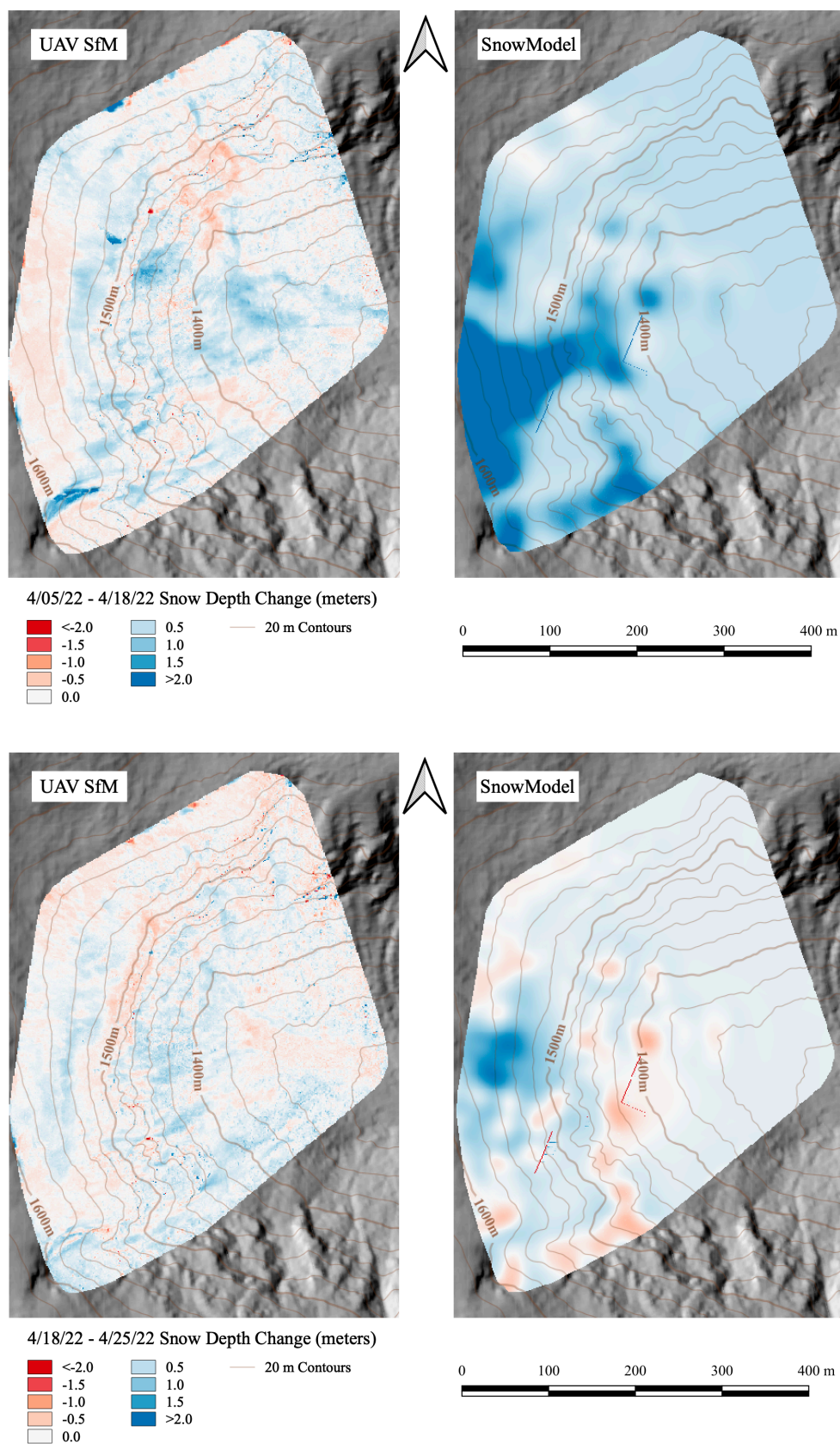


Figure A.8: SnowModel and UAV Snow Depth Change Map Comparison in Tuckerman Ravine Time Series

APPENDIX H – SNOWMODEL LANDCOVER INPUT

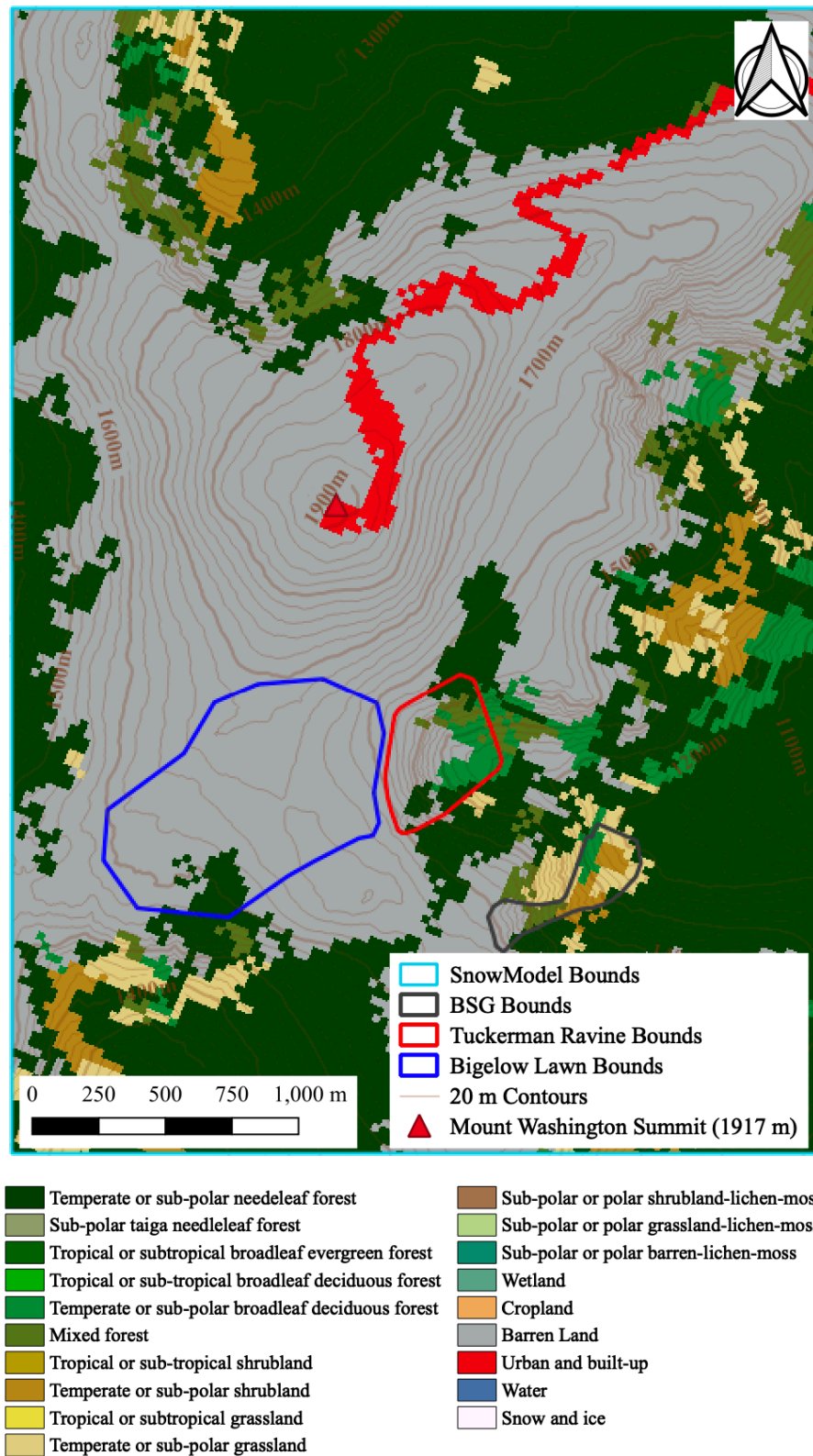


Figure A.9: North American Land Change Monitoring System 2015 30 m

